University of Stavanger

Faculty of Science and Technology

MASTER'S THESIS

Study program/ Specialization: MSc in Petroleum Engineering	Spring semester, 2016 Open / Restricted access
Writer: Rza Behbudov	…… (Writer's signature)
Faculty supervisor: Kjell Kåre Fjelde	
Thesis title: Full-scale and Small-scale Controlled Mud Level Drilling Simulations with the AUSMV Numerical Scheme	
Credits (ECTS): 30	
Key words: Dual Gradient drilling Controlled Mud Level EC-Drill AUSMV simulations	Pages: 105 + enclosure: 30 Stavanger, 14.06.2016

Acknowledgement

I would like to thank my supervisor Kjell Kåre Fjelde for his continuous support and guidance during this work.

I want to thank my family for their support during all these years of education. I would have not been able to be where I am right now without them.

I would like to also thank all my close friends that helped me in so many situations during my studies and life in general.

And at last I would like to thank University of Stavanger for the opportunity to build my career here in Norway.

Abstract

Due to an increased demand from operator companies for deep-water drilling solutions, an interest in Dual Gradient technologies has risen. An example of such a technology is Controlled Mud Level (CML) drilling, where a subsea pump integrated in one of the riser joints actively controls the riser level. Reducing the hydrostatic component of the system helps to control pressures down-hole very accurately and fast. For this type of pressure control, an understanding of down-hole parameters as well as precise pressure estimate is required. This can be done by different numerical schemes. The scheme used in this thesis is AUSMV numerical scheme used mostly for academic purposes. In this work, a coupling between this scheme and CML technology mentioned before has been introduced.

This thesis has undertaken a literature survey from which it was concluded that CML is a promising technology, which finds compromises between several drilling aspects and makes operations more simple and less time consuming. A detailed review of the historical, technical and operational aspects of the technology was performed. Already existing commercial field applications confirms the future interest in CML. One of the breaking innovations with CML is early kick detection, which allows determining the reservoir influx in less than a minute. Well Control procedures used for the CML are close to Driller's method. This is an advantage taking into consideration the time used for the training of the personnel.

After the technology has been reviewed in detail, simulations in Matlab have been performed to examine the ability of the AUSMV scheme to handle this type of well operations. Special focus was placed on the numerical boundary treatment on top of the well. Several ways of defining the outlet pressure boundary were investigated. In the end, setting the outlet pressure flux equal to 1 atm was concluded to be the best alternative. The scheme was available in two versions, 1st order and 2nd order. The updated 2nd order scheme differs from the original 1st order scheme by using slope limiters. This reduces numerical diffusion, which is a common problem with numerical schemes. After a comparison of the two schemes, the 2nd order showed more realistic and smoother results. The simulations of the 1st order scheme confirmed the problem of negative velocity fields for static conditions. Moreover, the

problem with an outlet pressure representation at the beginning of simulations was discovered, which needs further investigation.

Next objective for this thesis was to adapt the scheme for the small-scale experimental flow-loop located at University of Stavanger (UIS). Two methods for achieving stable numerical solutions were found. Since the pressures delivered by the approximated small-scale model were very low, the first method involved pressurizing the system with 10 bars. This was a remedy introduced due to the problems the model had with handling the low pressures encountered in this simulation set-up. This was not optimal since it would not be possible to pressurize the system experimentally. However, an alternative method was found by editing a specific pressure condition in the code, which was there initially to assure stability but in this set-up was causing a problem. Both methods were compared and the alternative method was concluded to be the best out of the two. Nevertheless, it is important to test the experimental set-up with the proposed method first to be able to assess its efficiency. The simulation results found that the model is extremely friction dominated, a very important conclusion in this case. This might cause problems in studying this particular simulation case as it mostly relies on pressure control based on manipulations of the hydrostatic pressure component. Furthermore, the results showed that the effect of these manipulations was almost entirely masked by friction. A possible solution for this problem would be to move the suction point higher up in the well, which would reduce the height of the fluid column above. This fluid column was found to be the main contributor to the negative friction effect.

Table of Contents

List of Tables

List of Figures

Nomenclature

List of Abbreviations:

BHP	Bottom Hole Pressure
CDPP	Constant Drill Pipe Pressure
CFL	Corant-Friedrichs-Lewy criterion
CMC	Controlled Mud Cap drilling
CML	Controlled Mud Level drilling
CSS	Continuous Circulation System
CTS	Cuttings Transport System
DAPC	Dynamic Annular Pressure Control
DG	Dual Gradient drilling
DSRM	Delta Seal Riser Module
DSV	Drilling Safety Valve
ECD	Equivalent Circulating Density
GOM	Golf of Mexico
HPHT	High Pressure High Temperature
IRIS	International Research Institute of Stavanger
JIP	Joint Industry Project
LRRS	Low Riser Return System
MCD	Mud Cap Drilling
MFC	Micro-Flux Control
MPD	Managed Pressure Drilling
MRJ	Modified Riser Joint
MRL	Mud Return Line
MSL	Mean Sea Level
NCS	Norwegian Continental Shelf
NPT	Non-productive Time
NTNU	Norwegian Institute of Science and Technology
OTC	Offshore technology Conference
PMCD	Pressurized Mud Cap Drilling
PWD	Pressure While Drilling
QCA	Quick Closing Annular
RCD	Rotating Control Device
RCH	Rotating Control Head
RKB	Rotary Kelly Bushing
RMR	Riserless Mud Recovery
SMD	Subsea Mudlift Drilling
SMO	Suction Module
SMP	Subsea Mudlift Pump
SPE	Society of Petroleum Engineers
SPP	Standpipe Pressure
UIS	University of Stavanger
WD	Water Depth

List of Symbols:

a	Sound velocity, m/s
A	Cross sectional area, m^2
F_w	Friction gradient, Pa/m
σ_a	Horizontal stress, median line, sg
$\emptyset$	Inclination (relative to vertical)
Δt	Time step, s
Δz	Box length, m
BHP	Bottom Hole Pressure, bar
d	Diameter, m
$Dmud$	Mud density, sg
f	Friction factor
F	Numerical fluxes
g	Acceleration caused by gravity, m/s^2
$Hriser$	Mud level inside the riser, m
K	Gas distribution coefficient
M	Mass rate, kg/s
p	Pressure, Pa
$Pbackpressure$	Backpressure, bar
$Pfric$	Friction pressure componet, bar
$Phyd$	Hydrostatic pressure component, bar
Po	Formation pore pressure, sg
$Priser$	Pressure inside the riser, bar
Psw	Seawater column hydrostatic pressure, bar
Pwf	Formation fracturing pressure gradient, sg
q	Source term, kg/s
Q	Source term, kg/s
Re	Reynolds number,
S	Gas rise velocity, m/s
U	Conservative variables
v	Velocity, m/s
V	Volume, m^3
α	Volume fraction
μ	Viscosity, Pa*s
ρ	Density, kg/m^3

Subscripts:

g	gas
l	liquid
mix	mixture
j	box number

Superscripts:

n	time level

1 Introduction

The Managed Pressure Drilling (MPD) concept is becoming more important for the industry today as more deep-water fields are being developed. MPD has evolved during last years and includes now a much wider spectrum of technologies available for the commercial use. Dual Gradient (DG) technology is one of these. Some of the available DG commercial technologies are still under development. An example of such a technology is Controlled Mud Level (CML) drilling. A significant difference between CML and other DG technologies is that the riser is partially evacuated. Active control of the mud level in the riser allows for more precise bottom hole pressure (BHP) control. For active control of the mud level in the riser, efficient software is required to be able to instantly calculate the pressures in the well and simulate fluid behavior. This type of software is based on different hydraulic models that are solved with the help of numerical schemes. An example of such a model-based scheme is called AUSMV. It is mainly used for academic purposes for improving the understanding of transient flow. It is important to test the coupling of the scheme with the CML case experimentally to validate that the model is able to represent the real physics of the flow configuration. This possibility is available at University of Stavanger (UIS) with the small-scale experimental flow-loop built for MPD related studies.

This thesis has several objectives related to DG technology and CML in specific:

1. First, a literature survey on CML and commercial application of this technology will be carried out. The purpose with this is to identify the relevance of this technology for the industry today.
2. The AUSMV numerical scheme mentioned earlier will be reviewed. The scheme is available in 1st and 2nd order versions, both of the versions will be adapted for the CML case and the results will be compared to each other. In these simulations a test case studied by Torsdal (2015) will be used.
3. After the comparison, the AUSMV scheme will be used for CML case simulations conducted with the small-scale flow-loop geometry. This is the first step in generating model results that can be compared with future experimental data generated in the small-scale loop at UIS.

To be able to reach the objectives above, the thesis has been structured in the following manner. First, a description of MPD concept together with the underlying technologies will be presented. This will be followed by the literature survey on CML, including the historical evolvement of this technology, non-commercial studies, already existing commercial applications and aspects related to those. A short description of the AUSMV numerical scheme will follow with the details on how the scheme has been updated for both simulation cases. The AUSMV scheme has been integrated in Matlab software. An already existing matlab code has been used as a basis for the simulations. Then description of the small-scale flow-loop geometry will follow, with the approximated model based on this geometry data that will be used for second simulations. The second objective in this thesis is related to the previous work done by Torsdal (2015), where simulations of the CML case were conducted with the 1st order scheme and the previous version of code. The updated matlab codes used for simulations will be included in the appendixes in the end of this thesis with all the changes marked with red color. First, simulations will be carried out with the purpose to adapt the new code for the CML case scenario, with the following comparison of the 1st order scheme to the 2nd order. At last, in the second example, simulations will be conducted with small-scale flow-loop geometry to be able to compare the results with experimental studies on CML in future.

2. MPD

Due to the depletion of already producing shallow water reservoirs, exploration takes it a step further by going into deeper waters (Hannegan, 2006). One important aspect of this tendency is that drilling becomes a more challenging process. This is mainly due to the increased pore pressure and steeper fracture gradient (Erivwo et al., 2012). Hence, there is the problem of a narrow operating window. This means that BHP variations should be limited as much as possible. One way to deal with this challenge was introduced by new a drilling approach called Managed Pressure Drilling (MPD).

The Underbalanced Operations and Managed Pressure Drilling Committee of the International Association of Drilling Contractors (IADC) define Managed Pressure Drilling as "an adaptive drilling process used to precisely control the annular pressure profile throughout the wellbore. The objectives are to ascertain the down-hole pressure environment limits and to manage the annular hydraulic pressure profile accordingly. The intention of MPD is to avoid continuous influx of formation fluids to the surface. Any influx incidental to the operation will be safely contained using an appropriate process." (Malloy et al., 2009) Moreover,

- "MPD process employs a collection of tools and techniques which may mitigate the risks and costs associated with drilling wells that have narrow down-hole environmental limits, by proactively managing the annular hydraulic pressure profile."
- "MPD may include control of back pressure, fluid density, fluid rheology, annular fluid level, circulating friction, and hole geometry, or combinations thereof."
- "MPD may allow faster corrective action to deal with observed pressure variations. The ability to dynamically control annular pressures facilitates drilling of what might otherwise be economically unattainable prospects."

In other words MPD represents a set of different technologies that allow dynamic BHP control. The pressure gradient consists of hydrostatic and friction gradients. The hydrostatic gradient is represented by effective mud-weight, where friction gradient is dependent on factors like flow-rate and flowing area. Refer to equation below (Malloy et al., 2009):

$$BHP = Phyd + Pfric \quad (1)$$

As stated earlier, the friction gradient is dependent on flow, if there is no flow, the contribution to BHP is lost. In conventional drilling operation during connections, when there is no flow, hydrostatic gradient stands on its own to represent BHP. Hence, since the friction is lost, BHP will be lower. Drilling High Pressure High Temperature (HPHT) or deep-water wells is a scenario where the margin between pore and fracture pressure gradients is very narrow (Erivwo et al., 2012). A slight change in BHP can result in an influx of reservoir fluids or a fracturing of the formation rock. It becomes critical to keep BHP constant and in one or another way compensate for frictional loss during connections, which MPD makes possible. Another important benefit of MPD to be mentioned here, is that this approach allows for much better well control. By means of constant flow control and monitoring of well parameters, kick detection is improved compared to conventional drilling (Malloy et al., 2009). Kick circulation might even be possible without closing BOP and shutting in the well (Choe et al., 2007). However, it often requires new well control procedures and crew preparation. The same benefits of constant flow control can be also used if a loss circulation scenario is experienced and BHP needs to be reduced in a quick manner.

MPD is represented by several technologies in the market (Rehm et al., 2008, Hannegan, 2006). The first and most popular technique is a traditional way of pressure control by means of Rotating Control Device (RCD) in combination with a choke and a backpressure pump. Another technique utilizing the same RCD equipment but different in principle is Pressurized Mud Cap Drilling (PMCD) (Rehm et al., 2008, Hannegan, 2006). However, it is important to mention that this method is mainly adapted for highly fractured carbonate reservoirs. The most promising method, which is suitable for many drilling environments but also relatively new, is Dual Gradient (DG) drilling (Rehm et al., 2008, D.Hannegan, 2006). DG means that hydrostatic pressure is represented by a combination of two fluid columns with different densities.

Since the simulations to be carried in this thesis deal with a DG drilling scenario, the focus will mainly be on the latter technique. A short description of each method will be presented in the subchapters below, with a main focus on DG drilling. There are several ways to drill a well in a dual gradient fashion, which will be further discussed in detail.

2.1 Backpressure MPD

In this subchapter, conventional backpressure MPD system will be shortly reviewed. As stated above, this system is commonly used and has found its application in many drilling environments (Hannegan, 2006). In general, there are two MPD systems, one open and one closed. In an open system fluid flows out of the well with atmospheric pressure, while in a closed one, fluid is pressurized (Rehm et al., 2008). The only way to maintain constant BHP with an open system in conventional MPD operation is to use Continuous Circulation System (CSS) (Rehm et al., 2008). This method allows continuous circulation even when connections are made. However, this method is outside of the scope of this work, for details refer to SPE 90702.

2.1.1 Principle of Backpressure MPD

The main principle behind this method is that to be able to compensate for frictional pressure loss a new variable is introduced, $Pbackpressure$ (Hannegan, 2006):

$$BHP = Phyd + Pfric + Pbackpressure \quad (2)$$

The system is a closed loop, where BHP is dynamically controlled by means of choke opening and backpressure pump. If the choke opening area is decreased, pressure will consequently increase. During connections, when $Pfric$ becomes 0, $Pbackpressure$ is increased to keep BHP constant. This is done by ramping up the backpressure pump to ensure flow across the choke. There are several basic equipment requirements for the backpressure MPD system (Rehm et al., 2008):

1. Rotating Control Device
2. Choke manifold
3. Backpressure pump
4. Mud gas separator

Rotating control device is an important pressure seal element located above BOP and below the drill floor. The main purpose of it is to direct the annular flow and create a closed loop system. The choke manifold can be used to regulate the pressure in the well. The way the choke is manipulated will differ from case to case. It can be either manual, fully automated or semi automated (Rehm et al., 2008). It can be used alone or in combination with backpressure pump. An example of a fully automated system is Dynamic Annular Pressure Control system (DAPC) (Chustz et al., 2007):

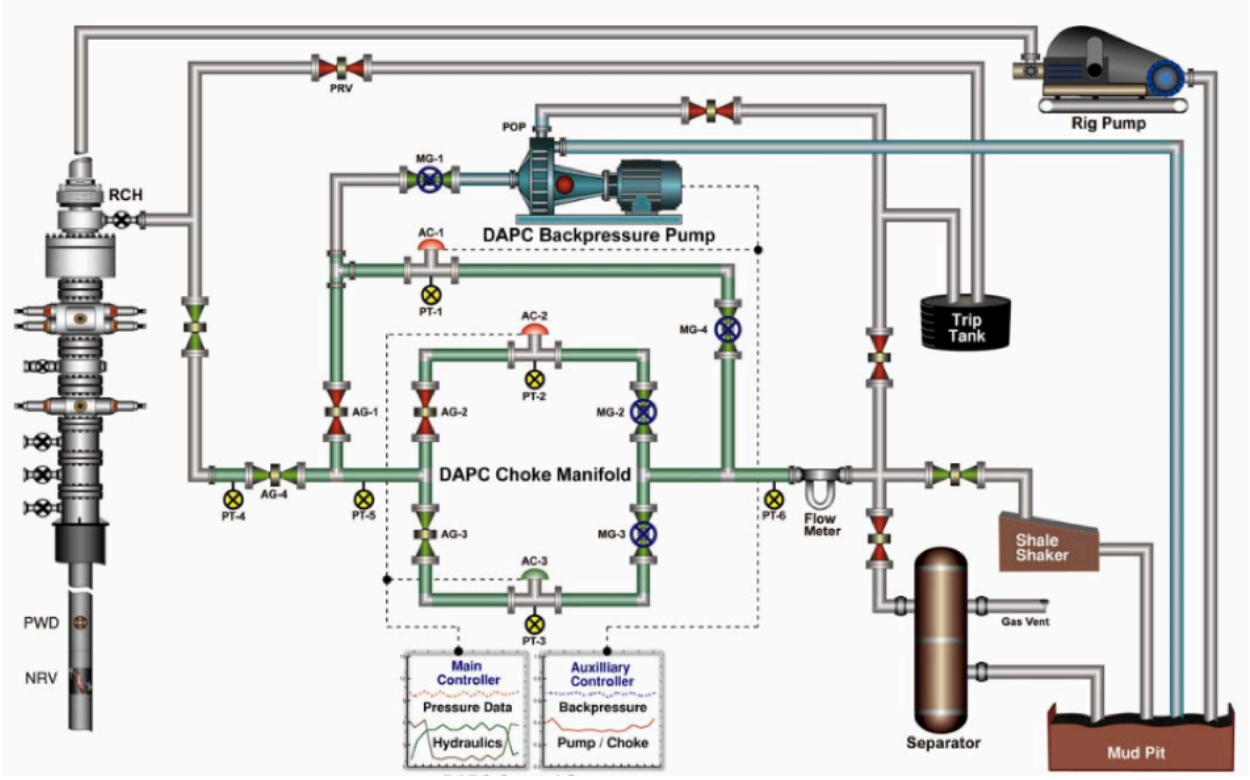

Figure 1: DAPC (Chustz et al., 2007)

The choke manifold in this case carries three chokes, one main and two secondary. Important additions to this system are integrated pressure management and hydraulic flow-model. The hydraulic model continuously updates flow parameters and based on that one responds to each pressure variation by changing the choke opening. It also contributes to early kick detection (Rehm et al., 2008). In the situation when the kick is taken by the well, a mud gas separator can be used to separate fluids even if the well is not shut-in and circulation is continued.

Another similar system commercially deployed but slightly different is Micro-Flux Control technology (MFC) developed by Weatherford (Santos et al., 2005). It is based strictly on real-time measurements and can work in a fully automated mode. The Choke manifold is replaced with a so-called Drilling manifold with two choke valves, a mass flow-meter and an intelligent control unit. Direct flow measurements from the flow-meter then, serve as an input for the intelligent control unit, so it can adjust the choke opening to provide backpressure or direct the flow either to shakers or mud gas separator if the kick is detected (Rehm et al., 2008).

2.2 Pressurized Mud Cap Drilling

PMCD (Terwogt et al., 2005) is an extended drilling method that developed from normal Mud Cap Drilling (MCD) (Rehm et al., 2008). Both of these methods are adopted for fractured carbonate systems where huge mud losses can occur. These formations are difficult to control in a conventional manner. If a kick is taken using MCD, kill mud is bullheaded down the annulus until no pressure is seen on the gauge (Rehm et al., 2008). Sacrificial fluid like water or any other economically friendly mixture is used in the drill-string. Water is pumped down with pressure so that all debris and cuttings from drilling are forced inside the fractures, while heavy kill-mud is holding the pressure on the annulus side. Hence, there is no cuttings-return to the surface. Moreover, another benefit is that corrosive gasses like H_2S are also kept down-hole (Rehm et al., 2008).

In PMCD, the only difference is that the kill-mud in the annulus is lighter, and to be able to maintain pressures down-hole, additional pressure is applied on top of it (Rehm et al., 2008). The well is sealed with a RCD on top and the equipment used for both PMCD and MCD is the same as for backpressure MPD (Rehm et al., 2008). Change in annular pressure is then used for kick detection. When influx is taken, pressure on the annular side becomes larger, because part of the fluid column is now replaced by gas with lower density. As the kick migrates towards the surface, the annular pressure will continue to increase. To prevent gas migration to the surface, additional fluid is pumped down the annulus until the annular pressure has been reduced to the previous value (Rehm et al., 2008).

2.3 Dual Gradient Drilling

Conventional MPD drilling operation offshore is performed with returns through the marine drilling riser. In other words, if we neglect temperature and pressure effects and assume no influx of formation fluids, there is a single gradient pressure profile in the annulus, from the top of the riser to the bottom of the well. All MPD systems described before are closed single gradient systems. In this chapter, Dual Gradient systems will be reviewed. As the name indicates, fluid column in the annulus is effectively represented by two fluids with different densities. Hence distinct pressure gradients are achieved in the well, one above the BOP and a different one below the BOP. Several commercially available technologies have been developed to achieve this (Stave et al., 2005, Smith et al., 2001, Ziegler et al., 2013). A simple example is

demonstrated below. The blue line is 1.5 sg all the way to the bottom of the well, while the red line is seawater gradient (1.03 sg) until 600 meter and 1.9 sg to the bottom:

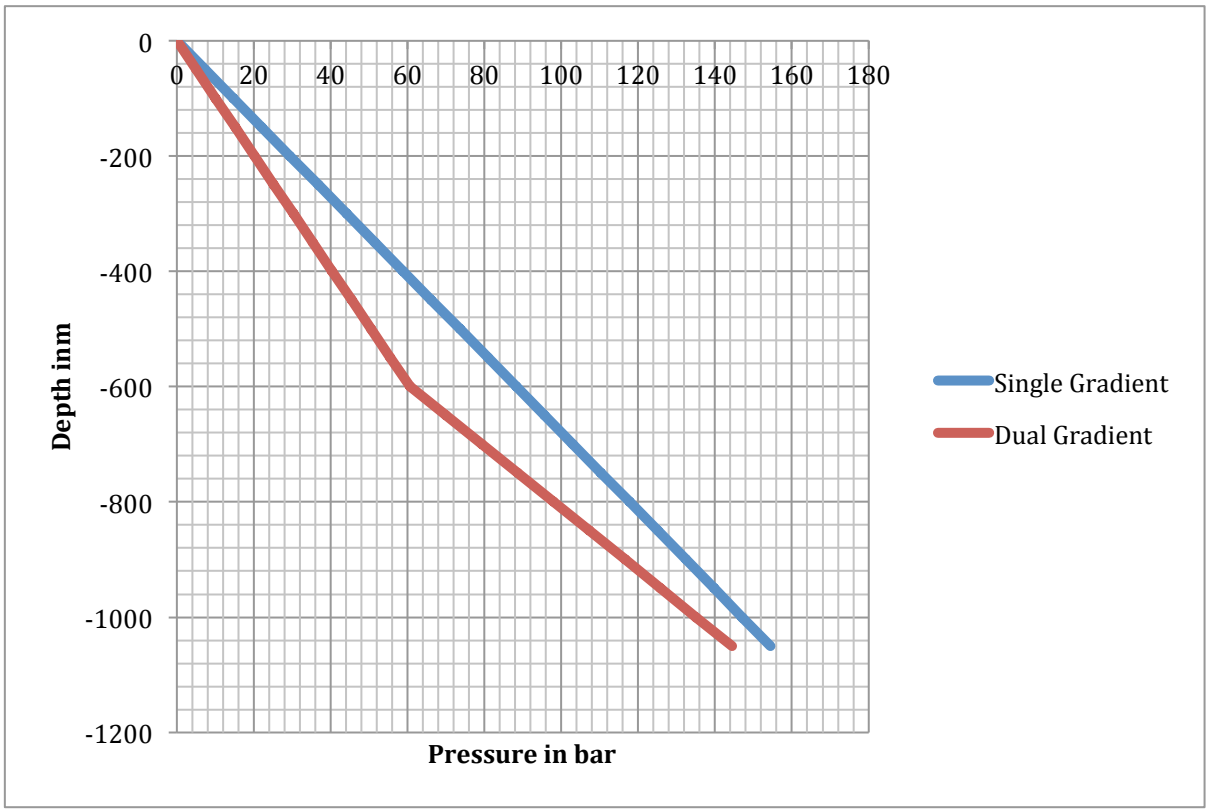

Figure 2: Dual Gradient vs. Single Gradient

The first attempt towards DG drilling was made back in 1996 with a Joint Industry Project (JIP) (Smith et al., 2001). It was a combined effort made by different deep-water drilling companies to drill the first DG well ever. As a result, the Subsea Mudlift Drilling (SMD) system was developed. The main principle is that riser is full with seawater and the rest of the annulus is filled with mud. The rotating diverter separates the riser and the well. A subsea pump lifts the mud out of the well. It is also this subsea pump that creates a seawater pressure below the RCD (Schumacher et al., 2001, Eggemeyer et al., 2001).

The Riserless Mud Return system (RMR) is similar to SMD with the main difference that there is no riser in place (Rezk, 2013, Cohen et al., 2010). A subsea pump lifts the mud returns and cuttings out of the well using a return line. The system is open to the sea with seawater above the wellhead and heavy mud in the well. Hence, this system has a natural dual gradient effect, but the main purpose of the system is to be able to

perform top-hole drilling with returns to the rig, avoiding cuttings accumulation at the seabed. RMR was the first commercially applied technology with a great success in top-hole drilling (Stave et al., 2014).

The most novel approach in DG drilling is so called Controlled Mud Cap drilling (CMC) (Fossli and Sangesland et al., 2004). It is also referred to as Low Riser Return System (LRRS) (Falk et al., 2011) or Controlled Mud Level (CML) technology (Fossli and Stave et al., 2014). Since CML is the most recent name for this technology, it will be used further in this work. This method is considered to be the most attractive so far and several commercial applications are taking place at the time this work is being written (Cohen et al., 2015, Hauge et al., 2015, Godhav et al., 2015). The main principle behind CML is that marine riser is filled with mud, but only partially. In this case the pressure column is represented by mud and air. Active lowering or elevation of the mud level inside the riser is possible, which gives great flexibility in BHP control. Another benefit is that CML is an open system.

RMR, SMD and CML were all commercially available technologies by the time this thesis was being written. The principles of DG drilling will be discussed further, followed by detailed review of these technologies. The main focus will be directed on CML. A separate literature survey on this method will be carried out in a separate chapter.

2.3.1 Principle of Dual Gradient

In this subchapter the main principles and benefits of DG drilling will be highlighted on the basis of different technologies. In the case of RMR and SMD, the pressure at the wellhead is always equal to hydrostatic pressure of the seawater column above. In combination with appropriate mud weight, the best possible pressure profile curve can be calculated. To demonstrate that, an example is provided below, where appropriate mud weight is to be determined. Well data is as follows:

Water depth (WD): 1500 m

Table 1: Well data, DG example

	Pore	Frac	MW	ECD	Median line
1500	1,03	1,07	1,05		1,05
1700	1,05	1,20	1,05		1,125
1900	1,09	1,32	1,15		1,205
2100	1,11	1,47	1,15		1,29
2300	1,13	1,55	1,42	1,43	1,34
2500	1,28	1,60	1,42	1,43	1,44
2700	1,31	1,63	1,42	1,43	1,47
2900	1,34	1,67	1,42	1,43	1,505
3100	1,38	1,70	1,42	1,43	1,54
3300	1,39	1,74	1,42	1,43	1,565
3500	1,43	1,77	1,68	1,70	1,6
3700	1,47	1,80	1,68	1,70	1,635
3900	1,49	1,83	1,68	1,70	1,66
4100	1,55	1,85	1,68	1,70	1,7
4300	1,57	1,87	1,68	1,70	1,72
4500	1,60	1,89	1,68	1,70	1,745
4700	1,62	1,91	1,68	1,70	1,765
4900	1,64	1,93	1,68	1,70	1,785
5100	1,69	1,95	1,87	1,91	1,82
5300	1,72	1,97	1,87	1,91	1,845
5500	1,74	1,99	1,87	1,91	1,865
5700	1,76	2,00	1,87	1,91	1,88
5900	1,78	2,01	1,87	1,91	1,895
6100	1,79	2,02	1,87	1,91	1,905
6300	1,80	2,03	1,87	1,91	1,915

Table 1: Depth in (Mean Sea Level) MSL, pore and fracture gradients, mud weight both static and dynamic (ECD), median line. The last column in the table is calculated on the basis of median line principle (Aadnøy, 2010). The optimal mud weight for the most problematic areas in isotropic conditions, when horizontal stresses are assumed to be the same, must be as close to this value as possible. This is described by the following equation (Aadnøy, 2010):

$$\sigma_a = \frac{1}{2} * (Pwf + Po) \tag{3}$$

Where Pwf and Po are fracturing and pore pressures respectively. In this way the formation remains undisturbed, and excellent hole-stability is achieved. Based on the data, the seawater column hydrostatic pressure is:

$$Psw = 1500m * 0.0981 * 1.03sg = 151.6\ bar$$

Pressure for the rest of the well is then calculated:

$$P(1700) = Psw + (1700 - 1500)m * 0.0981 * 1.6sg$$

$$P(1900) = P(1700) + (1900 - 1700)m * 0.0981 * 1.6sg \ldots\ldots\ldots$$

The figures below represent gradient and pressure curves for these cases. The dual gradient mud weight of 1.6 sg applies from the wellhead and down to the total depth of 6300 m below MSL:

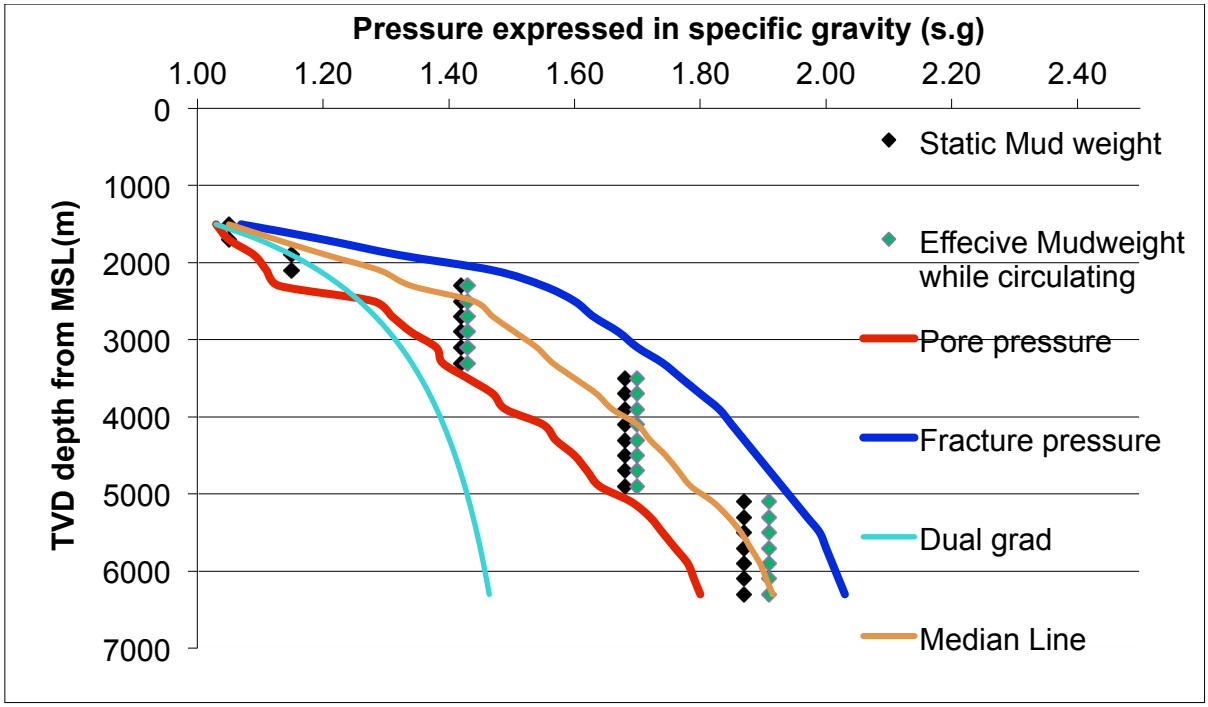

Figure 3: DG pressure profile vs. conventional, mud weight 1.6 sg

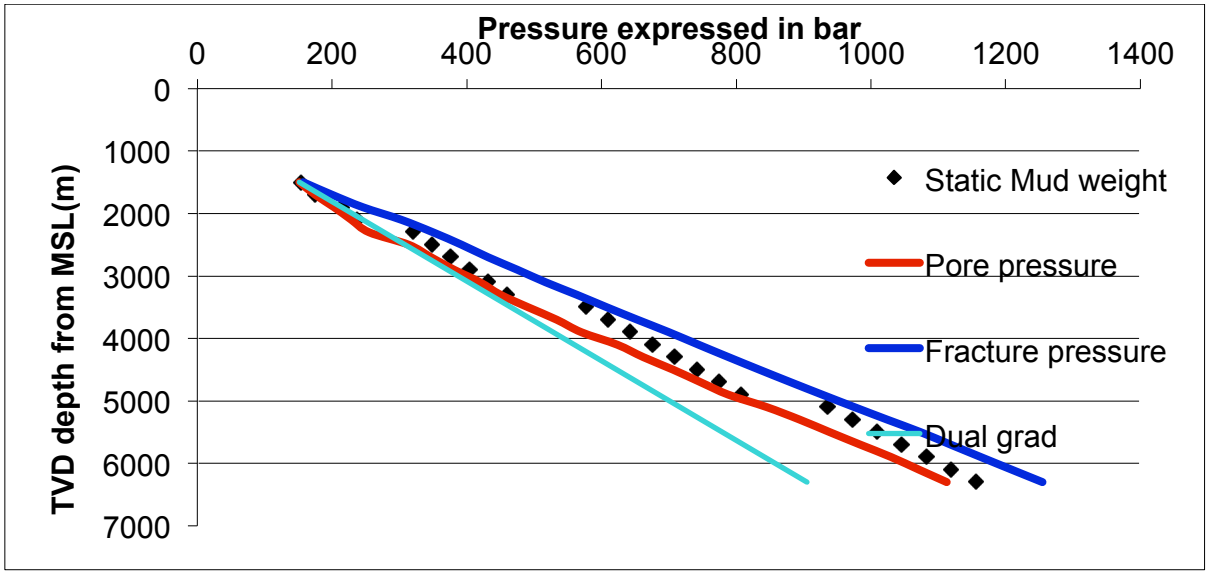

Figure 4: DG pressure profile vs. conventional, mud weight 1.6 sg

The light blue line represents the DG pressure profile using a 1.6 sg mud in the well. Obviously, a mud weight of 1.6 sg is not sufficient. Problems will occur as early as approximately 2500 meters. Next, DG mud weight is changed to 2.1 sg. *Psw* remains the same. By updating the calculation, the DG curve now becomes:

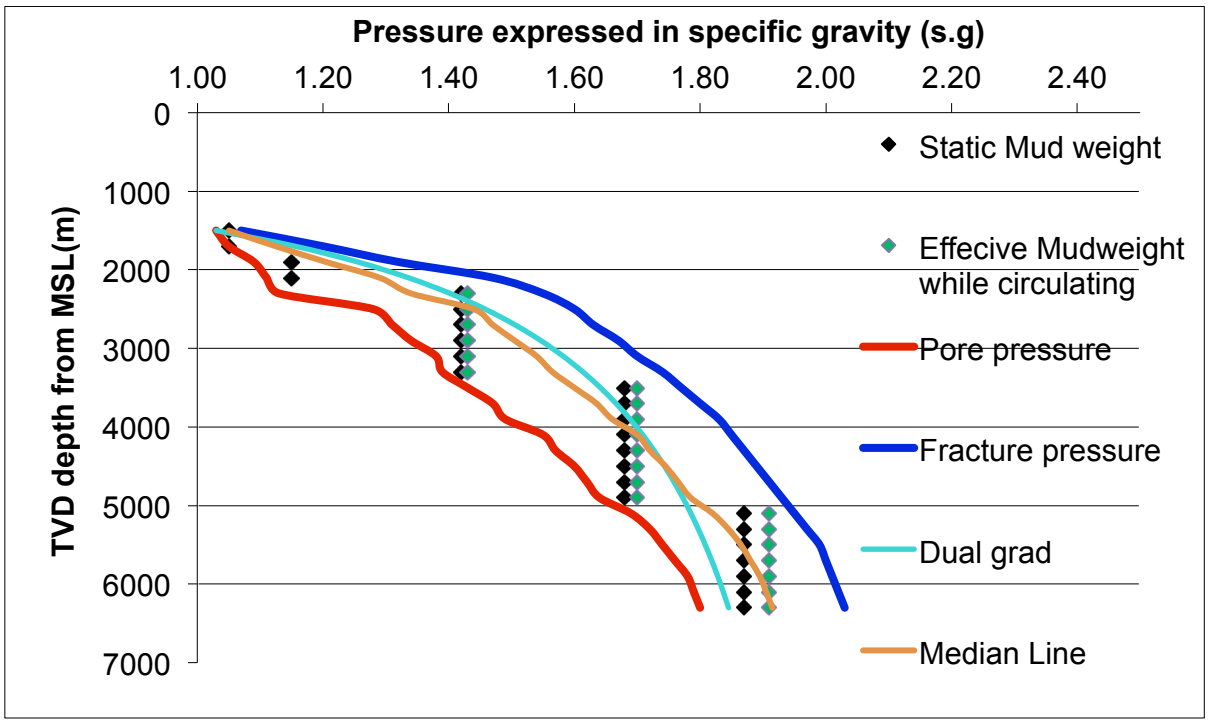

Figure 5: DG pressure profile vs. conventional, mud weight 2.1 sg

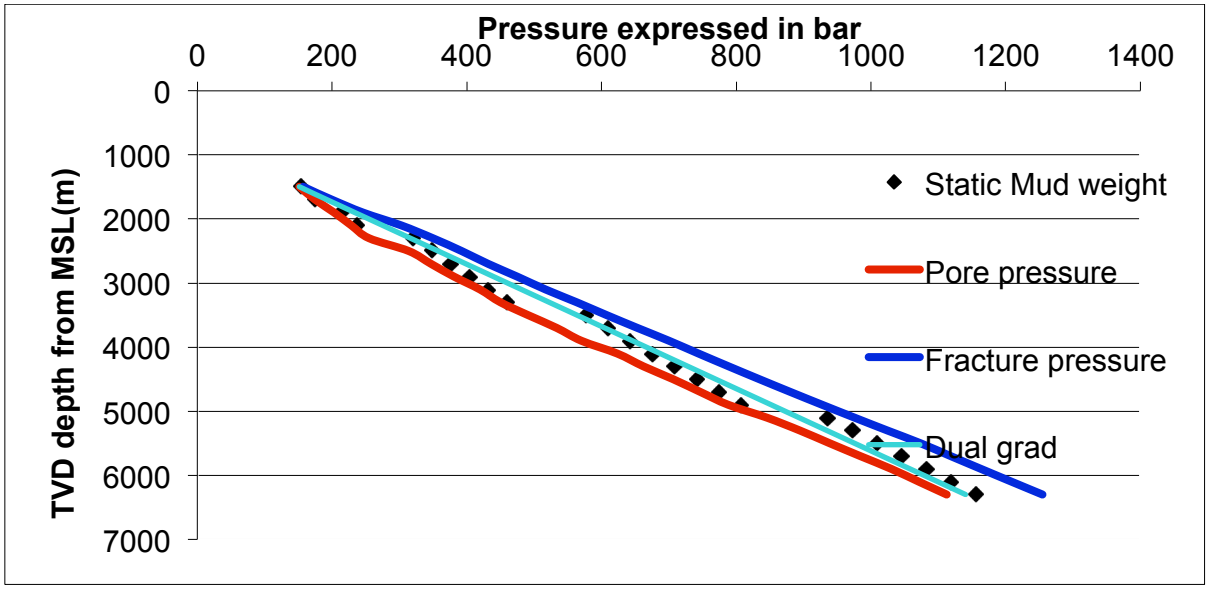

Figure 6: DG pressure profile vs. conventional, mud weight 2.1 sg

From the figures above it is clear that 2.1 sg suits better for the defined operational window. It is aligned with the median line principle quite well.

In the example above, Psw remains constant, which means pressure at the wellhead is always the same and equal to hydrostatic pressure of seawater column. It is the case for RMR, where the riser is not present, and it is the case for SMD where riser is in place but at the same time it is filled with seawater and Subsea Mudlift Pump (SMP) is responsible for creating the seawater pressure below the RCD. When it comes to CML, the dual gradient environment is now represented with air and mud, instead of mud and seawater as in the cases before (Fossli and Stave et al., 2014). A controlled mud level in the riser can either be increased or lowered. This directly affects BHP's hydrostatic component. Coupling this with the fact that the possibility to change mud weight is still present, the operation obtains even more flexibility in BHP control. An example below describes this case.

The well data is the same as before with the difference that instead of hydrostatic pressure of seawater, the riser is partially filled with mud. Instead of Psw we have $Priser$, which is equal to:

$$Priser = (WD - Hriser) * 0.0981 * Dmud \tag{4}$$

Where $Hriser$ is the mud level inside the riser relative to MSL. MSL is used as a reference in calculations to be persistent with other data. Note that to find actual riser level corresponding to Rotary Kelly Bushing (RKB), additional 25 meters must be added to this value. Typically, the air gap between RKB and MSL is about 25 meters. Now the task is to select the appropriate combination of these parameters. For 6300 m and 6100 m, optimal mud weights are 1.915 and 1.905 respectively. Setting the equation for general case:

$$\sigma_a = \frac{BHP}{0.0981 * MLS} \tag{5}$$
$$= \frac{(WD - Hriser) * 0{,}0981 * Dmud + (MLS - WD) * 0.0981 * Dmud}{0.0981 * MLS}$$

By using the provided information, optimal mud level in the riser was found to be at approximately 900 m and mud weight was equal to 2.2 sg. Following is the graph representing this case:

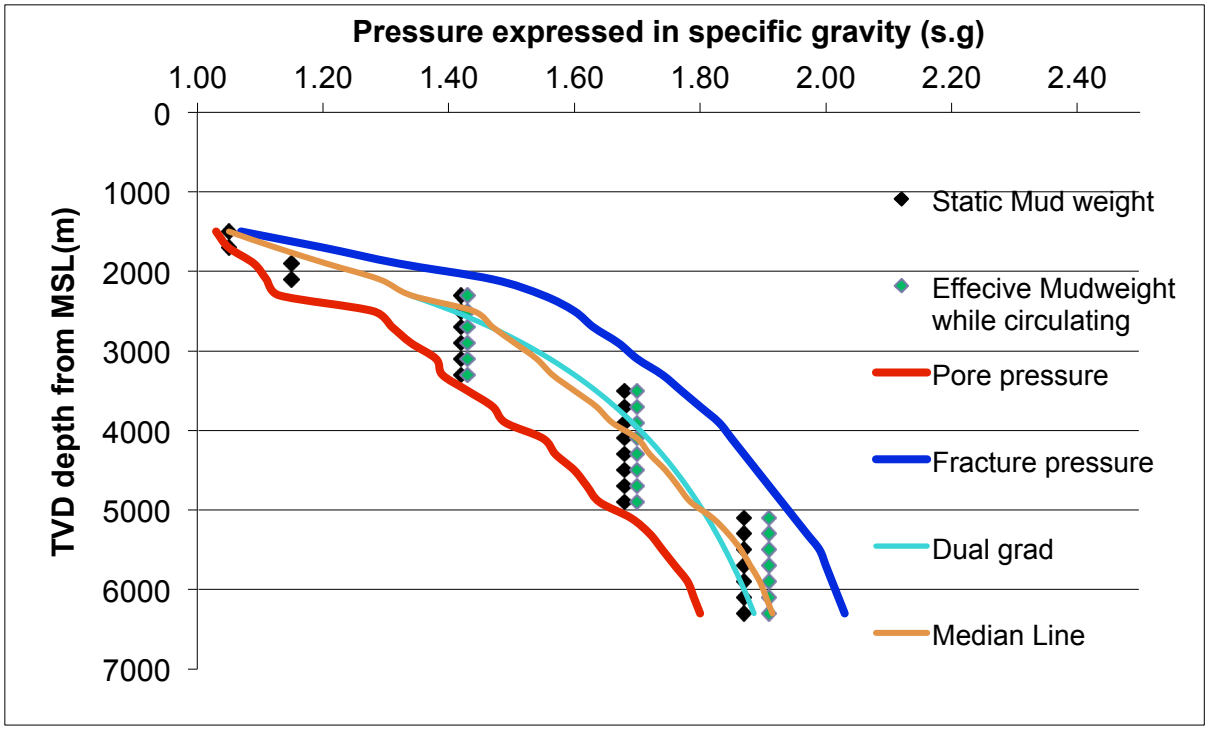

Figure 7: CML pressure gradient curves, riser level at 900m and mud weight 2.2 sg

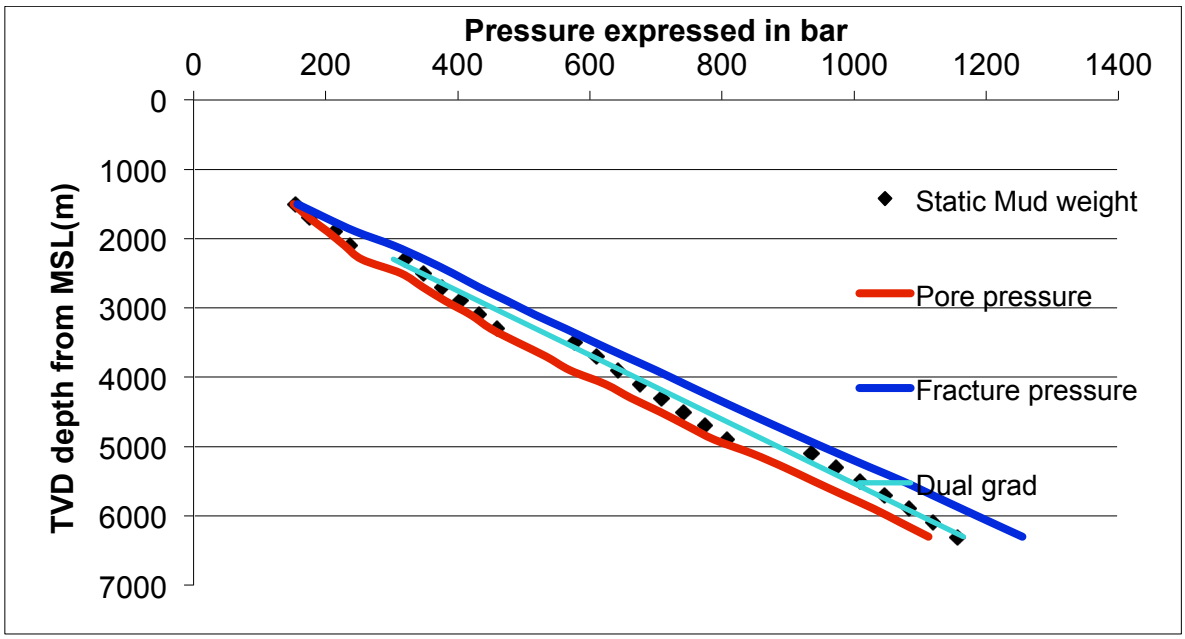

Figure 8: CML pressure gradient curves, riser level at 900m and mud weight 2.2 sg

With 1500 meters water depth, 925 meters air gap in the riser might appear to be big. The pressure outside the riser will be equal to 91 bars. The availability of this set up will then also depend on steel characteristics. From the examples in the literature, the Troll field can be mentioned here (B.Fossli and R.Stave et al., 2014). With a water

depth of 300 meters, the planned air gap in the riser was set to 200 meters, meaning that 2/3 of the riser was planned to be evacuated.

Compared with RMR and SMD, CML is aligned even better for this case with the median-line principle. The system provides a great degree of flexibility, which allows very accurate BHP control.

An important fact that can be observed from examples here is that originally, with conventional operation, five casing strings were planned. In both cases, using RMR/SMD or CML, fewer casing strings need to be installed for a single well, which results in time and cost savings. It is even possible in theory, with absence of problematic zones like, for example, unconsolidated clay formations, to drill the whole well to total depth without setting even one casing string. If aligned properly with the median-line principle, which is clearly the case here, hole stability should not be an issue. Having fewer casing strings on the other hand provides a much larger bore. Production is then increased at early stages of the project, which is important from an economical point of view. This means that projects that could not be carried out before now are economically possible.

2.3.2 SMD

As mentioned before, SMD was a first attempt towards DG technology. It began as a Joint Industry Project in 1996. The technology was developed and successfully tested, however, it still remains novel and it has not been applied much. The tests were completed in 2001 (Smith et al., 2001, Schumacher et al., 2001, Eggemeyer et al., 2001). In late 2006, Chevron raised the interest for SMD again (Dowell, 2010). Several studies were conducted on how to commercialize the technology in the best possible way. First, concept alternatives and feasibility analysis covered several possible configurations of the system (Smith et al., 2013). The main options were either to use a single riser with SMP integrated or located separately, dual risers with one marine riser and one auxiliary riser connected to the pump, or a configuration including marine riser, air buy and flexible riser joints. After careful examining the option with integrated single riser was selected (Smith et al., 2013). It was concluded to be the cheapest option that requires least rig modification and few new operational procedures compared to other alternatives. The technology was deployed in 2015, it was tested on a deep-water well operated by Chevron and located in Golf of Mexico

(GOM) (Rahman et al., 2015). The system was used with same type of equipment, but this time it was engaged as a single gradient SMD. Both the riser and the rest of the well were filled with mud of a constant weight, while the system configuration remained the same as for dual gradient SMD. In both cases, the main controlling element of the system is a mudlift pump, which allows controlling the pressure below the mud-line. More detailed description of SMD is provided below (Rahman et al., 2015). The schematic below shows the main principle of the system:

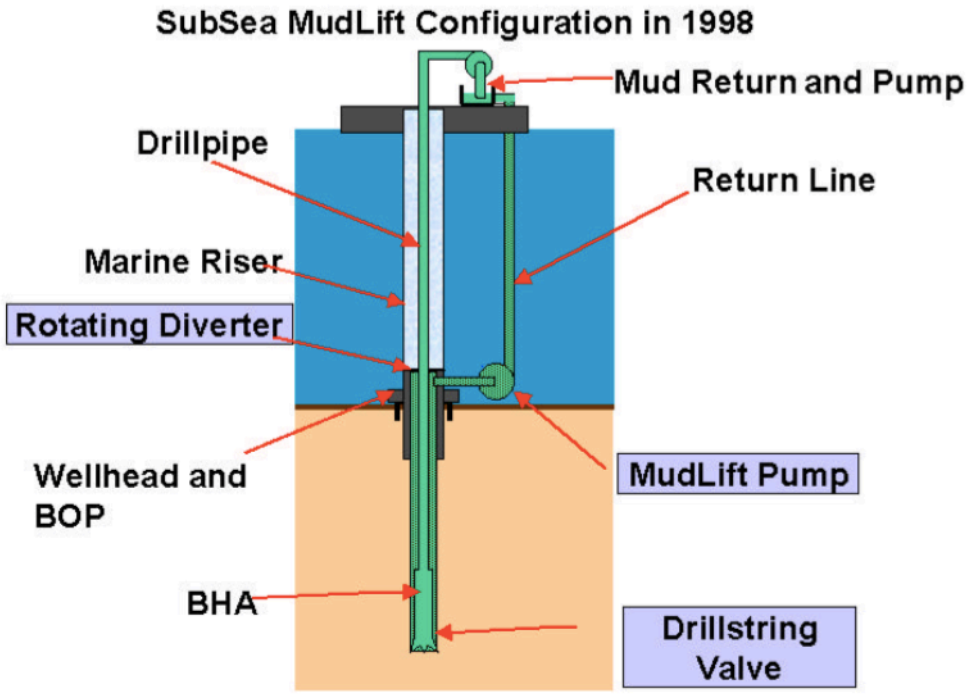

Figure 9: SMD system (Smith et al., 2001)

Equipment used in SMD (Smith et al., 2001):

- Subsea Mudlift Pump (SMP)
- Rotating diverter
- Return line
- Drill string safety valve (DSV)

The drilling mud circulates from the main pump down to the bit and then up through the annulus to the wellhead. The rotating diverter, which is similar in configuration with RCD, directs the flow to SMP and seals the wellhead from the riser filled with seawater, providing interface between two gradients. SMP then pumps the mud back

through the return line to the rig. Return line is a flexible rubber hose that connects SMP with the rig (Rehm et al., 2008).

SMP is the major component of the system and it is present in all of the available DG technologies. The pump uses a special impeller composed of discs with minimal profile. Friction between high speed spinning discs and fluid creates pumping power and lifts the fluid up. The pump can tolerate solids up to 3 inch in diameter (Rehm et al., 2008). It is the pump that defines the pressure below the RCD creating the DG effect.

Another important component is the DSV located inside the drill string, which prevents mud from U-tubing. U-tube effect is a natural consequence created by the difference in pressures between the drill string and annulus (Rehm et al., 2008). It occurs in a static condition when pumps are off. DSV is then designed in such a way that it allows flow to pass while circulation is on and holds back the mud column in the drill string when circulation is off (Rehm et al., 2008).

Several works discuss well control procedures for SMD (Schubert et al., 2006, Choe et al., 2007). Without DSV, it is important to keep kill mud circulation rate higher than mud free fall rate related to U-tube effect, although in some cases it can result in too high annular friction. Having DSV installed, additional pressure drop over the valve must be taken into account in kill calculations (Schubert et al., 2006). Kick detection becomes an issue with no DSV installed. When there is an influx in the annulus, and SMP is set on constant inlet pressure mode, pump speed will increase. U-tube free fall can give exactly the same indicator (Schubert et al., 2006). However, it is still possible to distinguish between those two, which is described by Choe et al. (2004) (Choe et al., 2007). Shut-in also becomes an issue with no DSV in place, as mud during U-tubing can fracture formation and additional influx can be taken. One solution for this is to follow procedures described by Schubert et al. (2006). These procedures outline how to circulate the kick without shutting in the well. In general, conducted studies highlight importance of DSV in dual gradient drilling operations.

Deployments of SMD so far have proven its relevance for nowadays industry and benefits of dual gradient drilling discussed before. The results from 2001 JIP were considered to be successful. In the case of a single gradient deployment, Chevron was pleased by the results. The future plan is to apply it more frequently in GOM deep-

water drilling. The main focus is to switch to fully dual gradient application (Rahman et al., 2015).

2.3.3 RMR

In deep-water offshore environment there are several problems associated with marine risers. First of all, when water depth is relatively high, there are many riser joints required. This creates additional load capabilities for the rig. Requirements for rig and deck space are then higher, and sometimes it is the only limiting factor for performing specific operation. This means that bigger and more expensive rig must be assigned for the job, which could be performed with smaller rig that cost less. Another additional cost is the volume of mud required to fill the riser. With such a long riser total cost for required volume can go up to 400000 USD (Rehm et al., 2008).

Considering challenges with marine risers in deep-water drilling described above, RMR becomes very attractive since this technology allows riserless operations to be performed. RMR is in fact the first ever DG system to be deployed commercially. BP in the Caspian Sea ran the prototype in late 2003 (Alford et al., 2005). Unlike SMD, RMR has found its application in many top-hole drilling operations around the globe. Regions like North Sea, Caspian Sea, Russia and Barents Sea, GOM, Malaysia, Egypt and Australia can be mentioned here (Smith et al., 2010). It developed originally from the Cuttings Transport System (CTS) (Stave, 2015), which has been widely used in the Norwegian Continental Shelf (NCS) before (Stave et al., 2014). The main purpose with CTS is to avoid cuttings accumulation around the wellbore during top-hole drilling. The CTS system utilizes the same subsea pump in combination with Suction Module (SMO) to dump the cuttings away from the well location (Stave, 2015). This is yet another benefit that RMR has, adopted from CTS, top-hole drilling with full returns. A Join Industry Project named DEMO 2000 in cooperation with PETRONAS was created by AGR subsea, BP America, Shell and Norwegian Research Council in 2003-2004. At first, RMR was limited to 549 meters water depth. Later, deep-water application of the system was successfully achieved in 2008 with a water depth of 1419 meters (Smith et al., 2010). A complete list of equipment used in RMR is presented below (Stave, 2015):

1. Suction Module (SMO)
2. Subsea Mudlift Pump (SMP)
3. Umbilical and Umbilical winch
4. Office and Tool container
5. Power and Control container
6. Return Line

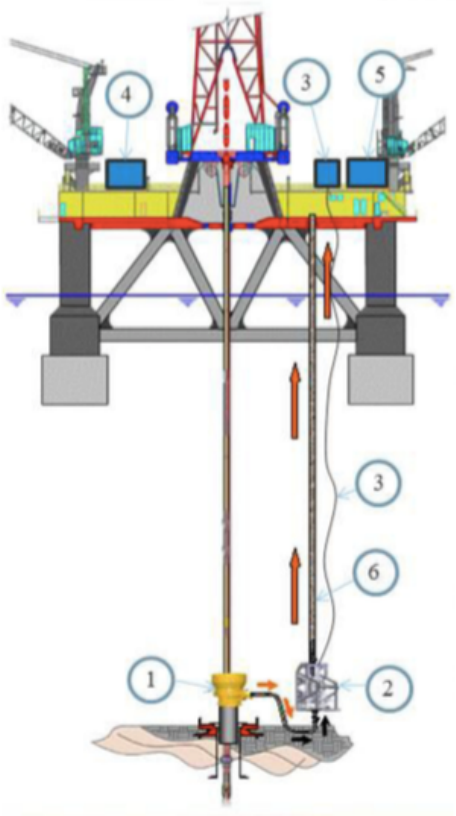

Figure 10: RMR system (Stave, 2015)

The deployment procedures and detailed description of equipment is well presented by Smith et al. (2010). The top-hole equipment, which consists of office and tool container together with power and control container, provides power and controls the system through the umbilical. SMO is attached to the wellhead and serves as an interface between two gradients (Rehm et al., 2008). It is monitored with video cameras and has remotely operated underwater vehicle (ROV) friendly connection points. Below is the picture of RMR work desk with active SMO monitoring (Smith et al., 2010):

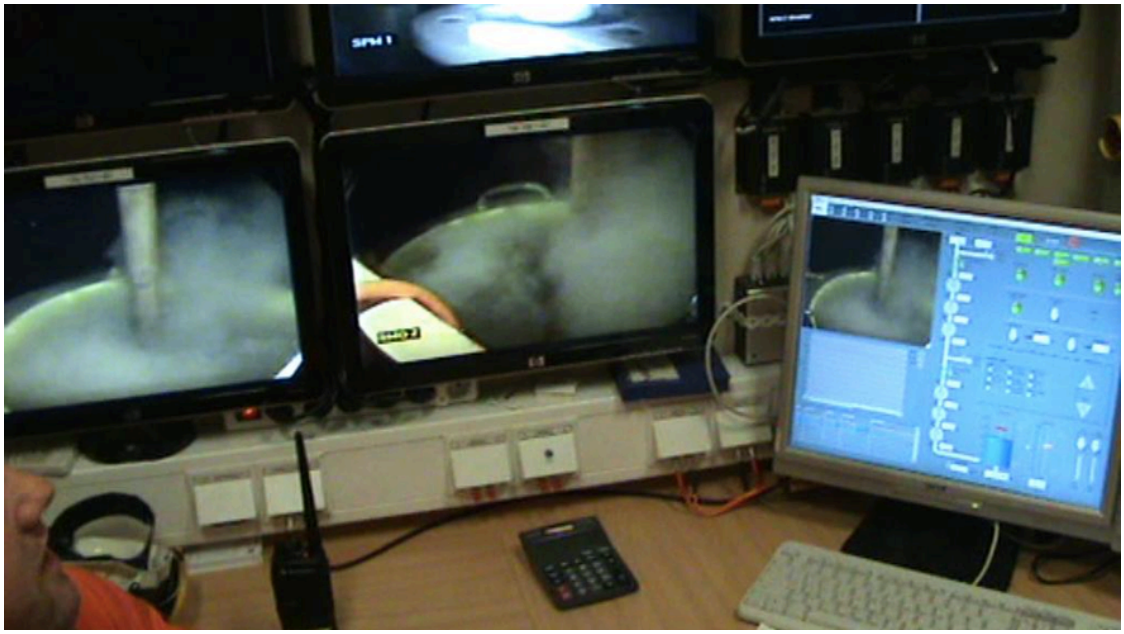

Figure 11: RMR work desk (Smith et al., 2010)

Its main purpose is to suck the return flow with cuttings and direct it to SMP. The SMP is set in automatic mode. There is a pressure transducer located on SMO that measures the suction pressure (Rehm et al., 2008). When the operation starts, the interface between seawater and mud is recorded with cameras as it is shown on the picture. The corresponding suction pressure is then set as a set point. Any changes in suction pressure are then compensated by SMP to keep the interface constant (Rehm et al., 2008). The cameras then can also be used to avoid any spills. This set up is beneficial for kick detection. If SMP pump speed is increased rapidly, such conclusion can be made that influx is taken by the system. When the pump speed reaches the predetermined value, the alarm goes off to notify the crew. The decisions to increase the mud weight can then be discussed to stop further kick occurrence (Rehm et al., 2008). These are the basic principles used in RMR operation. It is reasonable to mention that since there is no riser in place, the system is sensitive to excessive heave movements. The drill string can clash with the pump or tangle with return line. This is one of the few disadvantages of RMR (Rehm et al., 2008).

3 CML Literature Survey

3.1 About the Survey

This chapter presents a literature survey conducted on CML. The main database used for conducting it was www.onepetro.org. The search phrases include: "managed pressure drilling", "controlled mud cap", "dual gradient drilling", "evacuated riser", "low riser return system", "EC-drill", "LRRS". These search criteria were used to find any material related to CML or to the main principle behind this technology, drilling with partially evacuated riser. Results were then filtered by review of titles, abstracts and conclusions of the publications. In total, 10 SPE and 7 OTC publications satisfied the search criteria, refer to the Table 2:

Table 2: CML literature survey

SPE Publications			**OTC Puplications**		
Year	Authors	Paper	Year	Authors	Journal
2015	Udegbunam et al	SPE 168960	2015	Cohen et al	OTC 173822
2015	Godhavn et al	SPE 173814	2015	Hauge et al	OTC 26056
2014	Fossli B. & Stave R.	SPE 169178	2014	Malt R. & Stave R.	OTC 25455
2013	Ziegler et al	SPE 164561	2014	Stave R.	OTC 25222
2013	Ziegler et al	SPE 166272	2014	Halkyard et al	OTC 25044
2012	Mir Rajabi et al	SPE 151100	2014	Godhavn et al	OTC 25292
2012	Rajabi et al	SPE 156889	2013	Ganpatye et al	OTC 24081
2011	Falk et al	SPE 143095			
2009	Breyholtz Ø. & Nygaard G.	SPE 124631			
2006	Fossli B. & Sangesland S.	SPE 91633			

The purpose of the survey was to provide the current update on the technology including the historical development. Further, information about how is it used commercially and what kind of procedures exists, including well control procedures, is also provided. Since the main principles behind CML were discussed earlier, this

survey will review the application of those principles and the field experience. Based on these experiences, advantages and disadvantages together with future possibilities will be discussed.

EC-drill stands for the first commercially applied CML technology. The same company that released RMR and CTS projects, Enhanced Drilling, provides EC-drill to the market. This survey reviewed 11 papers, which describe EC-Drill general principles and field experience.

3.2 History of CML

The first application of a similar concept to CML took place on Gullfaks A and C fixed platforms, and ever since 1986, the concept was used for top-hole drilling of more than 80 wells. The static mud level on the return line inside the riser was kept lower by means of pumping speed to be able to lower BHP when necessary (Fossli et al., 2004).

The next step in the development of CML took place in Norwegian University of Science and Technology (NTNU) in 2004 (Fossli et al., 2004). The system developed by NTNU had partially evacuated the riser with split BOP. A small-scale model was built to test the system. BHP was used as a set point while riser mud level was adjusted accordingly to keep it constant. A continuation of this study was presented in 2011 (Falk et al., 2011).

Further development of CML, first field trial, commercial applications, development of the equipment and control systems are broadly described by Stave R. (2015). EC-Drill became a leading technology for the CML concept. The first steps were a simple upgrade of RMR system to be able to drill with evacuated riser (Stave, 2015). BP in Azerbaijan and Egypt used this system upgrade in 2008, and then Petrobras used the same set-up in Brazil (Stave, 2015). Those were top-hole drilling applications. The successful experience led to the first independent EC-Drill prototype development. This project started in 2011 with the installation of the system on Scarabeo-9 MODU, 6th generation semi-submersible rig (Mirrajabi et al., 2012, Ziegler et al., 2013). The installation process took two months, the first EC-Drill operation started on May 2012 (Ziegler et al., 2013). After a successful first field trial, it was then used on three wells in The Caribbean (Malt and Stave et al., 2014). In these cases EC-Drill covered full operational range until TD. In March 2014 Statoil adopted EC-Drill for the Troll field

multilateral drilling. The successful operation led into several studies focused on well control procedures (Cohen et al., 2015, hauge et al., 2015).

3.3 CML non-commercial studies

There are several studies conducted on CML. As mentioned before a small-scale model was built in NTNU to test different systems (Fossli et al., 2004). The figure below shows the model's configuration:

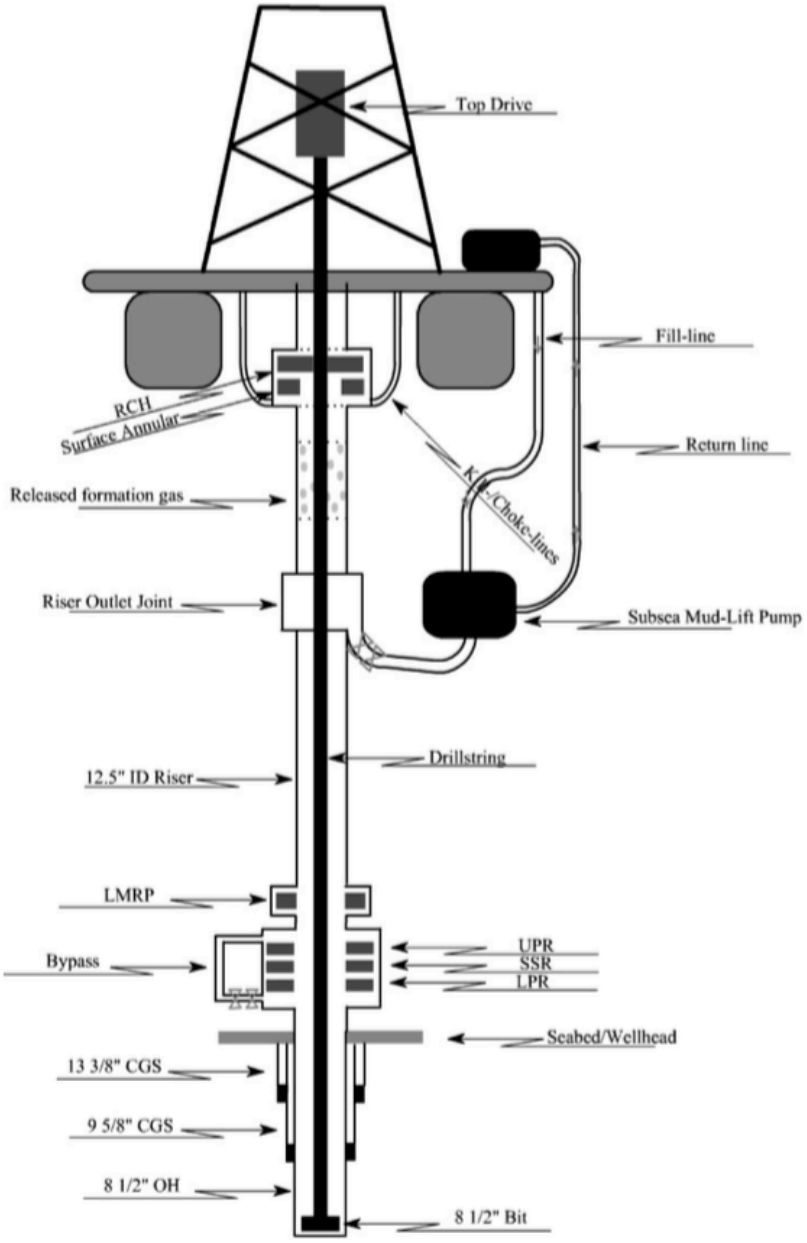

Figure 12: NTNU small-scale model (Fossli et al., 2004)

BOP is divided in this case into surface components and subsea components. The surface components include annular BOP and rotating control head (RCH), subsea

components are upper pipe ram, shear seal ram and lower pipe ram. There is a bypass line under the lower pipe ram for well control purposes, which also carries a subsea choke. If the kick is taken by the system, subsea BOP shuts in the annulus, while the bypass line provides a way to increase BHP by means of increasing riser mud level (Fossli et al., 2004). The modified riser joint (MRJ) is equipped with high-pressure isolation valves to be able to switch between conventional and CML. Several pressure sensors are located close to the pump to precisely control riser level. The fill line is used to pump additional fluid to change riser level during connections (Fossli et al., 2004). First, the ability of CML to keep constant BHP by active riser mud level adjustments was tested. By providing real-time down-hole pressure data the ability of the system to deal with stated challenge has been proven. The system uses a multiphase hydraulic model to calculate BHP at any depth and with reliable real-time pressure data no difficulties shall occur (Fossli et al., 2004). Further, well control methods for conventional drilling, MPD and CML were studied and compared. A specific well has been used as an example for calculations. CML addresses several challenges with the conventional MPD. Main advantages (Fossli et al., 2004):

- CML is an open system, which positively affects BHP sensitivity to rig heaves, a common MPD problem.
- Sluggish choke response during kick circulation with conventional MPD can be avoided.
- Riser margin is a big advantage over conventional MPD. In MPD lighter fluid is used, hence in situation with drift off, fluid circulation is lost and static hydrostatic pressure is not sufficient to keep overbalanced conditions. With CML mud weight is always sufficiently higher.
- When kick is taken and surface annular is closed, the riser can act as a fluid gas separator and there is still possibility to increase BHP with SMP. In this situation there is very little or no pressure at all seen on the surface.
- I was shown by the experiments that higher circulation rates that are possible due to the reduced hydrostatic pressure gradient increase kick margins.
- Trip margins can be easily introduced over a short period by increasing the mud level and hence the pressures.
- CML positively contributes to hydrates formation control due to lower pressure at the wellhead with partially evacuated riser.

The U-tube effect was concluded to be a main difficulty with CML in this study, together with unavailability of commercial technology at that time (Fossli et al., 2004).

A further update on CML came in 2011, it was a study published by the same coalition of Ocean Riser Systems and NTNU (Falk et al., 2011). This study focuses on well control issues of CML. It differentiates between two systems, in the first one the riser is full initially and SMP drops the mud level when circulation is started (Falk et al., 2011). The second system is of our main interest because the riser is partially evacuated from the start. The well control procedures for the first system are the same as for a conventional drilling operation (Falk et al., 2011).

For the second system, if there is a sign of influx intake, the main principle is to stop the pump to allow the riser level build-up, which in return will provide a higher BHP. The simulation of a well control incident was performed (Falk et al., 2011). The increase in pump speed gave indication of the influx, since the pump was running on constant riser level mode. As long as influx was identified, the pump was shut off and riser level began to rise. It took less than one minute to stop the influx and about 3 minutes to identify it (Falk et al., 2011). Some of the basic well control principles are discussed below (Falk et al., 2011):

- To be able to shut-in and avoid fracturing due to the u-tube effect, the mud level has to be u-tubed before the shut-in or DSV has to be installed.
- The choke line includes a bypass line, connecting riser with the annulus below BOP. This is similar to the already described small-scale model (Fossli et al., 2004).
- The bypass line provides possibility to regulate BHP after shutting in the well.
- The main well control method is Constant Drill Pipe Pressure (CDPP). The kick is circulated while the pressure in the pipe is kept constant by adjusting the subsea choke.
- The alternative circulation method is to keep the well opened, and regulate the pressure with mud level in the riser.

The study highlights the same benefits as before, availability of riser margin and improved kick margins. The case examples are used to demonstrate this (Falk et al., 2011). The well barriers for CML are discussed as well. There are two cases to

distinguish, moderate water depth (<4500 ft) and deep waters (below 5000 ft). For deep waters according to this study, barriers will remain the same as for the conventional drilling case (Falk et al., 2011). For the moderate water depths however, some of the common barrier elements are eliminated. The integrity of the BOP for example will not affect the primary barrier envelope. This applies only if the formation is sufficiently strong enough for the given mud-weight and the pressure at the seabed inside the riser is less than the pressure of the seawater column to that depth (Falk et al., 2011).

Another interesting aspect is the problem related to cementing. A narrow operational window can result in undesired low-density cement slurry or lower circulation rates to avoid formation damage and loss circulation. The first will affect the cement quality after settling, possibly lead to micro-annulus between casing and cement and weaken zonal isolation, while the latter can create problems during displacement and result in channeling (Falk et al., 2011). The paper provides examples of how CML can be used for BHP control during cementing operations. A similar approach of reducing the riser level is used to be able to compensate for high BHP and keep cement density together with the circulation rate at the desired level (Falk et al., 2011).

3.4 EC-Drill

EC-Drill is a commercially developed technology that has had several field applications already (Malt and Stave et al., 2014, Mirrajabi et al., 2012, Rajabi et al., 2012, Cohen et al., 2015) and is on its way to become more recognizable. EC-Drill can perform all operations after the riser has been run (Fossli and Stave et al., 2014). This includes drilling, completion, intervention and work-overs. To be able to use this technology on NCS, a minimum water depth of 300 m is required. This estimate is based on available ECD compensation. Since frictional component of ECD typically varies between 20 to 50 bars for reservoir sections on NCS (Fossli and Stave et al., 2014), a minimum water depth that will give required pressure reduction is around 300 m ($300m * 1.03 * 0.0981 = 30\ bars$). EC-Drill can be used on any rig with few modifications required (Mirrajabi et al., 2012). Below, a figure with typical system configurations and components is presented:

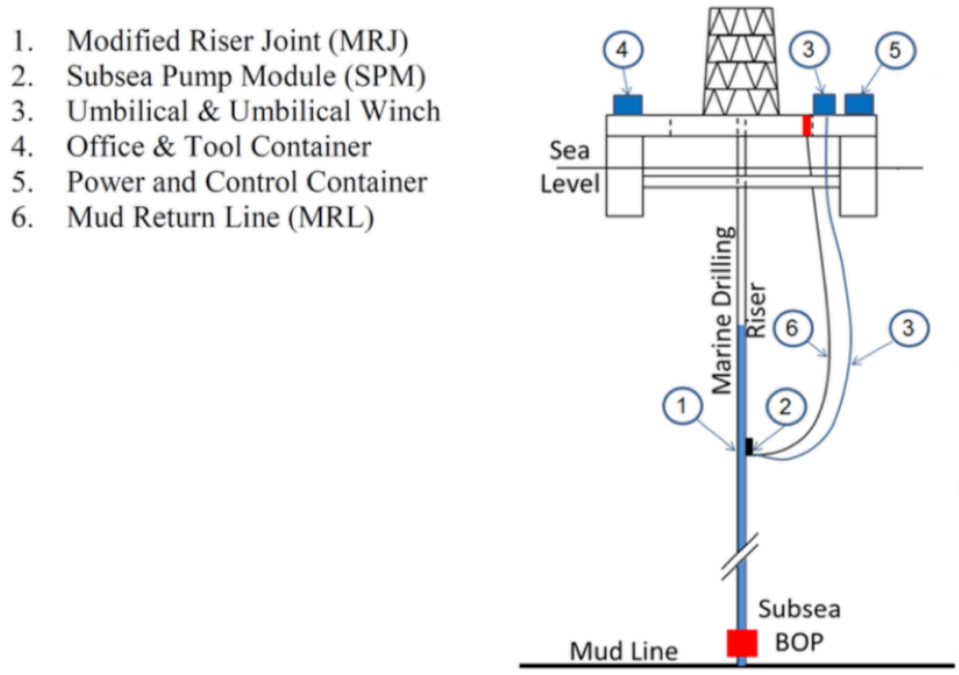

Figure 13: EC-Drill configuration (Stave, 2015)

The key components in EC-Drill are Modified Riser Joint (MRJ) and Subsea Mudlift Pump (SMP), referred to as Subsea Pump Module on the figure above. MRJ is specifically designed to be able to accommodate SMP. It has 6'' outlet to connect the pump to the annulus. Two remotely controlled valves of a fail-safe type are installed on MRJ with the purpose of sealing EC-Drill off and turning back to conventional operation in case of emergency (Mirrajabi et al., 2012). There are several pressure sensors installed on MRJ. The Riser Pressure Sensor is usually located inside, close to the suction outlet. It can precisely measure hydrostatic pressure above its location taking atmospheric pressure into account. There can be several sensors of this type to increase precision. Another sensor is called Suction Pressure Sensor and it is located in-between the isolation valves and the pump's suction connection. With the help of these sensors the pressure at any point in the well can be calculated by a built-in EC-Drill hydraulic model (Mirrajabi et al., 2012). Later, the calculated value is compared to the Pressure While Drilling (PWD) measurements to obtain the best possible estimate (Fossli and Stave et al., 2014). MRJ also has a docking platform, which supports the weight of SMP. SMP used in the system has same characteristics as the one used for RMR (Mirrajabi et al., 2012). The pump is integrated together with electrical motors and hydraulic equipment on the same frame. It can handle multiphase fluid with drilling cuttings up to 2.5'' and 10% gas volume. It can be

installed down to 1500 m deep. The pump is a three-stage pump, which can also be increased to four stages if needed. In case more pumping capacity is required, another SMP can be run in series (Ziegler et al., 2013). Mud Return Line (MRL) is composed out of number of joints each one being approximately 50 m long. One joint is a 6'' inner diameter flexible hose that is also adapted from RMR technology (Mirrajabi et al., 2012). The Office and Tool container is a place where the operator has an interface with the system and controls all the key parameters of EC-Drill. Another place on the rig with the same EC-Drill interface is the driller's cabin (Stave, 2015). Typical data monitored during operation is electrical power used by the pump, riser pressure, mud level in the riser, suction pressure, rig pump rate, return flow and position of the isolation valves (Mirrajabi et al., 2012). The Control Container is equipped with necessary electronics to control the SMP. The adjustments made by operator are then transferred via control container down to the pump through the umbilical, which includes hydraulic connections as well (Mirrajabi et al., 2012). The control system for EC-Drill provides several options (Fossli and Stave et al., 2014):

- Pump speed is controlled manually, based on readings of PWD and calculated pressure from the hydraulic model.
- The pump is set on the semi-automatic mode to keep the riser level at the same height.
- The pump is set on fully automatic mode where riser mud level is controlled accordingly to keep the desired BHP constant.

The most common according to this literature review is the semi-automatic mode. The increased pump speed can be an influx detector in this case (Mirrajabi et al., 2012). The control system is designed in agreement with industry standards: ISO 13628-6 and ISO 13628-6 (Stave, 2015). For semi-automated and fully automated modes PID controllers are used (Ziegler et al., 2013).

Another important component of the system is top fill pump. It is used when the riser mud level needs to be increased in short amount of time, like for example during connections (Ziegler et al., 2013). Another major function it has is that of keeping evacuated part of the riser gas-free. At an early stage of EC-Drill development gas accumulation in the top part of the riser and hazard of the gas entering the drill floor was identified as an issue (Fossli and Stave et al., 2014, Cohen et al., 2015, Hauge et

al., 2015). Several possibilities were considered, and in the end filling the riser from above was selected as the most effective solution. The mud runs down through a specifically designed mud funnel developed by Statoil (Fossli and Stave et al., 2014). The mud funnel is a circular flat nozzle, which creates a so-called "Mud wall" barrier to keep the gas inside. The barrier relies on the fact that downward fluid velocity is then greater than the slip velocity of gas inside the mud. In this case the gas will be pushed down and exit the riser through the return line. Additionally, closed diverter element is used as a secondary barrier (Fossli and Stave et al., 2014).

Enhanced Drilling built a dynamic training simulator in cooperation with Statoil (Fossli and Stave et al., 2014). It also offers training programs for operators to get familiar with the system before use. Based on formation data for a specific well, different case scenarios can be performed.

3.4.1 Advantages and Disadvantages

In addition to the already mentioned advantages and disadvantages of CML, the ones related to commercial technology in specific are described here.

- As mentioned before, U-tubing is the most challenging phenomenon in CML. EC-Drill introduces fingerprinting as the main solution to this problem (Fossli and Stave et al., 2014). Fingerprinting stands for comparing new data trend with old records to identify if there is any change in behavior. For example, change in the flow rate during new connection can be compared to the record of the old one. If there is a difference between flow rate records, an alarm goes off to notify the operator about possible gain or loss due to U-tubing (Fossli and Stave et al., 2014). It is obviously important to follow the same ramp schedule for the pump in this case.
- EC-Drill will become even more valuable in the future, as reservoir pore pressures in already producing fields will decrease (Fossli and Stave et al., 2014). Since pore pressure is decreasing, it is more difficult to compensate for the frictional effects by decreasing mud weight. Loss circulation is then becoming a major problem. Alternative solution has to be found for depleted reservoirs. EC-Drill provides such a solution.

- The fact that few modifications to the rig required to be able to install the system is a big advantage with EC-Drill. This makes it possible to use EC-Drill for any operation. (Ziegler et al., 2013).
- EC-Drill simplifies well testing procedures. To perform an inflow test on cement or bridge plug, operator can simply reduce the mud level in the riser (Malt and Stave et al., 2014).
- In conventional operation, minimal cuttings transport velocity is a key flow-regulating factor. Minimal cuttings transport velocity stands for minimal required velocity for proper cuttings transport. However, very high flow velocities can build ECD that formation will not be able to withstand. EC-Drill makes circulation with relatively high flow possible by adjusting the mud level in the riser (Rajabi et al., 2012).
- Due to the reduction of pressure related incidents and hence reduction of the non-productive time (NPT), EC-Drill reduces general costs of different operations (Rajabi et al., 2012).
- BHP control during connections is an important advantage of EC-Drill. Pump ramping down was identified to be vital for keeping BHP constant, as it takes time to fill the riser with the fill pump (Godhavn et al., 2015). In general, it was concluded that EC-Drill does not slow down connection time in any way.
- Kicks with low flow rate are difficult to identify with EC-Drill (Godhavn et al., 2015). During system deployment in GOM, an influx was undetected with EC-Drill parameters, only active volume showed an increase of 7 bbls in about 15 minutes. It was due to influx flow rate was low. These kicks are hard to detect with MPD (Godhavn et al., 2015). Well was shut in and EC-Drill was isolated, kick was circulated conventionally.

3.4.2 EC-Drill extensions

There are two extensions of EC-Drill presented by Statoil (Godhavn et al., 2014, Godhavn et al., 2015). The first one is called ECD-Management. Statoil differentiates between two CML versions, CML-O and CML-U. “O” stands for overbalanced and this is the same concept as been described before. In CML-O, in case of an emergency, for example when rig pumps are shut off, the well remains in overbalanced condition. This is opposite for CML-U. “U” stands for underbalanced, which means that overbalance is lost. ECD-Management describes CML-U and introduces several new

system modifications to be able to deal with the underbalanced condition (Godhavn et al., 2014).

An important addition to the system is Delta Seal Riser Module (DSRM). It is installed directly above the SMP, limited by maximum water depth of 400 m (Godhavn et al., 2015). DSRM is more compact than the normal BOP and delivers higher hydraulic power. It includes Quick Closing Annular (QCA) for trapping pressure below the SMP. The closing time for open hole is 5 seconds and for drill pipe is 2 seconds (Godhavn et al., 2015). The bypass line is present to be able to control BHP in a closed position. Additionally, DSRM has a second annular element called Riser Drilling Device (RDD). It provides an annular seal during connections and stripping. DSRM has a separate control system from EC-Drill (Godhavn et al., 2015).

By providing a seal during connections, DSRM helps to avoid U-tubing and eliminates the need of filling the riser from above (Godhavn et al., 2014). Additionally, a gas handler is installed in the riser together with a gas sensor. Hence, there is no need for the mud funnel anymore. There are new pressure compensated seals between motor and the pump for better system integrity (Godhavn et al., 2014). With DSRM, CML-U is similar to conventional backpressure MPD systems.

The second extension is ECD-Control, which has a normal RCD in the riser and SMP creating a loop from below RCD trough bypass line and above (Godhavn et al., 2014). In this case, DG effect is lost, therefore it will not be described in detail in this thesis.

It is also important to mention here that both extensions have conventional well control procedures (Godhavn et al., 2014).

3.4.3 Well Control with EC-Drill

3.4.3.1 Early kick detection

Kick detection with EC-Drill has been studied and tested in several publications (Godhavn et al., 2015, Cohen et al., 2015, Hauge et al., 2015). Different parameters used for this purpose are described here. As mentioned before, SMP can be run in different modes, constant pump speed or constant inlet pressure. Kick detection varies depending on which mode is used.

Examples demonstrate how riser pressure together with pump speed can be used as an early kick detector. If the pump runs in a constant speed mode, the increase in pressure inside the riser recorded by riser pressure sensor is a direct indicator of an influx. It was concluded that kick is detected earlier than with conventional volume measurements (Godhavn et al., 2015). This was tested both during normal circulation and during connections where rig pumps are shut down and parameters change rapidly (Godhavn et al., 2015). Additionally, riser can be considered as a separate active pit and together with other active pits on the rig it forms a unified fluid system (Godhavn et al., 2015). Volume measurements with this system support kick detection in this case. Statoil claims that kick detection is improved with such an approach.

Another approach is to use pump speed or power consumed by SMP as a main kick detecting parameter (Cohen et al., 2015). If SMP is running in a constant inlet pressure mode, mud level in the riser is maintained constant at any time, hence, if influx is taken by the system, pump will speed up to compensate for the volume increase. That will also affect power consumption. The monitoring of these parameters gives early kick detection (Cohen et al., 2015, Hauge et al., 2015), which can also be supported by flow out of the well measurements (Cohen et al., 2015).

Different field tests showed that using the parameters and different modes of SMP, in all cases both with gas and liquid, system was able to detect an influx in less than one minute (Cohen et al., 2015). Liquid influxes as small as 80 liters per minute and gas influxes of 0.5 m^3 were easily detected with EC-Drill (Hauge et al., 2015).

3.4.3.2 Well control procedures

Well control has been an important aspect for EC-Drill as it diverts from the conventional drilling. Originally configured well control procedures involved dynamic kill method to avoid U-tubing (Cohen et al., 2015). In this method, the riser level is raised first to stop the influx. The second step is to shut-in the well and to use the bypass line to circulate the influx without shutting off the rig pumps. The bypass line leads the influx out of the well through the return line and surface choke installed at the end is regulating the pressure differences (Cohen et al., 2015). After careful evaluation and risk assessment by members of the DEMO 2000 JIP's technical committee, this method was considered to be challenging and difficult from

regulatory point of view (Cohen et al., 2015). As an alternative solution use of DSV was proposed. SMP is then switched from constant pressure to constant pump speed mode. The rest of well control procedures are similar to Driller's method (Cohen et al., 2015). For further description refer to the figure below:

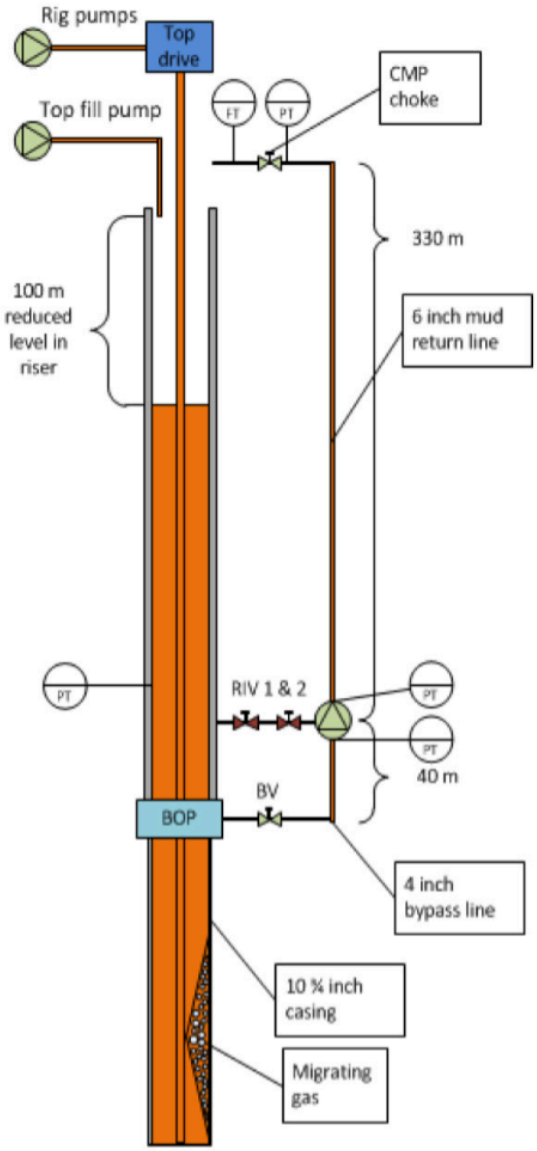

Figure 14: EC-Drill Well control (Hauge et al., 2015)

As an example the test set up from one of the Statoil's field trials is used here (Hauge et al., 2015). After the well is shut in, the bypass line is used to circulate the influx out through the MRL (Cohen et al., 2015). EC-Drill isolation valves marked RIV 1 and RIV 2 on the picture are closed (Hauge et al., 2015). SMP is set to constant speed mode. To control the pressures and compensate for gas expansion subsea or controlled mud pressure (CMP) choke is used (Hauge et al., 2015). The bypass line

can be fingerprinted after installation and SMP parameters can be adjusted accordingly to account for the pressure drop over the line in case of well control event (Cohen et al., 2015).

Well control procedures above are similar to non-commercial CML studies described earlier. Field trials were carried out to test the ability of EC-Drill to handle well control events (Hauge et al., 2015, Cohen et al., 2015). Several tests were performed, cement unit was used to simulate gas kick situation by pumping gas down the drill pipe. The driller's method with CDPP was used. The surface choke (CMP choke) was responsible to keep the standpipe pressure (SPP) constant. The operator tried to keep SPP at 8 bars during the whole circulation time (Hauge et al., 2015). Three tests were carried out with different kick sizes. It turned out that it is more difficult to keep SPP constant while circulating bigger amounts of gas. Apart from that, gas front has been concluded to be the most challenging part of circulation, while tail requires less choke manipulation. A sluggish response at the choke was also recorded in these cases (Hauge et al., 2015).

As mentioned in non-commercial studies, alternative well control method is to circulate the influx with an open BOP. This was tested as well which resulted in mud spill on the drill floor (Hauge et al., 2015). When circulating with an open BOP, 50% of the gas went through the pump and the rest went into evacuated part of the riser. This was the reason for the spill. The practice was concluded to be unsuccessful (Hauge et al., 2015). In general it was noticed that the amount of gas venting to the evacuated part of the riser is decreasing with increasing suction speed (Hauge et al., 2015). It is also important to mention here that during this test, mud funnel was not a part of the system yet.

4 AUSMV Scheme And Drift Flux Model

This describes the basics behind the AUSMV scheme and related formulations. AUSM stands for Advection Upstream Splitting Model and V stands for Velocity. It is a numerical scheme that is based on the Drift Flux Model (Udegbunam et al., 2015). The main advantages of this scheme are that formulation is relatively simple and the scheme is quite efficient and robust. As it was stated earlier, EC-Drill relies on precise and fast down-hole calculations. This scheme can be used for calculating pressures and predicting flow behavior for CML technology. However, the application of the scheme used in this thesis has first of all an academic relevance. To be able to apply the scheme for CML technology, more accurate sub-models must be implemented. The scheme will be adapted for a CML case scenario and tested with different simulations in the end of this thesis. The relevance of such a hydraulic model for the EC-Drill technology has been already mentioned in chapters two and three. To briefly describe the model, works by Fjelde et al. (2016) and Udegbunam et al. (2015) were used as the two main sources. For more detailed explanation one should consult the sources mentioned above.

The transient Drift Flux model is a one dimensional two-phase flow model that is based on mass and momentum conservation laws (Udegbunam et al., 2015). These are two mass conservation equations for each phase and one mixture momentum equation for both liquid and gas. The Drift Flux model is built on a more fundamental two-fluid model (Fjelde et al., 2016). The model considered here involves the following assumptions (Fjelde et al., 2016):

- No mass exchange between the two phases
- Isothermal flow
- No changes in the area along the flow

A more general description of the model can be found in the work by Udegbunam et al. (2015). Based on the assumptions above, the conservation laws take the following form (Fjelde et al., 2016):

$$\frac{\partial}{\partial t}(\alpha_l * \rho_l) + \frac{\partial}{\partial z}(\alpha_l * \rho_l * v_l) = 0 \tag{6}$$

$$\frac{\partial}{\partial t}(\alpha_g * \rho_g) + \frac{\partial}{\partial z}(\alpha_g * \rho_g * v_g) = 0 \quad (7)$$

$$\frac{\partial}{\partial t}(\alpha_l * \rho_l * v_l + \alpha_g * \rho_g * v_g) + \frac{\partial}{\partial z}(\alpha_l * \rho_l * {v_l}^2 + \alpha_g * \rho_g * {v_g}^2 + p) = -(F_w + \rho_{mix} * g * \cos(\emptyset)) \quad (8)$$

$$\rho_{mix} = \alpha_l * \rho_l + \alpha_g * \rho_g \quad (9)$$

Equation 6 and 7 are mass conservation equations and equation 8 is a mixed momentum equation. Index "l" stands for liquid and "g" stands for gas. The variables α, ρ, p and v are volume fraction, density, pressure and velocity respectively. The sum of the volume fractions is equal to 1. ρ_{mix} stands for mixture density of two phases and F_w represents the frictional forces. To include the inclination of the well, the hydrostatic parameter in equation 8 was multiplied by $\cos(\emptyset)$. For the first simulation this angle is equal to 0 as we consider a vertical well. In the case of the small-scale experimental loop the angle is close to horizontal and equal to 84 degrees. $\frac{\partial}{\partial t}$ represents the change in parameters through time, and $\frac{\partial}{\partial z}$ is the change along the depth. Here it should be noted that the area variable has been excluded in the conservation laws when presenting the model, but it is included in the codes found in appendixes.

4.1 Sub-models or closure laws

To make the model complete sub-models or closure laws have to be introduced. For example the gas slip model creates a coupling between phase velocity fields (Udegbunam et al., 2015). It makes it possible to use one mixed momentum equation instead of two, which simplifies the model mathematically. The gas slip relation has the following form:

$$v_g = K * v_{mix} + S = K * (\alpha_l * v_l + \alpha_g * v_g) + S \quad (10)$$

$$v_g * (1 - K * \alpha_g) = K * \alpha_l * v_l + S \quad (11)$$

$$v_g = \frac{K * \alpha_l * v_l + S}{(1 - K * \alpha_g)} \quad (12)$$

The variable K stands for distribution coefficient and S stands for drift velocity of gas relative to liquid, also known as gas rise velocity (Fjelde et al., 2016). These coefficients are usually flow-dependent and vary with different types of flow like slug,

bubble flow, etc. For the simulations conducted in this thesis fixed values are used for simplicity: K is equal to 1.2 and S is equal to 0.5. The slip coefficients are interpolated towards no-slip conditions (K=1, S=0) when approaching pure gas region. This is done to avoid singularity in the slip model, which occurs when $(1 - K * \alpha_g) = 0$ (Udegbunam et al., 2015). The coefficients for pure gas flow are then equal to K=1 and S=0. For the details and how it has been integrated in the code refer to Appendix A or Appendix B. The gas rise velocity in static conditions is also referred to as the rise velocity of gas bubbles (Fjelde et al., 2016). With this gas slip sub-model, gas always travels faster than liquid due to the mathematical construction of the model.

Density sub-models used for simulations have the following form (Fjelde et al., 2016):

$$\rho_l = \rho_{l,0} + \frac{(p - p_0)}{{a_l}^2} \tag{13}$$

$$\rho_g = \frac{p}{{a_g}^2} \tag{14}$$

Where a_l, a_g are the speed of sound in liquid and gas respectively, $\rho_{l,0}$ and p_0 is liquid density and pressure at standard conditions and p is pressure at the particular depth. The speed of sound in gas a_g has a standard value of 316 m/s and a_l is equal to 1500 m/s.

The friction sub-model has the following form (Udegbunam et al., 2015):

$$F_w = \frac{2 * f * \rho_{mix} * v_{mix} * abs(v_{mix})}{(d_o - d_i)} \tag{15}$$

Here d_o and d_i are the outer and the inner diameter respectively. To find the friction factor f, a Reynolds number has to be calculated first to determine the flow regime, whether it is laminar or turbulent. The formula for the Reynolds number is (Udegbunam et al., 2015):

$$Re = \frac{\rho_{mix} * abs(v_{mix}) * (d_o - d_i)}{\mu_{mix}} \tag{16}$$

Mixture viscosity μ_{mix} is found similarly to mixture density and mixture velocity. The friction will be crucial for the simulations of CML case scenario, as will be

pointed out later in the chapter dedicated to the simulation analysis. For the Reynolds number values greater than or equal to 3000 the flow is considered to be turbulent and a Blasius-type equation $f = 0.052 * (Re)^{-0.19}$ is used to find the friction factor. For the values lower than or equal to 2000 the flow is laminar and fanning friction factor is used: $f = \frac{24}{Re}$. For all the other values in between, interpolation between two friction factors is used.

4.2 Conservative and primitive variables

Another, more general way to write the equations 6-8 is presented below (Fjelde et al., 2016):

$$\frac{\partial}{\partial t}U + \frac{\partial}{\partial z}F(U) = Q(U) \tag{17}$$

$$U = \begin{bmatrix} u_1 \\ u_2 \\ u_3 \end{bmatrix} = \begin{bmatrix} \alpha_l * \rho_l \\ \alpha_g * \rho_g \\ \alpha_l * \rho_l * v_l + \alpha_g * \rho_g * v_g \end{bmatrix} + \begin{bmatrix} 0 \\ 0 \\ q_3 \end{bmatrix} \tag{18}$$

U is then the vector of the so-called conservative variables u_1, u_2 and u_3. They consist of primitive variables like densities, volume fractions and phase velocities. F(U) represents fluxes which will be introduced in the next sub-chapter and Q(U) stands for the source term (Fjelde et al., 2016). The AUSMV scheme updates the conservative variables after each time-step and updates the primitive variables on that basis (Fjelde et al., 2016). With the help of u_1 and u_2, pressure and consequently densities and phase volume fractions can be determined (Udegbunam et al., 2015). When it comes to phase velocities, the gas slip sub-model together with u_3 can be used. After new primitive variables are found based on the updated conservative variables, the scheme can move to the next time-step and further until the end of the simulation time. For detailed information on how this is being executed one should consult the work by Udegbunam et al. (2015). In the appendixes one can see how this was implemented in the code. The source term defines if additional mass is being added to the system or extracted from it and it also contains the gravitational and frictional terms that are the main responsible for the pressure development in the well. The source terms for mass conservation equations are equal to 0, while the source term for momentum conservation equation q_3 will be introduced later.

4.3 Discretization

The discretization process is the dividing of the well into number of boxes, starting with the box number 1 at the bottom of the well and ending with box number N at the top (Fjelde et al., 2016). The length of each box dx is then equal to the total depth of the well MD divided by the total number of boxes. Each box has a set of primitive and conservative variables, which correspond to the center of that box. In each box variables are considered to be constant at each time-step. The AUSMV scheme updates conservative variables after each time-step dt. The scheme is explicit, which means that variables are being updated based on variables from the old time-step (Fjelde et al., 2016). The borders of each box are called fluxes. Hence, there is a total number of N+1 fluxes in the well. Here mass and momentum are transferred between the boxes. For the graphical representation refer to the figure below:

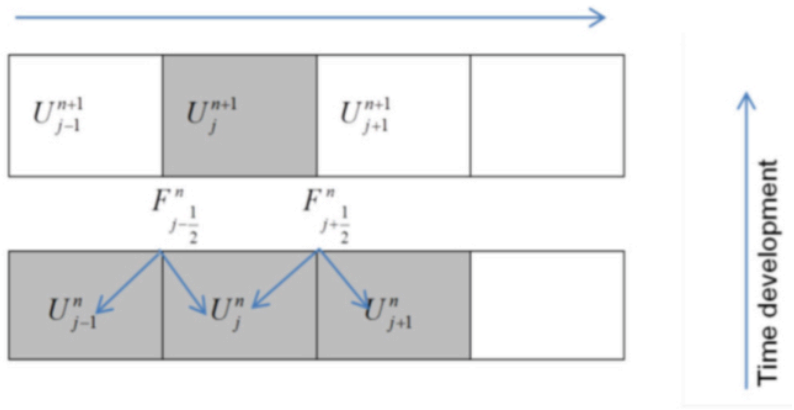

Figure 15: Discretization (SPE 190053)

F stands for fluxes and indexes "j" and "n" refer to the number of the box and time-step respectively. The formula that the AUSMV scheme uses to update conservative variables in each box for each time-step is:

$$U_j^{n+1} = U_j^n - \frac{\Delta t}{\Delta z} * \left(F_{j+\frac{1}{2}}^n - F_{j-\frac{1}{2}}^n \right) + {Q_j}^n \tag{19}$$

Udegbunam et al., (2015), describe the way fluxes are found in detail. One can also refer to the Appendixes for more information. Here "n+1" refers to the new time step and "n" refers to the old one, Δt and Δz are the same as dt and dx. The source term ${Q_j}^n$ is related to the momentum equation.

Since the scheme is explicit, there are limitations related to dx and dt (Fjelde et al., 2016). The criterion that dictates the relation between them is called Courant-Friedrichs-Lewy (CFL) criterion (Udegbunam et al., 2015):

$$\Delta t \leq CFL * \frac{\Delta z}{\max(|\lambda_1|, |\lambda_2|, |\lambda_3|)} \tag{20}$$

CFL varies between 0 and 1 and depends on the formulation of the scheme for the particular case (Fjelde et al., 2016). Variables λ_1 and λ_3 are eigenvalues and correspond to pressure pulses (sonic waves) propagating downstream and upstream (Udegbunam et al., 2015). Eigenvalue λ_2 corresponds to the speed of the gas bubble traveling downstream in a pure liquid region. The eigenvalues representing pressure pulses have the largest value. Time-step dt will be then limited by the wave propagation speed up to 1500 m/s in pure water (Fjelde et al., 2016). The propagation of sonic waves and their magnitude depend on flow-rate changes or choke adjustments. They are also referred to as acceleration effect.

4.4 Boundary condition

All fluxes are calculated by the AUSMV scheme except of the inlet and outlet boundaries. The process of defining the inlet and outlet fluxes is also referred to as a boundary condition. The boundary condition depends on the physical condition of the system (Fjelde et al., 2016). As it was mentioned in chapter two, there are open and closed systems. CML is an open system, which means that pressure at the outlet boundary must be close to 1 atm. Unknown variables can also be found by the technique called extrapolation. Instead of assuming that the pressure at the outlet boundary is equal to 1 atm, one can find it by extrapolation. The AUSMV scheme and the code used for this thesis offer the possibility to choose between open and closed well conditions depending on the case to be simulated.

For an open system, the mass flow rates at the bottom are known (Fjelde et al., 2016). They are specified for each simulation example later in chapter six. Based on the flow rates one can find mass and convective momentum fluxes. The only unknown parameter is the inlet pressure flux. There are two extrapolation methods to determine that pressure flux, the first one presented by Udegbunam et al. (2015):

$$Pinlet = P(1) + 0.5 * \big(P(1) - P(2)\big) \tag{21}$$

And the second one, more recently presented by Fjelde et al. (2016):

$$Pinlet = P(1) - 0.5 * \Delta z * \rho mix * g * \cos(\emptyset) - 0.5 * \Delta z * Fw \quad (22)$$

For the inlet pressure flux in the scheme presented in this thesis the more recent method described in equation 22 is used. When it comes to the outlet boundary, mass and convective momentum fluxes are extrapolated using the values in the boundary boxes (Fjelde et al., 2016). As it was stated above, the outlet pressure flux is set to 1atm.

For a close well, all mass and convective momentum fluxes are set to 0 since there is no fluid circulation in the system (Udegbunam et al., 2015). The inlet pressure flux can be extrapolated the same way as for an open well using equation 22. The outlet pressure flux can be extrapolated in the following way (Fjelde et al., 2016):

$$Poutlet = P(N) - 0.5 * \Delta z * \rho mix * g * \cos(\emptyset) - 0.5 * \Delta z * Fw \quad (23)$$

The conditions specified above are valid for normal circulation. One of the main challenges in this thesis was to determine how to specify the outlet pressure flux while introducing the suction point and simulating a CML operation. The way the inlet boundary conditions were specified remained the same as for an open well. The outlet boundary conditions had to be changed because the physical conditions of the system were different. In case of CML operation fluid in the upper boxes is replaced by air, and the suction point or the theoretical SMP located in the middle of the well replaces the flow-line. To be able to reproduce a realistic scenario, outlet liquid fluxes were set to 0. That was to ensure that the well would not refill itself from the top after the suction point was introduced. The gas fluxes were extrapolated the same way as during normal circulation for an opened well. That meant that the gas was allowed to be sucked from the top. The outlet pressure flux could be expressed in three different ways.

1. Fixed pressure equal to 1 bar: $Poutlet = 100000\ Pa = 1\ atm = 1\ bar$
2. New extrapolation method described by Fjelde et al. (2016):
   $Poutlet = P(N) - 0.5 * \Delta x * \rho mix * g - 0.5 * \Delta x * Fw$
3. Old extrapolation method described by Udegbunam et al. 2015:
   $Poutlet = P(N) + 0.5 * (P(N) - P(N-1))$

The simulations of each method and the conclusion on which method delivered the most appropriate results are presented in chapter six.

4.5 Extension to Second Order AUSMV scheme

The sub-chapters above give a brief description of the AUSMV scheme. As it was mentioned before, it is a numerical scheme designed to simulate down-hole two-phase flow behavior. The main disadvantage of a scheme like this is a phenomenon called numerical diffusion (Fjelde et al., 2016). This tends to smooth out sharp physical interfaces. Numerical diffusion is a consequence related to discretization effects (Udegbunam et al., 2015). To avoid numerical diffusion one can increase the number of boxes and so, increase the accuracy of the results. However, this will lead to an increase in the computational time (Udegbunam et al., 2015). Another possibility to solve this problem is to upgrade the AUSMV scheme to a 2nd order by using slope limiters. The CML case has been simulated before using the 1st order scheme and a different code (Torsdal, 2015). The goal for this thesis was to use the same simulation case with the updated code and to simulate with both 1st order and 2nd order schemes to be able to compare the results. The simulation and comparison of the 1st order scheme to the 2nd order are presented in chapter six. Here the difference between two schemes is presented.

When introducing the slope limiters, the variables are no longer constant in a particular box. The slopes are used to calculate the boundary value in each box. To calculate the fluxes, instead of using values corresponding to the center, the 2nd order scheme uses the calculated boundary values (Fjelde et al., 2016). This approach requires less computational effort and fewer boxes. The convergence towards a solution is faster (Fjelde et al., 2016). The figure below shows the concept of slope limiters:

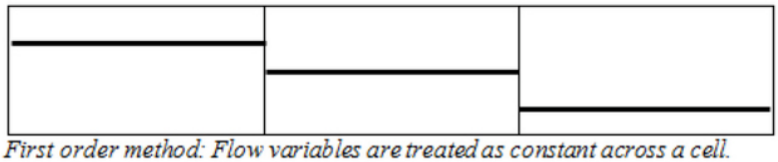

First order method: Flow variables are treated as constant across a cell.

Second order method/ Slope limiter concept: Gives better resolution of gas distribution in a well.

Figure 16: Slope limiters (SPE 180053)

For more details on how this was implemented in the code refer to the appendixes.

4.6 Introducing the suction point

To be able to simulate a CML operation, changes to the code had to be made. Equation 19 is a discretized form of equation 17. Here, the source term was zero for the mass conservation equations and non-zero for the momentum equation. To introduce a suction point, a source term had to be introduced in the liquid mass conservation equation in the box where the SMP is placed. The way this was implemented in the liquid mass conservation law was by updating the discretization formula:

$$U_j^{n+1} = U_j^n - \frac{\Delta t}{\Delta z} * \left(F^n_{j+\frac{1}{2}} - F^n_{j-\frac{1}{2}} \right) - \frac{\Delta t * q}{A * \Delta z} \tag{24}$$

In equation 24, q stands for the suck-rate in kg/s. The number of the box "j" defines at what depth the suction point will be introduced. For both simulations in chapter six, "j" is equal to 14. Given that in total there are 25 boxes in both cases, that corresponds approximately to the middle of the well. The rest of the simulation continues as before with already updated fluxes near the suction point. Hence, the volume of the liquid will gradually reduce in the boxes above the suction point. For more details one should consult appendixes. Here it should be noted that in the appendixes source term has the form $\frac{\Delta t * q}{dx}$. This is because during the implementation the area was included in the conservative variables in the code. Another very important detail with introducing the suction point is a specific pressure condition or so called fix that has been introduced to make simulations stable. This pressure condition assures that pressure in each box during the simulation will not fall below atmospheric pressure 1atm. After the suction point is introduced, liquid volume is reduced in the upper boxes. This leads to very low pressures close to vacuum condition. It was observed that eventually the pressures obtain negative values, which terminates the whole simulation. The pressure condition described here, does not allow pressures in each box to be lower than 1 atm. Without this pressure condition, simulation would not be feasible. The pressure condition is marked with red color in the appendixes and referred to as "important pressure test and correction on pressure".

5 Small-scale Experimental Loop at UIS

The simulations in this thesis are conducted on the small-scale flow-loop, which was built in 2010/2011 as a combined project between UIS and the International Research Institute of Stavanger (IRIS). Initially it was built with the purpose of studying conventional backpressure MPD systems and the possibility for completely automated rig systems (Torsvik, 2011). Experiments on DG systems with this flow-loop are also possible. The pictures of the experimental set-up can be found in Figure 17 and Figure 18.

Figure 17: The small-scale flow-loop, UIS, front view. Photo: Rza Behbudov

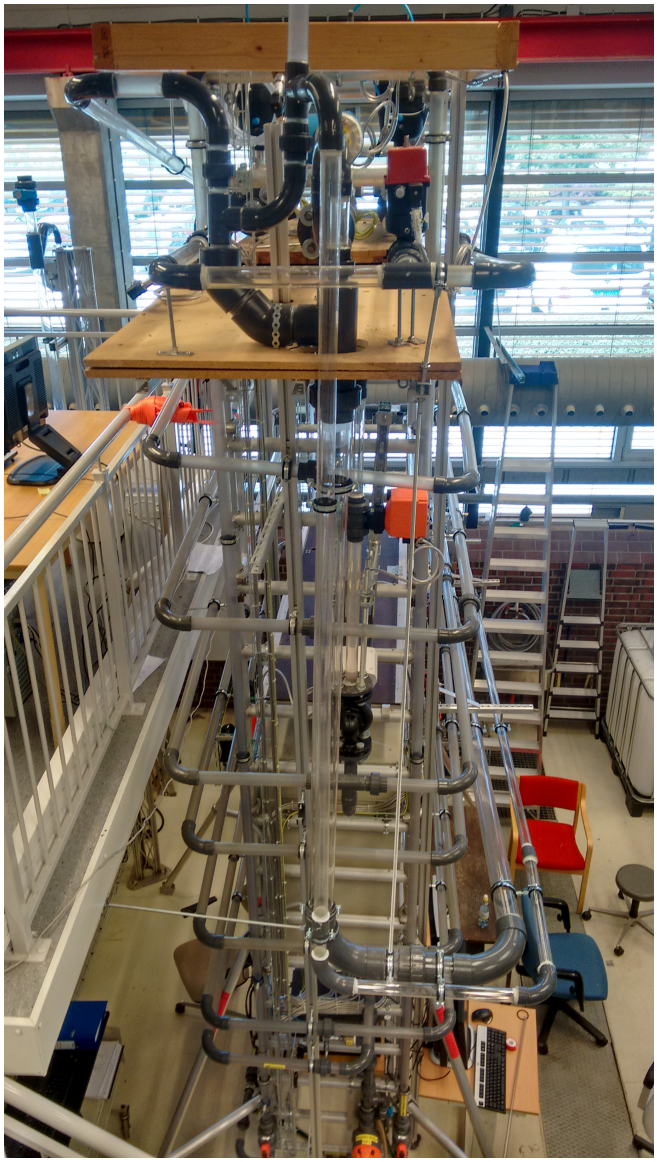

Figure 18: The small-scale flow-loop, UIS, top view. Rza Behbudov

The most important parameters for the simulations conducted in this thesis are the geometry and pipe inner diameter. An approximated model will be used. Each loop segment consists of eight pipe pieces, four short and four long (Torsvik, 2011). The length of the long piece is 1400 mm, and the length of the short one is 400 mm. There are four bent connections that create a rectangular shape and four connections between the pipes. In total there are seven loop segments (Torsvik, 2011). For simplicity these connections are neglected and the whole loop is considered as a straight pipe. The total length of that pipe is then 50400 mm, which has been approximated to 50 meters for the simulations. For the graphical representation of the loop segment refer to the Figure 19.

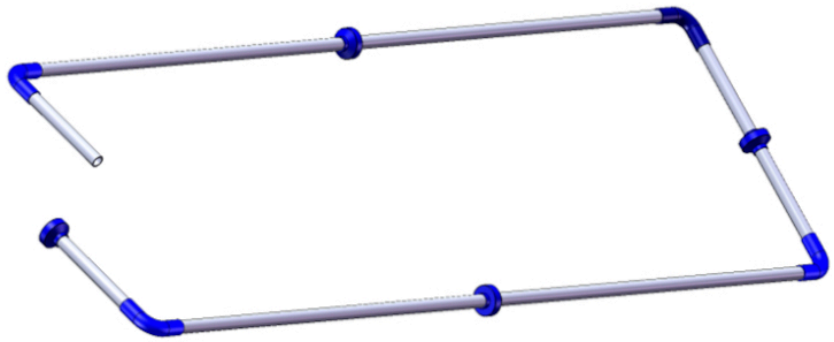

Figure 19: Loop segment (Torsvik, 2011)

The height of the construction is 5 meters, which gives an inclination angle of 84 degrees. For the approximated model refer to the Figure 20.

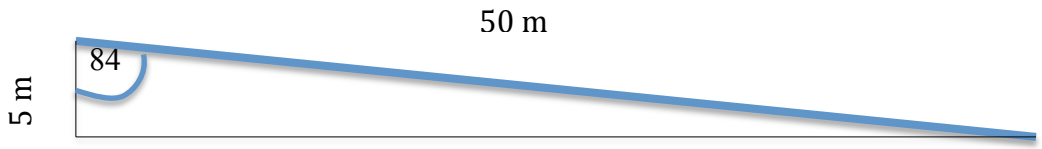

Figure 20: Approximated model

The model in Figure 20 will be used for the simulations conducted in chapter six. The inner diameter of the pipe is equal to 0.033 meters. The geometry has been implemented in Appendix B and marked with red color.

6 Simulations and Analysis

This chapter examines the simulations conducted with the AUSMV scheme. The results of the defined research areas are described here. The simulations were divided in two major parts. First, the goal was to adapt the 2nd order AUSMV scheme for CML case scenario and compare the results to the 1st order scheme simulations. In the second part the goal was to adapt the scheme to the small-scale loop at UIS and test if a CML case can be simulated. For the first simulation, we will use the scenario simulated by Torsdal (2015).

6.1 Simulation one

In this example mud level in the annulus will be lowered by introducing a suction point to the system. Suction point is a theoretical representation of SMP located in the middle of the well. A vertical well is assumed. Well data is given below:

Table 3: Well data, Simulation One

Fluid data:		Well Geometry	
Liquid Viscosity:	0.001 Pa*s	Well depth:	2000m
Gas Viscosity:	0.0182*10^(-3) Pa*s	Inner Diameter (ID):	0.127m
K:	1.2	Outer Diameter (OD):	0.2159m
S:	0.5		
P standard conditions:	100000 Pa		
ρ standard conditions:	1000 kg/(m^3)		

We assume a uniform annular well geometry neglecting any flow area changes. The well is 2000 meters deep and the SMP is placed at 920 meters RKB. The simulations are run for 1000 seconds. The total length of the well and 25 discretization boxes gave a value of dx equal to 80 meters. Time-step dt was selected accordingly and was equal to 0.01 seconds. This gave an acceptable CFL value of 0.1875. The fluid rates entering and exiting the system can be found in Table 4:

Table 4: Liquid rates, Simulation One

Time (sec)	Liquid rate in (kg/s)	Time (sec)	Liquid rate out (kg/s)
0-150	0	0-150	0
150-160	22*(time-150)/10	150-160	0
160-300	22	160-300	0
300-310	22-22*(time-300)/10	300-400	0
310-800	0	400-410	22*(time-400)/10
800-810	22*(time-800)/10	410-1000	22
810-1000	22		

The fluid enters the system through the bottom at 150 seconds and continues to flow until 310 seconds. Between 310 and 800 seconds the flow at the bottom is stopped. It is initiated again at 800 seconds and continues until the end of simulation time. The liquid rate out corresponds to the suction point, which is initiated at 400 seconds. It is important to introduce interpolation for all rate changes to avoid numerical instabilities. An interpolation period of 10 seconds was used. The way this data has been implemented in the code can be found in Appendix A. As mentioned earlier the suction point is introduced at the box number 14, which corresponds to 920 m RKB.

6.1.1 EC-Drill case with 2nd order scheme

The EC-Drill case has not been simulated with the 2nd order AUSMV scheme before. In the master thesis written by Torsdal (2015) this case was considered, but the 1st order scheme was used with an older version of the code. One of the challenges was to find appropriate boundary condition at the outlet of the well when introducing the suction point. Several possibilities were studied. In all of the cases liquid outlet fluxes on the top were set to 0 to ensure that the well would not refill itself from the top. The pressure flux on the top could be expressed in several ways:

1. Fixed pressure equal to 1 bar: $Poutlet = 100000\ Pa = 1\ atm = 1\ bar$
2. New extrapolation method described by Fjelde et al. (2016):
   $Poutlet = P(N) - 0.5 * \Delta x * \rho mix * g - 0.5 * \Delta x * Fw$
3. Old extrapolation method described by Udegbunam et al. (2015):
   $Poutlet = P(N) + 0.5 * (P(N) - P(N-1))$

The results are shown in the Figure 21. Pressure at he bottom of the well is plotted. As one can see, even though the suction rate is equal to the liquid rate entering the system, extrapolation methods do not seem to work properly.

According to Table 4, liquid stops to enter the well at 300 seconds. Then, the mud level begins to drop at 400 seconds after the SMP is initiated. This is because the well is not refilled from the bottom. This results in a pressure drop due to a lower fluid column. When the liquid flow at the bottom is ramped up again at 800 seconds the pressure should stabilize. It should remain stable since the inlet and outlet liquid rates are equal and there will be no more mud level reduction. Method 1 gives appropriate results. Pressure stops to drop after 800 seconds and evens up to 162 bars. Both methods 2 and 3 show an increase in pressure despite the fact that fluid leaves and enters the system at equal rates.

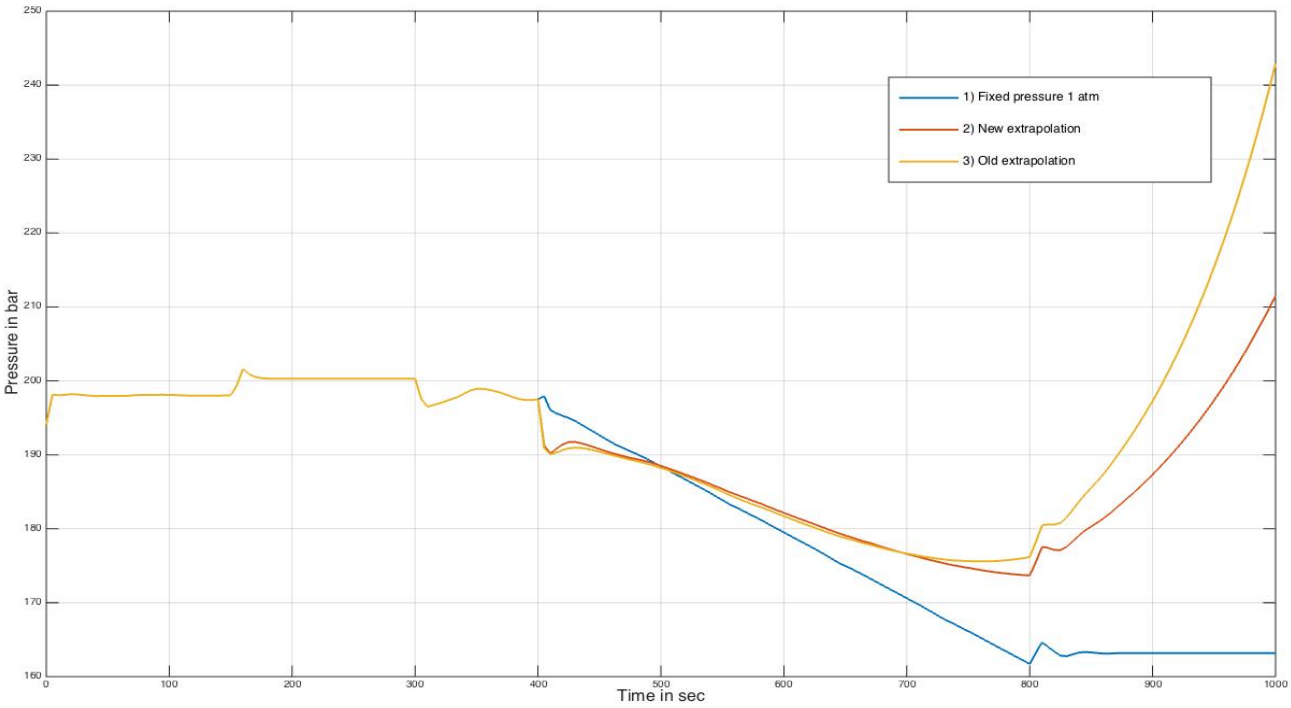

Figure 21: BHP vs. time

In all three methods only liquid fluxes at the top were set to 0. It is obvious that the pressure build-up in methods 2 and 3 must have an explanation. It is logical to propose that if liquid fluxes are 0, this pressure build-up can be somehow related to the gas in the well. Therefore, the next step was to set gas fluxes at the top equal to 0 as well. The simulations of methods 1, 2 and 3 were repeated with the same system parameters. The results are plotted in Figure 22.

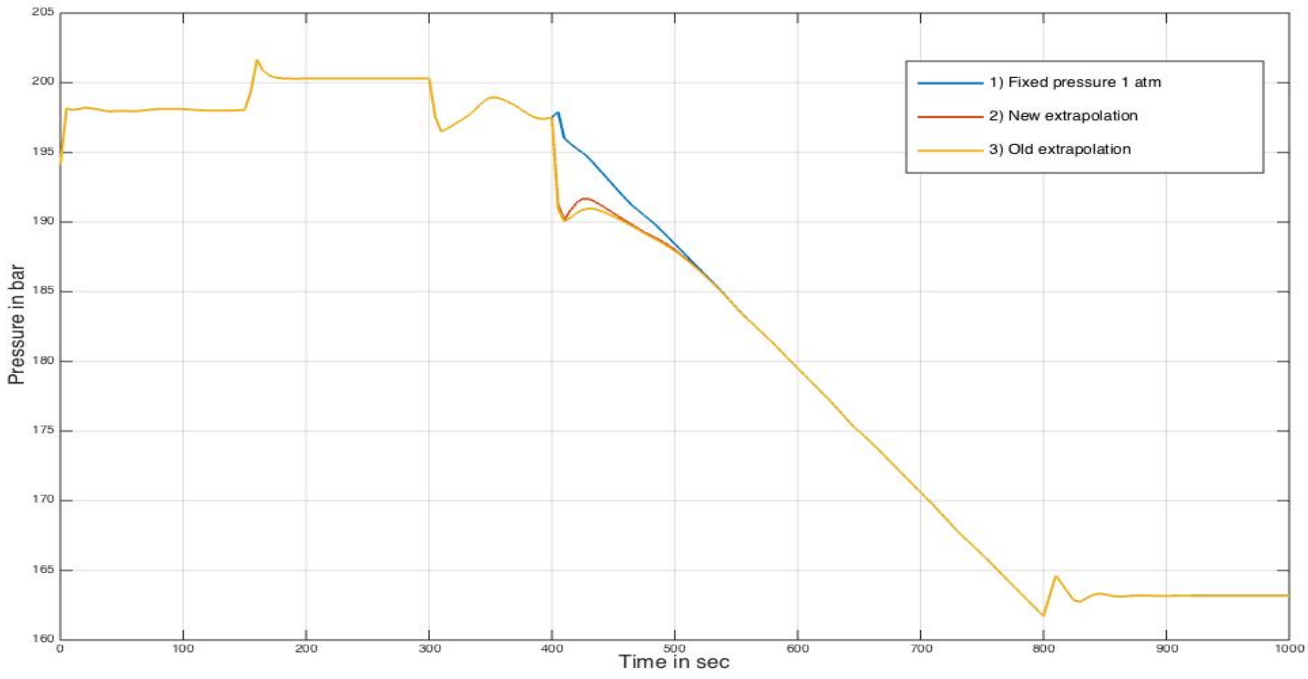

Figure 22: BHP vs. time, gas fluxes equal to 0

When gas fluxes are set to 0, both extrapolation methods work. The pressure increases by 4-5 bars around 150 seconds. Before this time the well is in static condition and the BHP is represented only by the hydrostatic component. After circulation at the bottom is initiated at 150 seconds, the friction component adds to the hydrostatic, which results in 4-5 bars increase in the BHP. The drop in the BHP around 300 seconds is also explained by friction. Since circulation is stopped, the frictional component is equal to 0. There is a slight difference in pressure between extrapolation methods and method 1 around 400 seconds, around the same time when the SMP is initiated. The pressure has a small build-up equal to approximately 1 bar before the eventual drop in method 1, where in method 2 and 3 it drops rapidly with 8-9 bars and goes slightly up again before continuing to decrease further as mud level falls. This can be explained by the fact that extrapolation methods include the friction parameter and method 1 does not. This drop is the result of friction forces obtaining negative sign when the suction point is introduced. The fluid starts to flow downwards in the system in the negative direction. Unlike this, Method 1 has a fixed pressure on the top, which is independent of friction forces. That is the reason why the pressure does

not drop so rapidly as for methods 2 and 3. Moreover, this pressure drop seems unphysical. As mentioned earlier, around 150 seconds when the circulation from the bottom was initiated with 22 kg/s, the increase in BHP due to the friction component was around 4-5 bars. When the SMP is initiated with the same circulation rate of 22 kg/s, only half of the well is circulating since the suction point is located at the middle. Hence, the decrease in BHP due to the negative friction component should be half of the initial increase since the rates are opposite in direction but equal in magnitude and only half of the well is circulating. This corresponds better with the method 1 where BHP decreases with 2-3 bars instead of 8-9 bars as it does in methods 2 and 3.

Another important aspect to mention here is that while introducing the suction point to the system, it was observed at the beginning that the top boxes tend to obtain very low pressures close to vacuum condition. This affected the whole simulation process and after 400 seconds the simulation failed. To resolve this problem a special condition was introduced in the code by which pressure in any box would not go below 1 bar. Refer to Appendix A for the details. The condition is marked with red color.

To be able to assess reliability of simulations hand calculations were performed. The volume of the empty annulus after the mud level reduction was compared to the amount of fluid withdrawn from the system during the whole simulation time. According to the simulation results, the mud level is between 280 and 440 meters. This spread is due to numerical diffusion and inaccuracy in the numerical solver. Refer to the Figure 23. Without these factors, the interface between the mud level and the air would be a straight line.

For simplicity, it is assumed that half of this interval is filled with gas. Hence, a midpoint of 372 meters was selected for calculations. This corresponds to the volume of:

$$V = A * H = \frac{\pi}{4} * (OD^2 - ID^2) * H$$
$$= \frac{\pi}{4} * (0{,}2159^2 m - 0{,}127^2 m) * 372m = 8{,}89m^3 \quad (25)$$

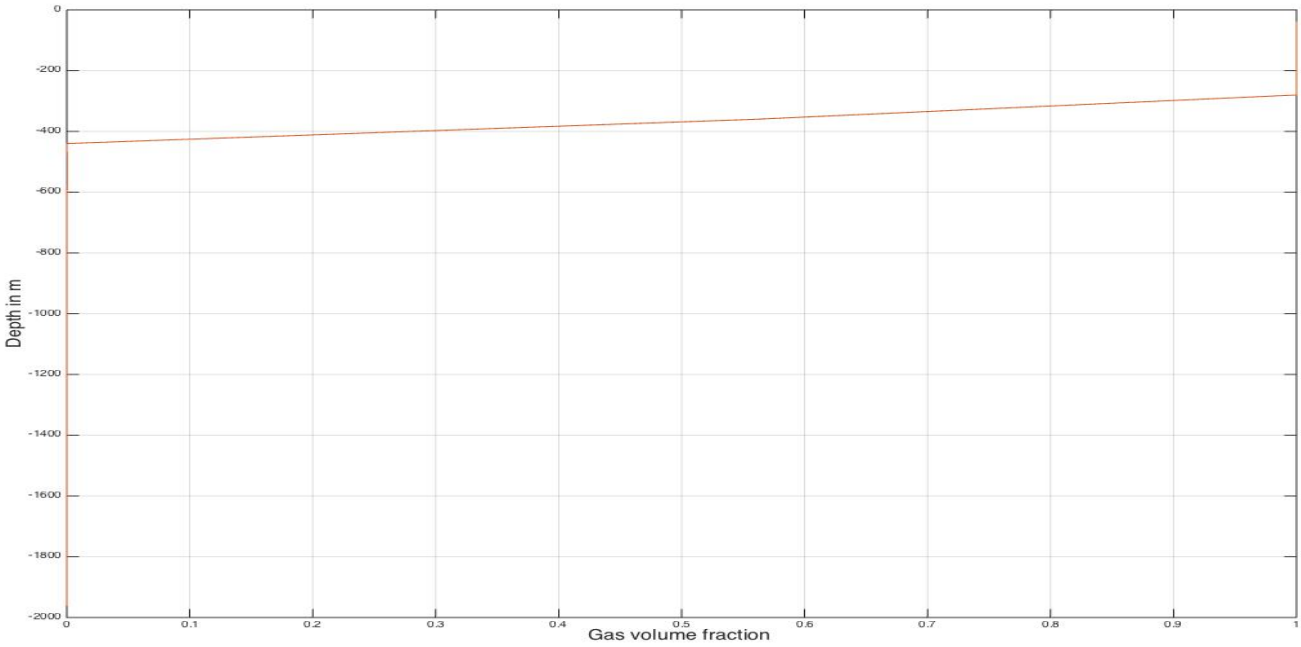

Figure 23: Gas Volume fraction vs. depth

The total amount of liquid pumped out of the system according to the Table 4 is equal to:

$$Mout = M_{400-410} + M_{410-800} + M_{800-810} = 22kg + 390sec * 22kg + (220kg - 22kg) = 8800kg \quad (26)$$

In the equation above, the amount of gas sucked during interpolation is counted as well, both during the start of the suction and when the pumps are ramped back at 800 seconds. After 800 seconds liquid-rate-in is equal to liquid-rate-out. The total volume of the liquid sucked from the system can be calculated:

$$V = \frac{Mout}{\rho} = \frac{8800kg}{1000(\frac{kg}{m^3})} = 8{,}8m^3 \quad (27)$$

As one can see, measurements of the empty volume in the annulus obtained from simulation results correspond quite well with the amount of liquid withdrawn from the system. This proves the reliability of AUSMV scheme for this type of simulations.

6.1.2 AUSMV 1st vs. 2nd order

After the AUSMV scheme was adapted for EC-Drill case scenario, further simulations were conducted to compare the 1st order scheme with the 2nd order. The

EC-Drill case scenario has been simulated with the 1st order scheme before (Torsdal, 2015). One of the major issues with the 1st order scheme is numerical diffusion (Fjelde et al., 2016). Numerical diffusion is a result of discretization and it has not been fully understood yet (Udegbunam et al., 2015). It can be avoided by increasing the number of boxes, which will result in an undesired increase in computational time. Another way is to upgrade the scheme to 2nd order. This problem mostly affects sharp transition zones, for example gas liquid interface (Fjelde et al., 2016). A comparison between different well flow parameters that can be executed with the AUSMV scheme will be introduced. To define the outlet pressure flux at the suction point, method 1 from the subchapter above was selected. The simulation well data in tables 3 and 4 was kept the same.

The AUSMV scheme provides many different well flow parameters like pressure, liquid and gas mass rates, velocities of different phases, phase fractions and more. Graphic representation will be used for 1st and 2nd order schemes. First, time dependent graphs will be presented. Afterwards, the change of well parameters versus depth for different time steps will be presented as well.

6.1.2.1 Time plots

Figure 24 compares BHP. As one can see, the 2nd order scheme is quite similar with the 1st order, apart from minor differences. For instance, at the very beginning the 1st order scheme causes an oscillatory behavior, although later around 40 seconds it becomes smooth and very similar to the 2nd order. The same type of oscillatory behavior is observed with the 2nd order scheme right before the suction point is initiated and once more after the pumps are ramped back. The last oscillation in the 2nd order scheme is quite small, but the first one seen at 350 seconds reaches $\pm 1\ bar$. The same difference of $\pm 1\ bar$ is true for to the 1st order scheme oscillation mentioned earlier. Apart from these minor differences it can be concluded that in case of BHP both schemes provide similar results.

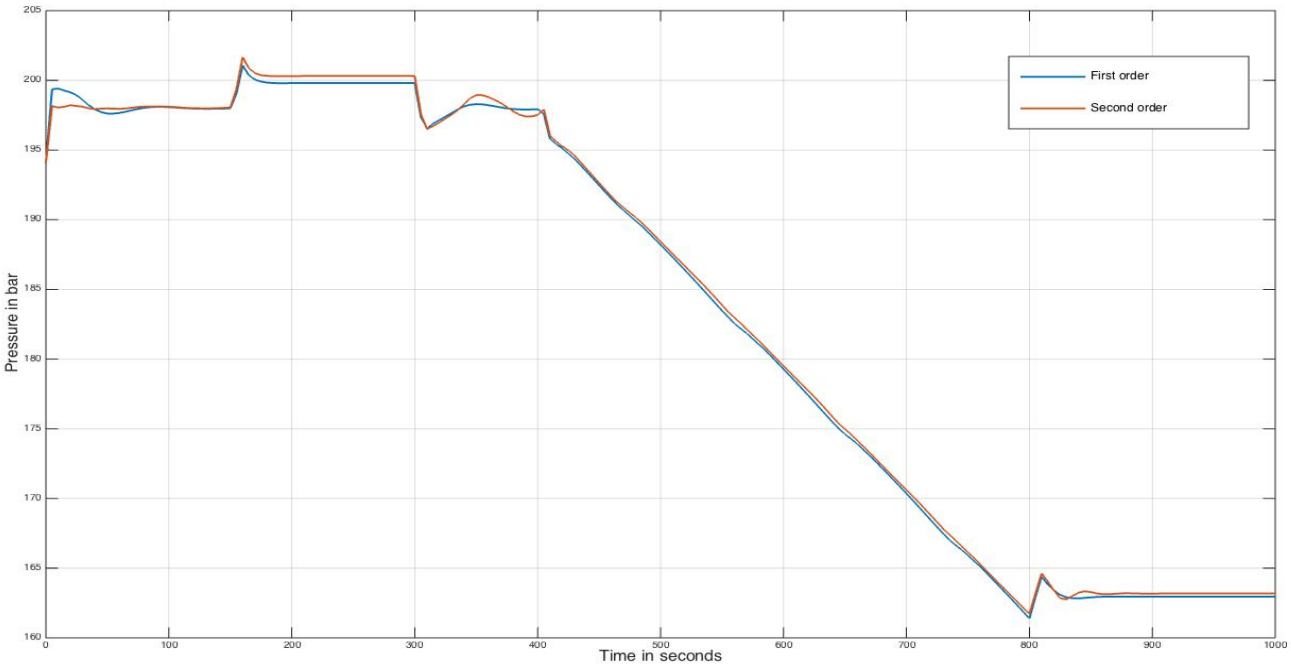

Figure 24: BHP vs. time, 1st vs. 2nd order

Next, pressure on the outer boundary is considered. Refer to the Figure 25. There is a significant difference between the 1st and 2nd order scheme before 400 seconds or before suction point is initiated. The 2nd order scheme has 1 bar overpressure compared to the 1st order. However, in both cases outlet pressure measurements are higher than one would expect them to be. In an open system, pressure at the outlet boundary must be equal to 1 bar atmospheric pressure unless it is specified differently. This was investigated to assure that this problem has a local nature and is not affecting the rest of simulation results.

At the same interval BHP is equal to 196 bars, which agrees with the hand calculations. This means that the rest of the simulation must be correct. The representation of the outlet boundary in the end of the code needs further investigation. After the suction point is initiated, outlet pressure drops to negative values. This is a temporary effect due to the air being sucked from the top and around 500 seconds the pressure condition described in the chapter four starts to apply. The pressure equalizes at 1 bar.

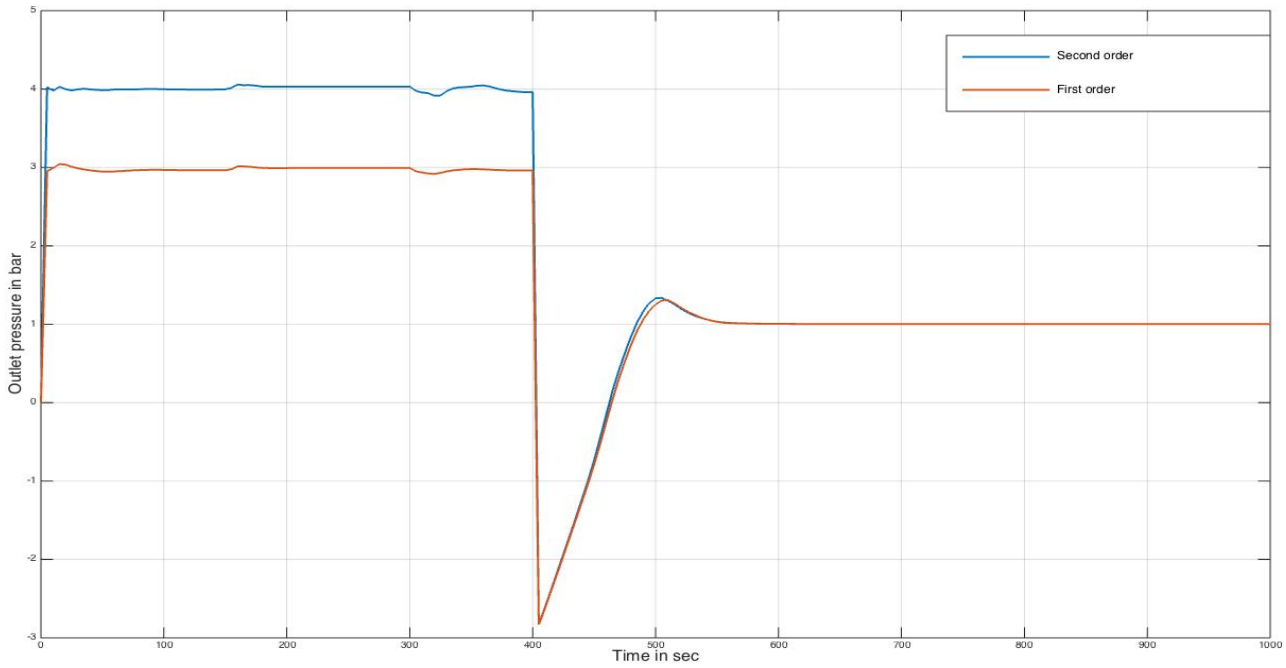

Figure 25: Outlet pressure vs. time, 1st vs. 2nd order

A comparison between friction gradients of 1st and 2nd order schemes is plotted in Figure 26. The 2nd order shows a slightly higher pressure during static conditions, which becomes larger during circulation. An interesting observation here is that friction takes a negative sign when liquid is sucked from the system. This might be again explained with a negative velocity sign, since the fluid is moving downwards. The plot appears less steady during this interval due to pressure pulses in the system. However, with the 2nd order scheme this effect is less noticeable. The reason why the pressure pulses are so evident is unclear. It can be argued that the start-up of the SMP could be the cause of it. If this is the case and the pulses have a physical nature they should be damped by using a more viscous fluid instead. One can also argue that the reason why it takes time for the pulses to damp out can be the fact that the lower part of the well is static. When the circulation in the lower part of the well is initiated again at 800 seconds, there is a small pressure pulse at the beginning, which is damped out instantly. These observations may lead to the conclusion that friction forces could be the main cause behind the damping of the pressure pulses. Pressure pulses are more evident in static conditions, when friction is equal to 0.

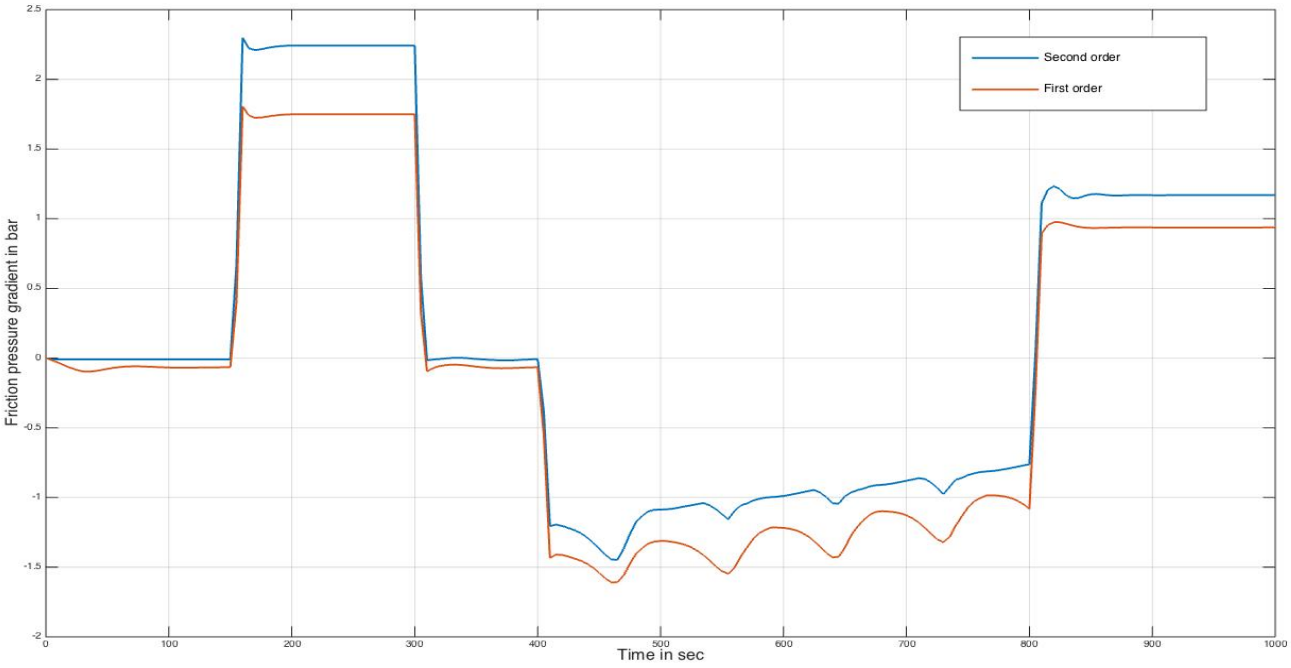

Figure 26: Friction pressure gradient vs. time, 1st vs. 2nd order

An interesting observation on Figure 26 is the way negative friction changes after 400 seconds. The friction is increasing in magnitude. The reason for this is that more gas enters the system from the above and reduces the overall mixture viscosity of the system. Only the falling liquid column above the suction point contributes to the negative friction and this column is reduced in height with time as more liquid is pumped out of the system.

Although, simulation scenario does not introduce any gas to the system from the beginning, fluid is replaced by air in the upper boxes. To illustrate this, gas rate entering the system from the top is plotted in Figure 27. Between 400 and 800 seconds liquid level in the annulus drops and air is being sucked on the top, this is seen in the plot. The gas behavior during this period is diverse and quite similar for both of the schemes. Negative values around 500 seconds might be explained again by direction of the gas flow.

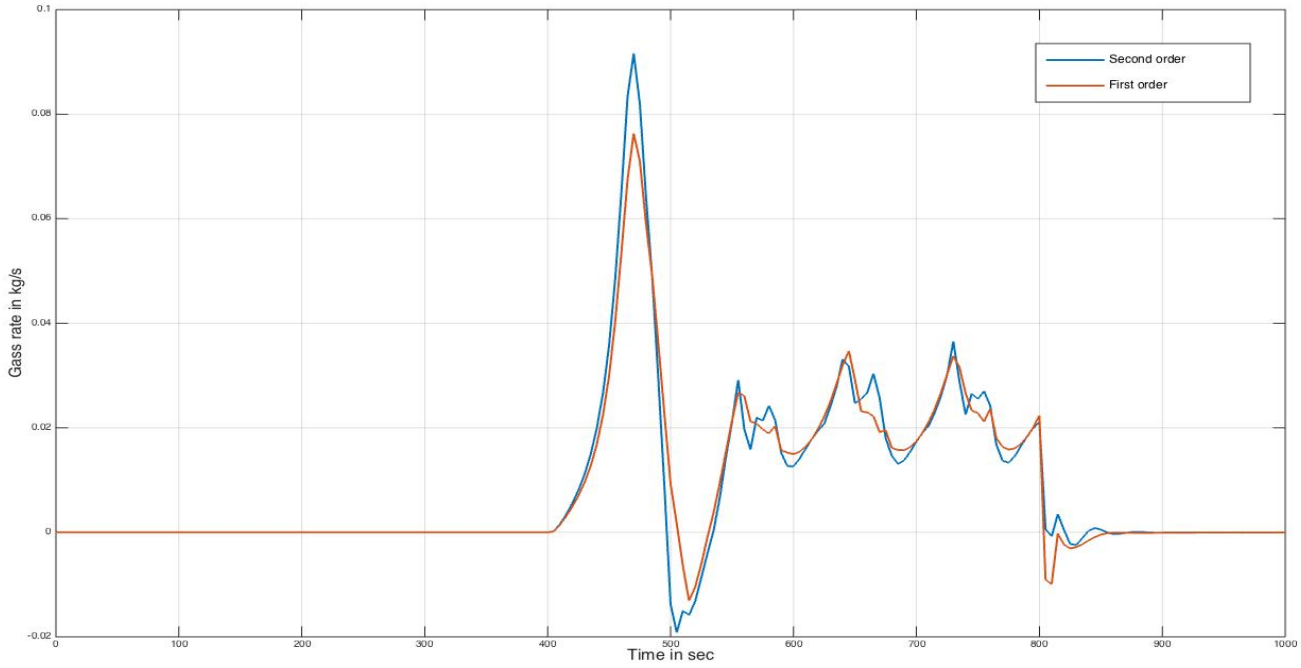

Figure 27: Gas mass-rate-in vs. time, 1st vs. 2nd order

The total amount of gas during simulation is plotted in Figure 28. The 2nd order scheme has slightly higher amount of gas around 500 seconds, which corresponds with the gas rate on figure 27. Apart from that, the results are quite similar.

The rate of the liquid exiting the system is plotted in Figure 29. As expected, the rate varies between 0 and 22 kg/s. The AUSMV scheme takes into account both the liquid leaving the system between 150 and 300 seconds through a conventional flow-line and after 400 seconds through the suction point. The difference between 1st and 2nd order schemes is minor here as well. The behavior of 2nd order scheme is smoother at the start. The 1st order scheme creates a pressure pulse of approximately 2.5 bar amplitude, while the 2nd order propagates relatively smooth with very small oscillations. There is another pressure pulse between 300 and 400 seconds where oscillations are slightly higher for the 2nd order scheme. Neither of the intervals have fluid exiting the system, so liquid rates must be equal at 0. The first oscillations at the start are probably some disturbances caused during the initialization of the well. It takes time for the scheme at the beginning to adjust all the parameters in realistic manner. The second oscillations between 300 and 400 seconds can be explained by

the fact that the pump is shut down and there is no circulation in the system. That is the reason that the pressure pulses are more evident in this interval compared to the pump start-up around 150 seconds where friction damps the pressure pulses instantly. This corresponds well with the observations of pressure pulses on Figure 6 discussed earlier.

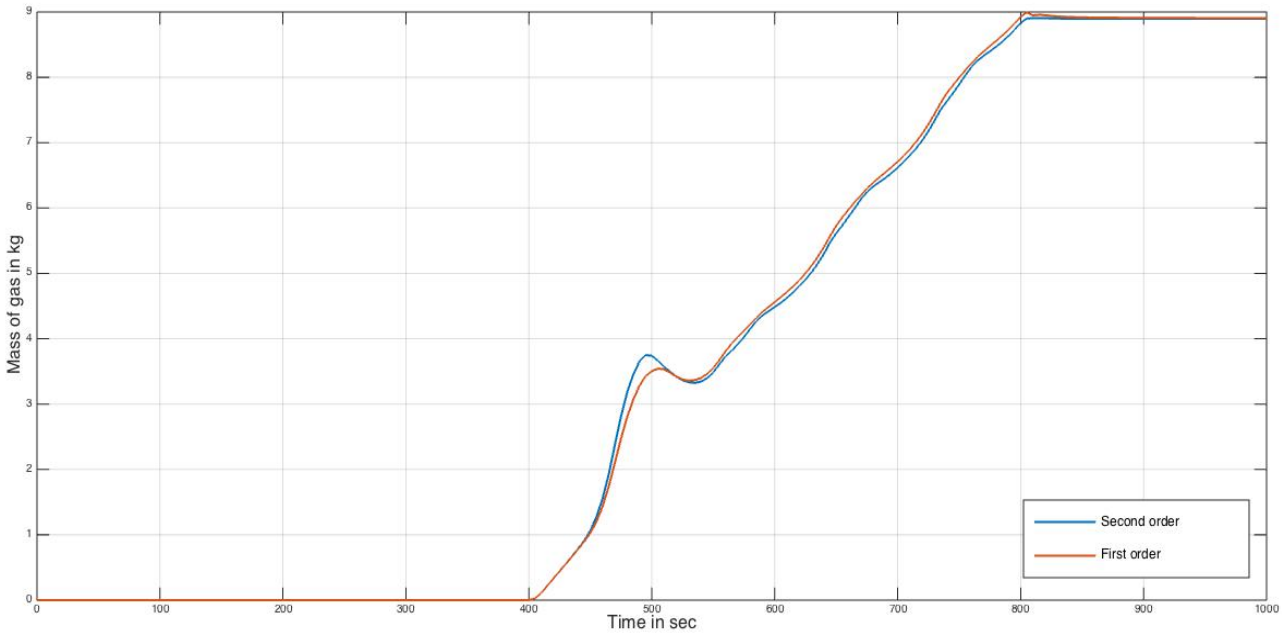

Figure 28: Total mass of gas vs. time, 1st vs. 2nd order

Changes in other well parameters through time, such as hydrostatic gradient, total mass of liquid in the well, rate of liquid entering the system and total volume of gas in the well were identical for both schemes. The pressure pulses seen on different plots are quite normal for this type of system. To try to reduce these, one can use liquid with a higher viscosity. Other than that, time dependent plots show little difference between 1st and 2nd order schemes.

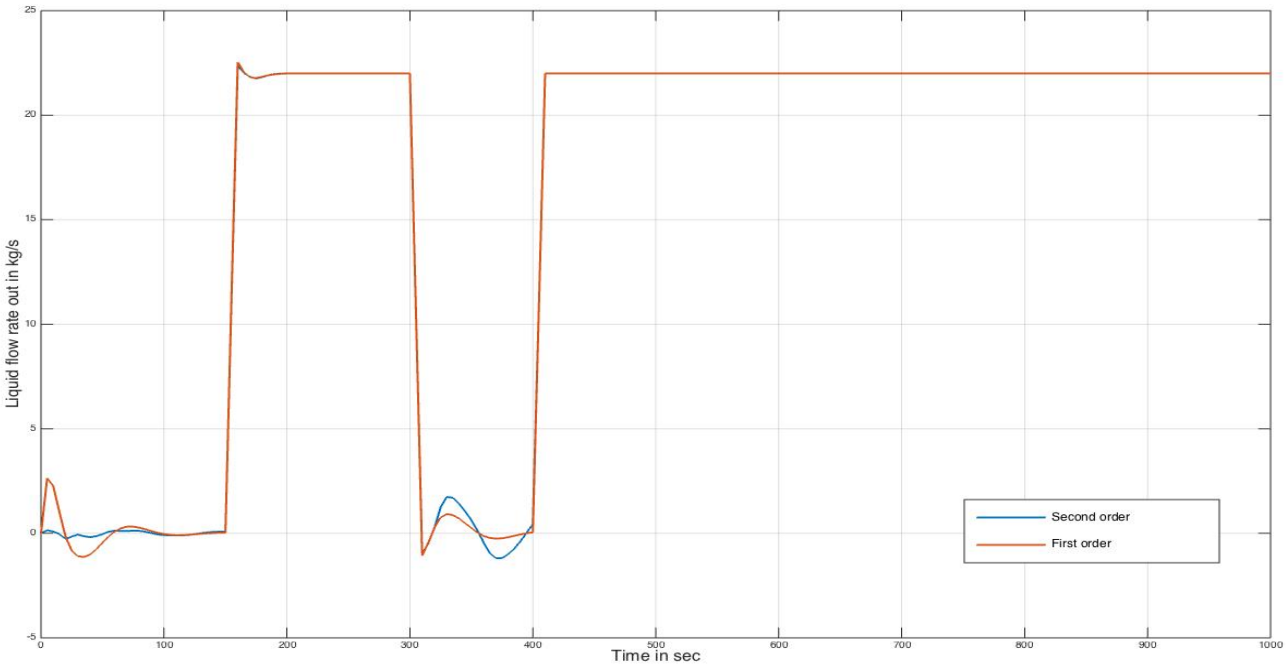

Figure 29: Liquid mass-rate-out vs. time, 1st vs. 2nd order

6.1.2.2 Depth plots

Apart from the time dependent plots, depth related changes for different well parameters were investigated. Three time situations will be considered here. The first time situation is at 250 seconds during first circulation, the second at 600 seconds when mud level in the annulus is dropping and finally at 1000 seconds which is the end of simulation time where the mud level is stable. Liquid and gas velocities at 250 seconds are plotted in Figures 30 and 31 respectively.

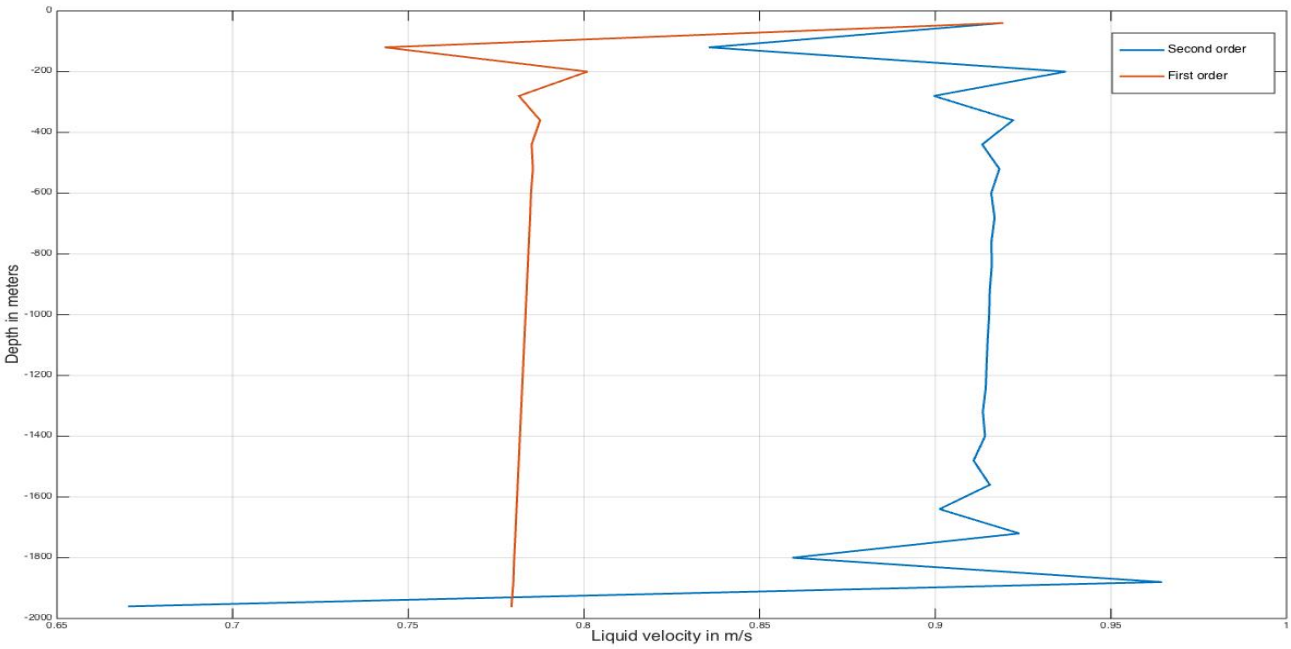

Figure 30: Liquid velocity vs. depth, 250 sec

The plots for gas and liquid are very similar with the one difference that gas travels faster. This can be explained by the gas slip model. The model is constructed mathematically in such a way that gas travels faster than liquid. Refer to the chapter four for details. For both phases velocity should not change a lot through depth at this time situation since fluid column is uniform and circulation is constant.

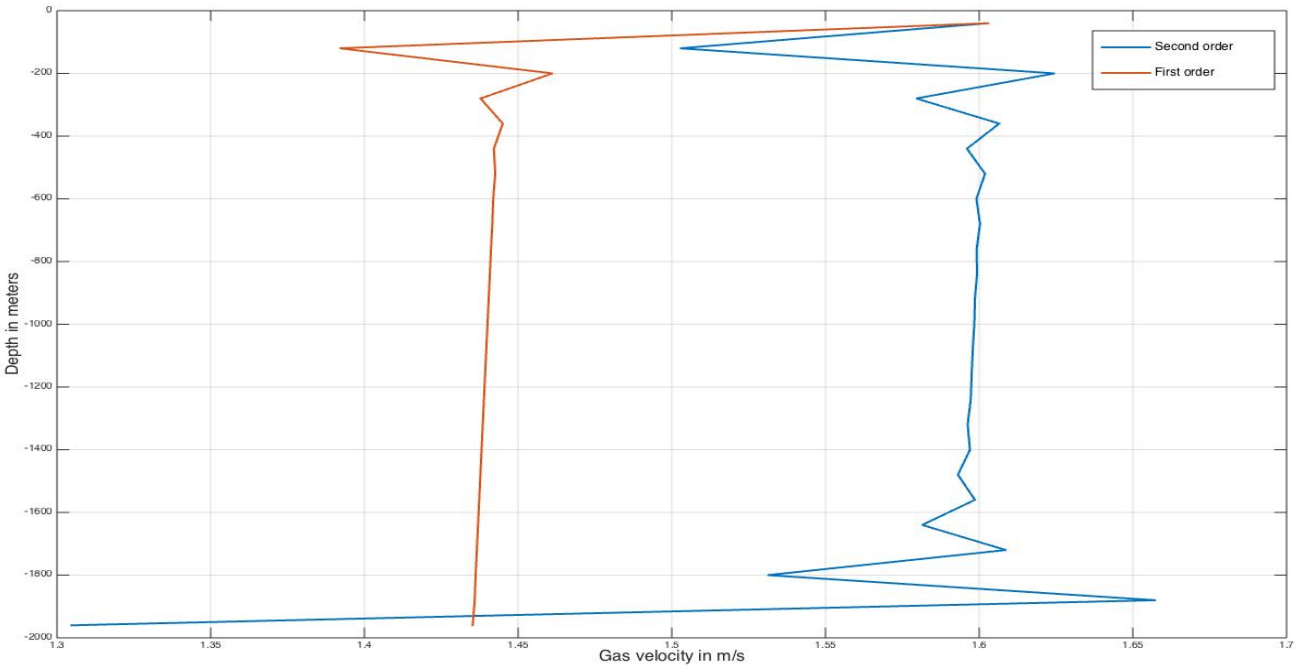

Figure 31: Gas velocity vs. depth, 250 sec

When it comes to the difference between 1st and 2nd order schemes, the 2nd order scheme shows higher values for both phases with much more disturbance at the bottom of the well. It is important to mention that the slope limiters in the 2nd order scheme were used on all parameters except on phase velocities. This makes it difficult to explain such a disturbance at the bottom of the well. Since these disturbances are closer to the boundaries they can be explained by the numerical boundary treatment. More investigation on the boundary treatment to find best possible solution is required.

Gas concentration plots were almost the same for 1st and 2nd order schemes. At this time situation there is very little gas in the system so the values were very small. The same can be said about the pressure profile versus depth, the plots are nearly identical.

The next time situation to be considered is 600 seconds. At this time, the mud level in the annulus is dropping and the rig pumps are shut off. For the velocity profiles refer to Figures 32 and 33 for liquid and gas respectively.

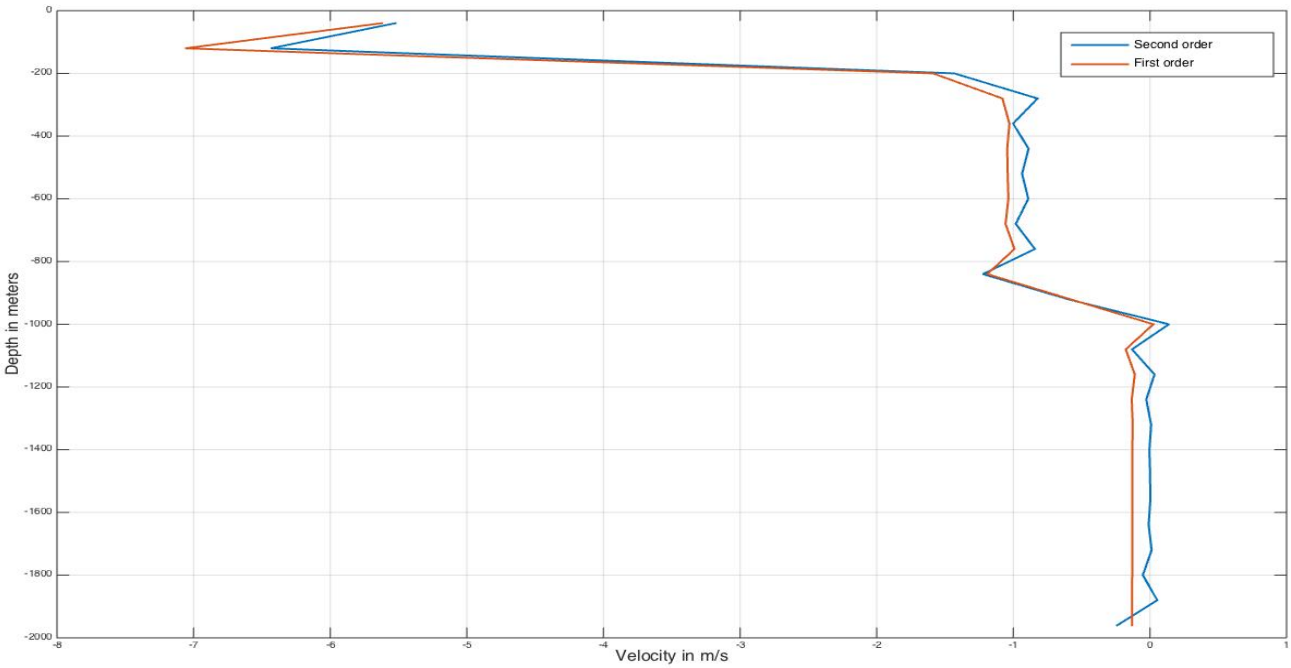

Figure 32: Liquid velocity vs. depth, 600 sec

At this stage of the simulation the well parameter plots have changed. The gas concentration is higher at the top. The SMP has been pumping the fluid out for 200 seconds already and the mud level in the annulus has dropped to 325 m RKB according to Figure 34. Below 1000 meters, the liquid is in static condition, no circulation is happening here. Around 1000 meters, where the suction point is located, both velocities change their sign to minus. This is because liquid and gas above the pump are traveling now in an opposite direction downwards. The velocities are even higher around 300 to 200 meters, which is an interval with higher gas concentration. This can be again explained by the numerical boundary treatment. In general the plots correspond well with the simulation scenario.

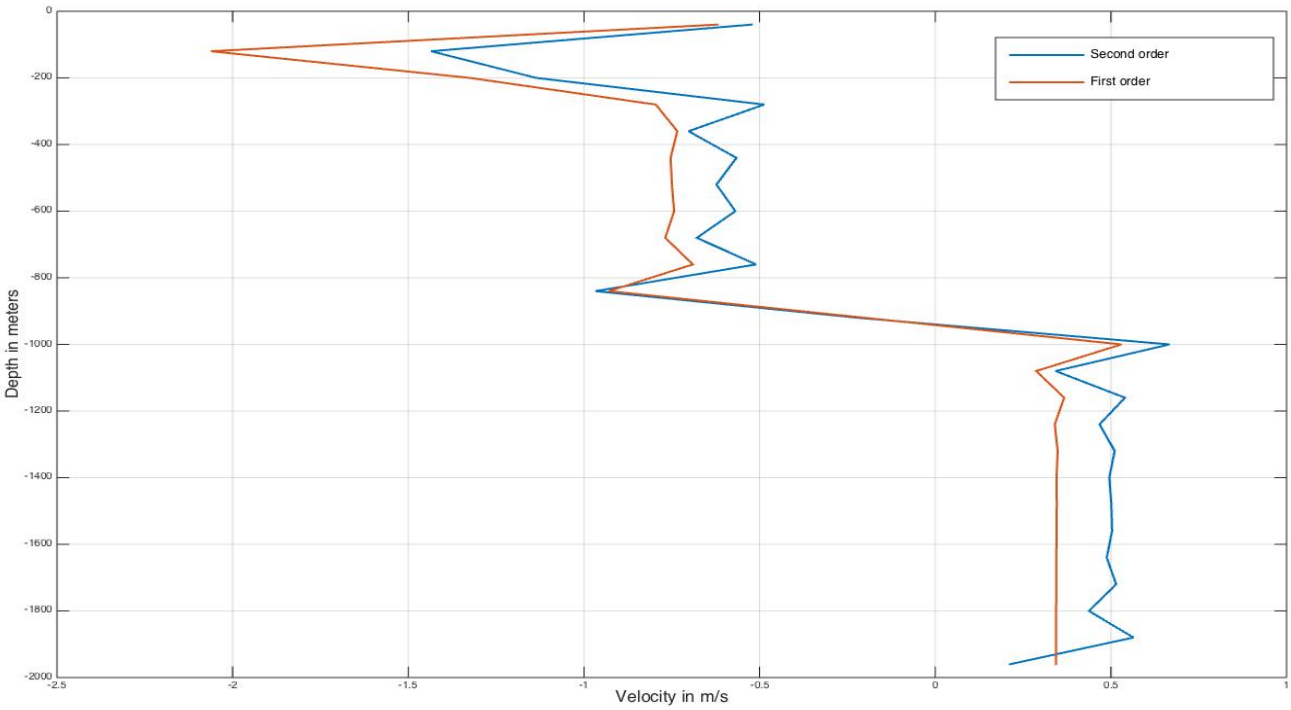

Figure 33: Gas velocity vs. depth, 600 sec

When it comes to the comparison of two schemes, the 2nd order scheme delivers more accurate results in case of velocity profiles. There is less diffusion of the gas/mud interface on top of the well even though the difference is quite small. Another very interesting aspect should be mentioned here. In Figure 33, below 1000 meters liquid velocity is supposed to be 0 as there is no circulation in this part of the well. This is the case for the 2nd order scheme, but not for the 1st order. The problem of the 1st order scheme delivering a negative velocity field for static conditions has been encountered before (Fjelde et al., 2016). The 2nd order scheme seems to solve this problem and deliver more realistic results. In general, the velocity profile delivered by the 1st order scheme is also somewhat lower in other parts of the well. When it comes to gas concentration, both plots are quite similar. There is less diffusion with the 2nd order scheme as the plot seems to look more like a straight line at around 200 meters, but the difference with the 1st order scheme is very small. The same can be said about the pressure profile, plots are nearly identical.

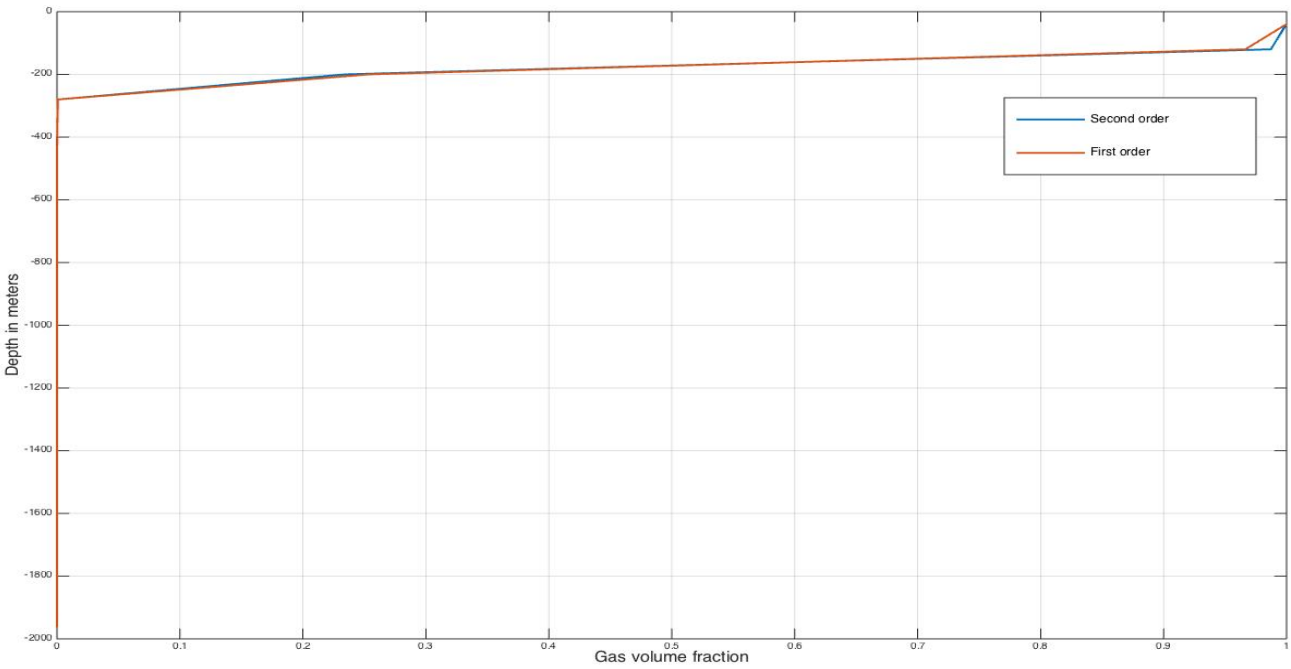

Figure 34: Gas volume fraction vs. depth, 600 sec

The last time situation to be considered is 1000 seconds, the end of the simulation. The gas volume fraction versus depth has already been plotted in Figure 23. The rig pumps were ramped up again at 800 seconds. Before that, the mud in the annulus has dropped to 440 meters and stabilized at that level. The pressure has dropped accordingly due to loss of the hydrostatic head on the top. This can be seen in Figure 15. Above 400 meters it is close to 1 bar atmospheric pressure. The velocity profiles are plotted in Figures 36 and 37.

At this stage the liquid column above the SMP is kept "static", the fluid enters the well from the bottom and exits at approximately 1000 meters. The 2nd order scheme describes this scenario quite well. The same problem of negative velocity occurs with the 1st order scheme above SMP and below 400 meters, where the liquid velocity must be close to 0. The mean value of the velocity in that interval seems to be close to 0 for the 2nd order scheme, which again proves its advantage over the 1st order.

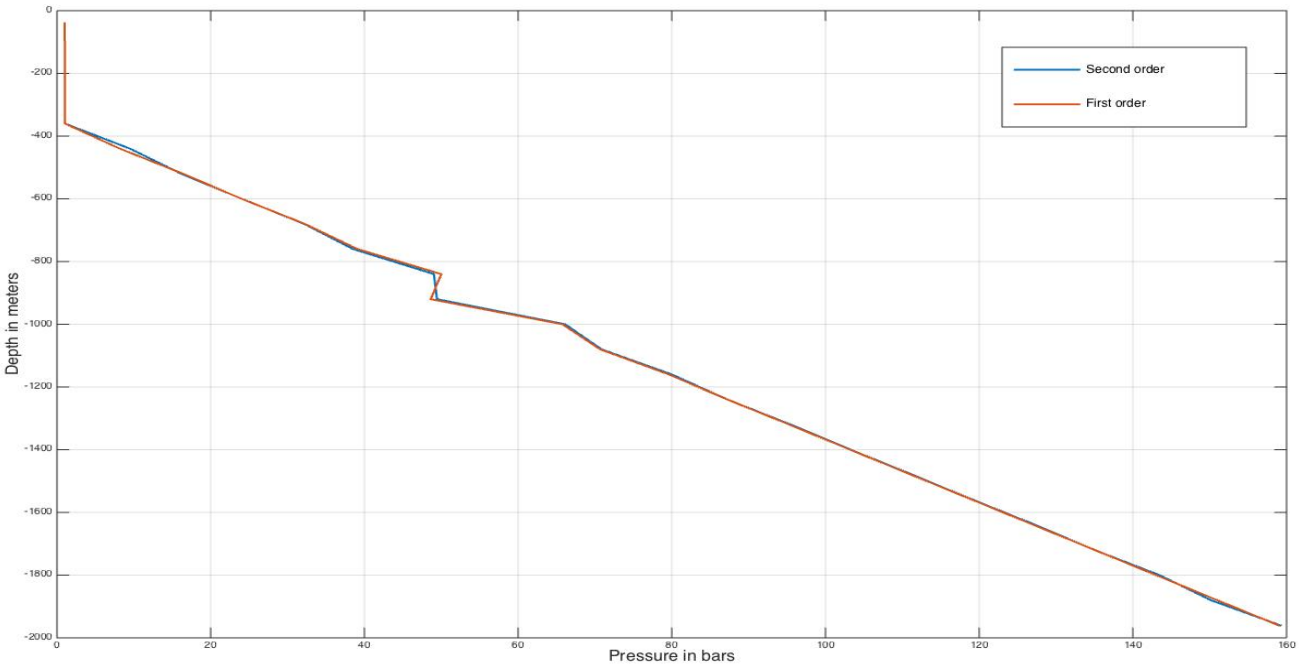

Figure 35: Pressure vs. depth, 1000 sec

A negative unphysical liquid velocity spike on top can be caused by boundary conditions. However, this rare liquid velocity profile does not seem to cause any problem for the rest of the results since liquid concentration is very little. In both plots for liquid and gas, the phase velocities are quite disturbed above the mud/gas interface. This was even more pronounced compared to the time situation at 600 seconds. These disturbances are understandable due to very difficult scenario from the simulation point of view. The liquid is being injected and withdrawn from the system at the same time, the behavior of the "static" two-phase flow region above the SMP can be very hectic. This case can be considered as a good test of the robustness of the AUSMV scheme.

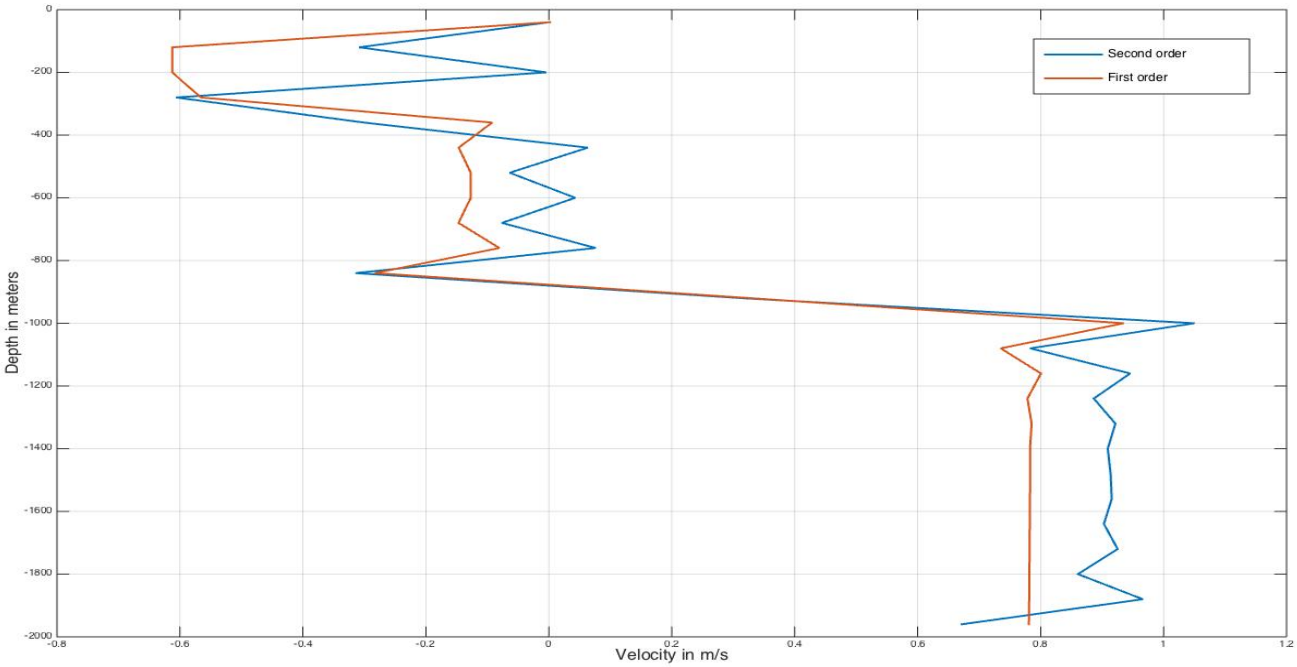

Figure 36: Liquid velocity vs. depth, 1000 sec

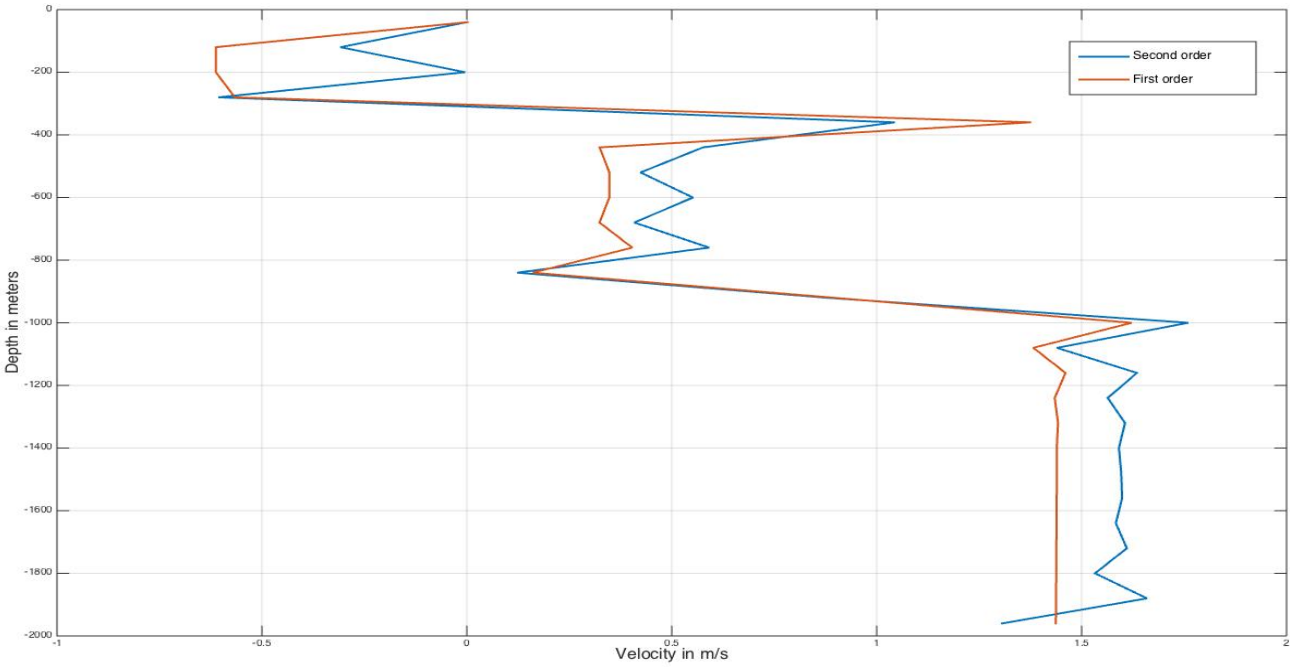

Figure 37: Gas velocity vs. depth, 1000 sec

6.2 Simulation two

The goal for this simulation was to adapt the already tested CML case with the 2nd order scheme for a small-scale experimental loop at UIS described in chapter five. The necessary changes to the code have been made in Appendix B. For well data refer to Table 5:

Table 5: Well data, Simulation Two

Fluid data:		Well Geometry	
liquid Viscosity:	0.05 Pa*s	Well depth (MD):	50m
Gas Viscosity:	0.0182*10^(-3) Pa*s	Inner diameter (ID):	0m
K:	1.0	Outer diameter (OD):	0.033m
S:	0.5	Inclination:	84
P standard conditions:	100000 Pa	Well depth (TVD):	5m
ρ standard conditions:	1000 kg/(m^3)		

The liquid viscosity was increased to 0.05 Pa*s in order to reduce pressure pulses. The well depth in MD has been changed according to the small-scale geometry. The number of discretization boxes was kept the same. This affected the CFL condition as value of dx decreased, therefore dt value had to be changed accordingly. After several attempts it was concluded that dt equal to 0.00025 seconds gives the best results with respect to computational time and accuracy of simulations. With these parameters the CFL value was again equal to 0.1875. The K value was set to 1 instead of 1.2. The annulus flow in the previous simulation was changed to the pipe flow with diameter of 0.033 meters equal to the flow loop diameter. To reproduce realistic small-scale configuration and take inclination into account, each calculation involving hydrostatic pressures was multiplied by $\cos(84)$. This made the theoretical well almost horizontal and kept parameters like friction gradient and length of boxes dx unchanged. The TVD of the well is then equal to 5 meters. The way all these changes have been integrated in the code is marked with red color in Appendix B. For the liquid rates in and out of the system refer to Table 6:

Table 6: Liquid rates, Simulation Two

Time (sec)	Liquid rate in (kg/s)	Time (sec)	Liquid rate out (kg/s)
0-5	0	0-5	0
5-10	0	5-10	0.5*(time-5)/5
10-30	0	10-30	0.5
30-35	0.5*(time-30)/5	30-35	0.5
35-50	0.5	35-50	0.5

In the first five minutes of simulation no liquid enters or exits the system. Next, interpolation is introduced, the same way as for the first simulation but this time it was only 5 seconds. The suction point begins to reduce the mud level in the loop. This continues with steady liquid-rate-out equal to 0.5 kg/s. At 30 seconds liquid starts to reenter the system from the bottom with the same rate. Liquid rates in and out remain unchanged until the end of the simulation. The whole simulation takes 50 seconds. The scenario is similar to Simulation One, with the difference that this time mud level is reduced first and then stabilized at a constant level. The theoretical SMP is placed at the same box number 14, which in this case equals to 23 meters, approximately half of the well. The changes to fluid rates can be tracked in Appendix B marked with red color.

6.2.1 EC-Drill case for the small-scale loop

From the early stages it was clear that the main difficulty with the stated task was the size of the small-scale loop. The high inclination angle, small diameter and short length of the pipe resulted in very low BHP. If the model simulated in Simulation One delivered pressures in the range of 200 bars, then in case of Simulation Two hydrostatic pressure component was equal to approximately 0.5 bars. The absolute pressure is then equal to 1.5 bars and that is very close to the atmospheric pressure. This created problems for the AUSMV scheme. The BHP pressure plots showed an unrealistic increase in pressure right when the suction point was introduced reaching as high as 1500 bars. After already 10 seconds the simulation failed. This was obviously a mistake that had its roots some place in the code. Several parameters like outlet pressure, liquid rates and simulation scenario were adjusted in order to find a solution but with no success.

After further investigation the problem was found in the pressure condition described before in chapter four when adapting the scheme to CML case. This condition was

specifically related to the upper boxes to ensure a realistic behavior of the model and to avoid vacuum condition. It was stated in such a way that pressure in each box would have a minimum value of 1 bar. However, since pressures in the small-scale model are very low, after introducing the suction point to the small-scale loop, this condition was interfering in the boxes below the SMP. This was not the initial intention. Hence, the condition itself needed to be changed or another way of dealing with this problem needed to be found.

The first solution was found by pressurizing the well from the top with 10 bars to expand the simulation capacity. The total pressure is then represented by hydrostatic pressure, friction and surface pressure equal to 10 bars. To implement this change, the outlet pressure fluxes mentioned in 5.1.1 were then set to 10 bars instead of 1 bar as before. The system behavior was then stabilized and simulation was adequate until the end. The BHP has been plotted in Figure 38.

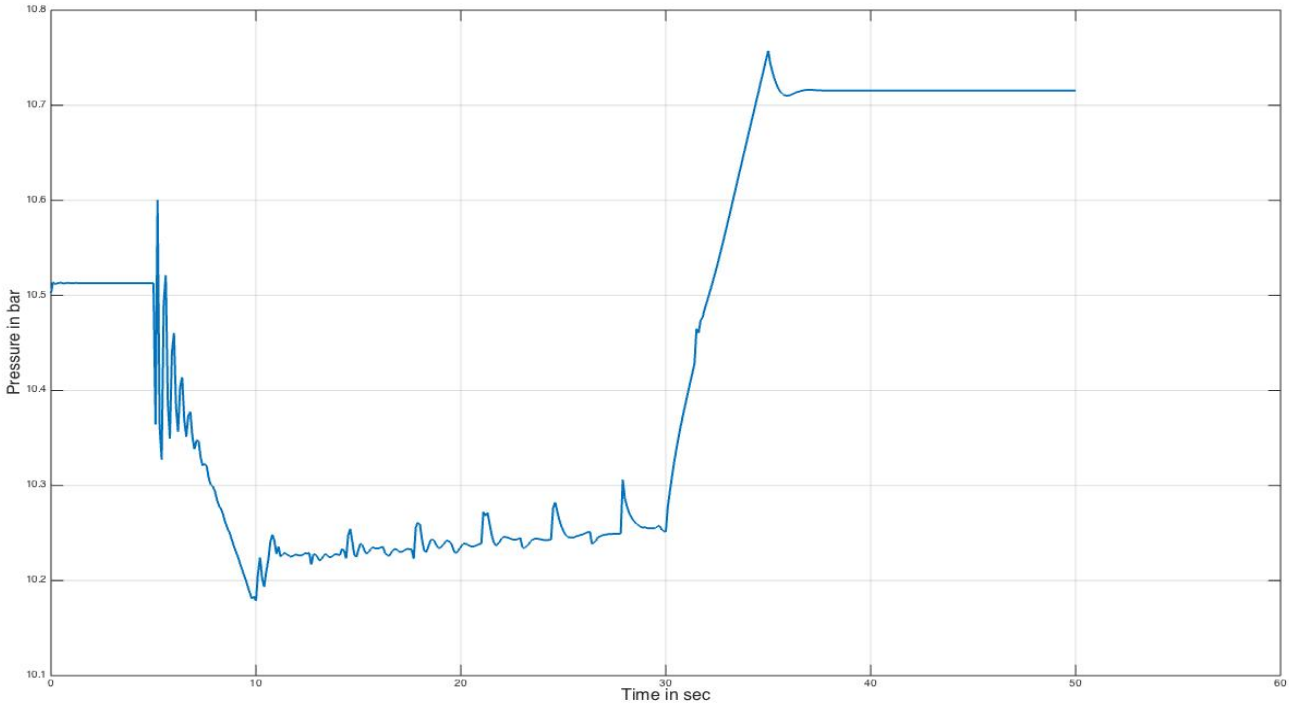

Figure 38: BHP vs. time, 10 bar overpressure

As one can see, pressure drops with approximately 0.35 bars after the suction point has been introduced. It later stabilizes at around 10.21 bars and goes up again when liquid starts to enter the system from the bottom around 30 seconds. Eventually it

becomes stable at 10.72 bars, when liquid-rate-in is equal to liquid-rate-out. The pressure pulses are still quite high at the beginning despite the fact that viscosity has been sufficiently increased. The BHP behavior is as expected apart from the period between 10 and 30 seconds when liquid is extracted from the system. During this time the suction rate is constant and equal to 0.5 kg/s according to Table 6. This means that after 10 seconds from the simulation start the mud level is still dropping which should be reflected in the BHP. The BHP should decrease, however, on Figure 38 it is clear that pressure slowly increases until 30 seconds. To understand better this phenomenon several additional plots were taken. For hydrostatic and friction gradients refer to Figures 39 and 40 respectively. Gas volume fraction is plotted in Figure 41.

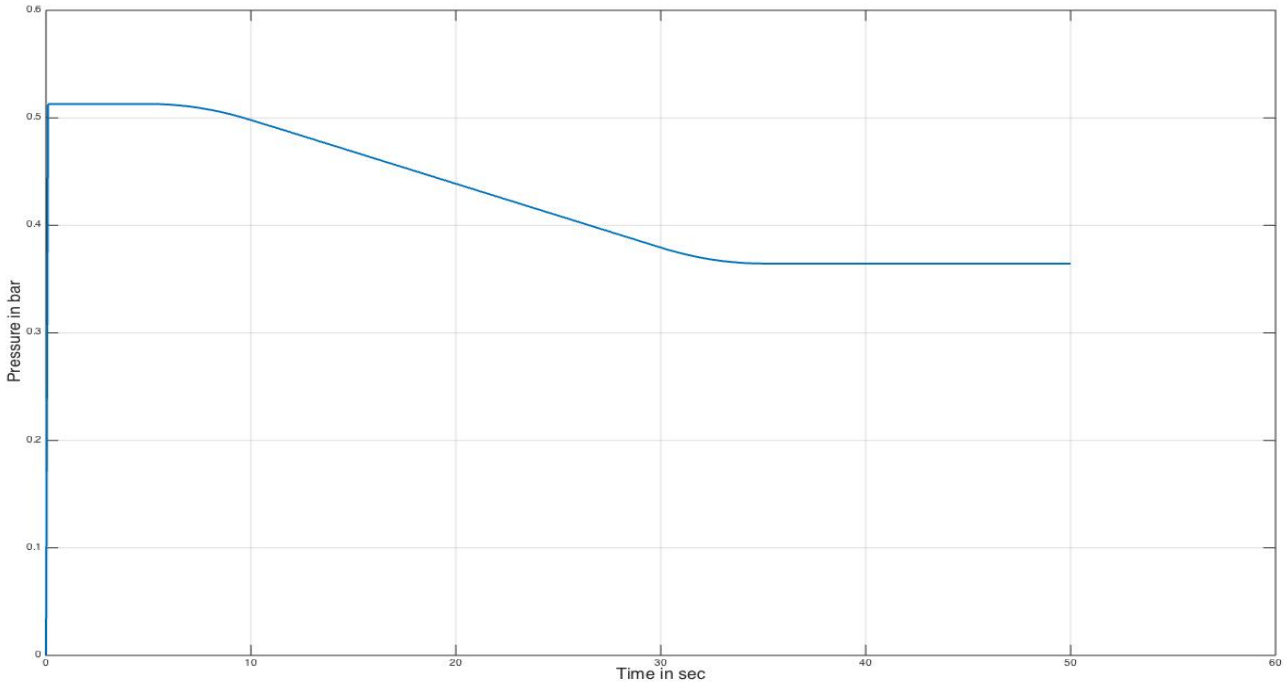

Figure 39: Hydrostatic pressure gradient vs. time, 10 bar overpressure

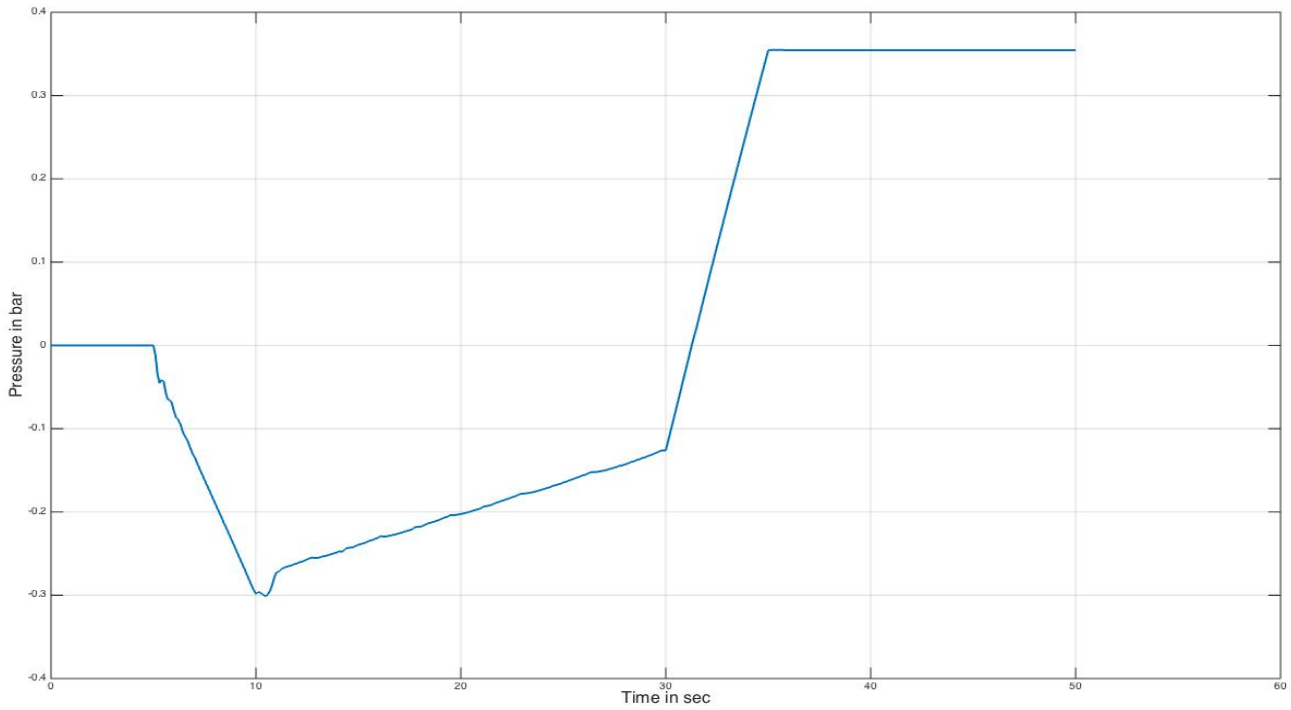

Figure 40: Friction pressure gradient vs. time, 10 bar overpressure

The hydrostatic pressure gradient is reduced as expected. The mud level in the flow-loop has dropped to 17 meters, this can be confirmed by Figure 41. These factors are indicating that the changes made to the code are adequate and the simulation is running the way it should. The only parameter that can explain the pressure behavior between is friction. As one can see, friction becomes negative when interpolation starts at 5 seconds. This negative friction causes the largest pressure drop between 5 and 10 seconds seen on the Figure 38. The reason for that was already discussed in Simulation One. This is due to the negative direction of the flow since the fluid is moving downwards. This effect is expected, however, after interpolation is over at 10 seconds and liquid-rate-out becomes constant and equal to 0.5 kg/s, negative friction begins to decrease in magnitude for the rest of the interval. This can be explained by the mixed viscosity parameter in the friction model. The same behavior of friction forces was observed in Figure 26 in Simulation One. Since gas is beginning to fill the upper part of the well, the mixed viscosity is reduced, and that reduces the friction in magnitude although it is still negative. This explains the fact that the BHP increases between 10 and 30 seconds in Figure 38, and not decreases due to reduced hydrostatic component. Considering Simulation One the decrease in hydrostatic pressure gradient

was the dominant factor for the BHP behavior, however, the example here is totally dominated by the friction pressure gradient. This again comes from the high inclination angle, small pipe diameter and the resulting low hydrostatic pressure of 0.5 bars. The largest pressure drop equal to 0.35 bars between 5 and 10 seconds is related mostly to friction, as the mud level has not been dropped sufficiently to influence the BHP at this time. From Figure 41, the reduction in mud level at the end of simulation time equal to 34% caused only 0.15 bars reduction in the hydrostatic pressure and consequently the BHP. It is worth to mention here that with the small-scale model like this, pressure pulses can reach very high values. The AUSMV scheme has an integrated acceleration parameter, the actual reason for the pressure pulses. With the small pipe diameter of 0.033 meters like in our case, even small changes to the system can result in high pressure pulses.

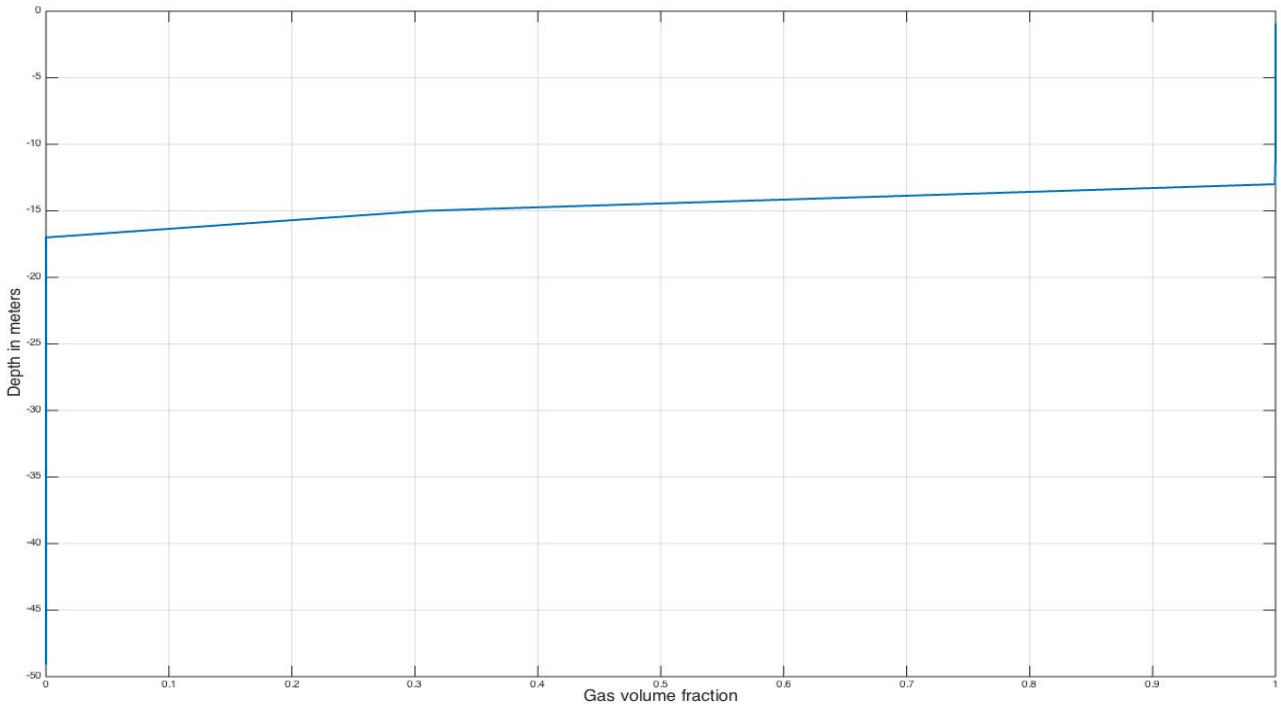

Figure 41: Gas volume fraction vs. depth, 10 bar overpressure, 50 sec

Even though the proposed simulation solution worked quite well and can be used for the actual small-scale loop experiments, a pressurized model is not a realistic scenario. In the method described above the pressure in static conditions is composed of 10 bars overpressure and just 0.5 bars actual hydrostatic pressure. To make simulations

more realistic, the pressure condition that caused the problem was investigated further. An alternative solution that delivers more realistic results was found. This solution involves changes to the pressure condition itself rather than manipulation with the outlet pressure fluxes. To avoid the problem of the pressure condition interfering the scheme sequence below the suction point, the condition was made specifically to act in discretization boxes above that point. In addition to that it was written in such a way that it would work only in the boxes where liquid volume fraction is less than 0.1. The intention with that was to separate the boxes filled with gas from the ones filled with liquid after the mud level reduction. This way of rewriting the pressure condition made it possible to operate within realistic pressure regimes delivered by the model, without over-pressuring the system from above. The way this was implemented in the code can be found in Appendix B marked in red color. The BHP with the alternative method is plotted in Figure 42. The friction pressure gradient and gas volume fraction are plotted in Figures 43 and 44 respectively, together with the previous plots for comparison. The change in hydrostatic pressure gradient through time is identical with Figure 39.

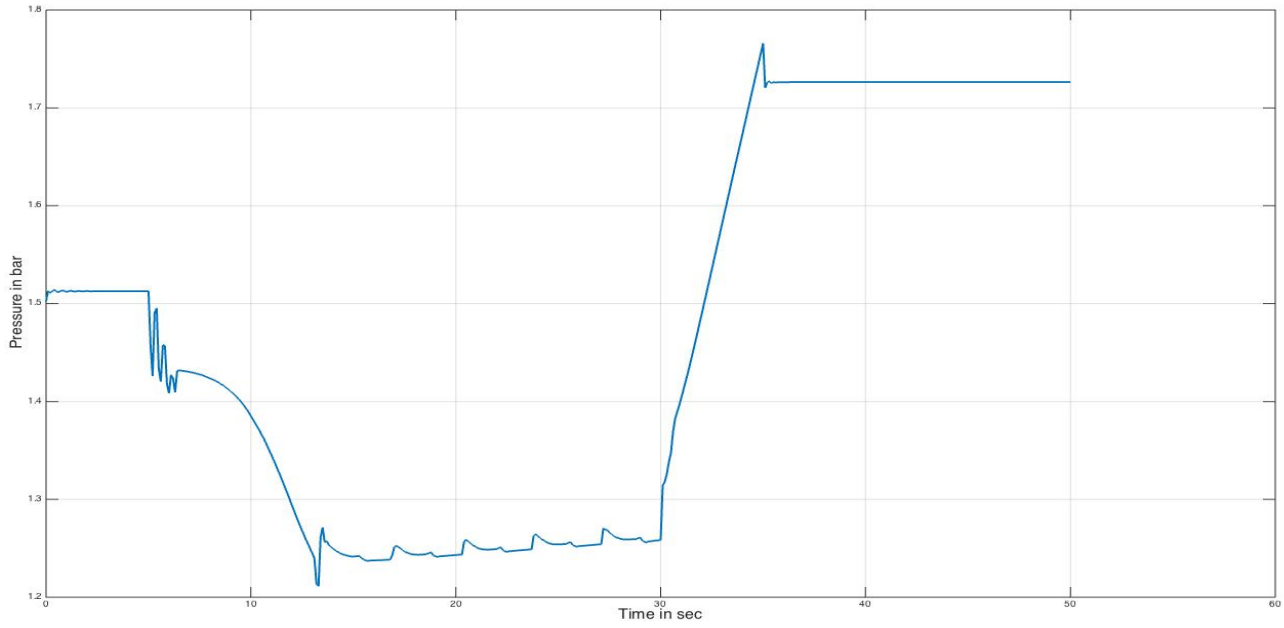

Figure 42: BHP vs. time, alternative method

The BHP behaves much smoother with the alternative method. The pressure pulses are significantly smaller during interpolation of the rate and later when the mud level continues to drop. Between 5 and 15 seconds, plots are different. The initial pressure

drop is actually less than in Figure 38, 0.3 bars instead of 0.35. During this interval the BHP with the alternative method drops gradually, where in Figure 38 the drop is more rushed. After 15 seconds the behavior is almost identical. The model proves to be friction dominated as it can be seen in 43. The difference between abrupt and more gradual change is clear here as well.

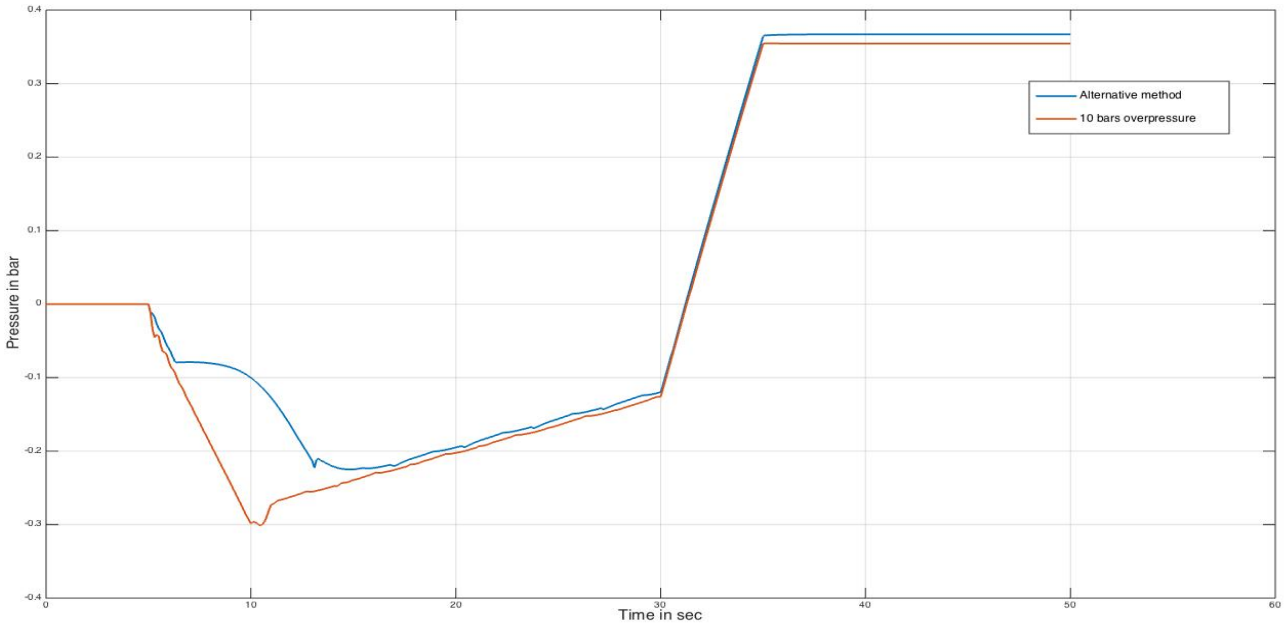

Figure 43: Friction pressure gradient vs. time, alternative method

An interesting observation from Figure 44 is a sudden increase in gas volume fraction at 23 meters, the depth where theoretical SMP is located. The explanation for this gas bubble right at the suction point lays in the pressure condition. After setting the pressure for the boxes filled with gas equal to 1 bar, primitive variables for these boxes are calculated again based on the new pressure value and old conservative variables. Since the liquid phase's conservative variable for this particular box is lower than for other boxes after introducing the suction point, this affects the new gas volume fraction. This problem is not seen with the 10 bars overpressure method. Further investigation is required. Because of this gas bubble the mud level in the flow-loop with the alternative method is higher. When using the overpressure method the level drops to 17 meters, but with the alternative method it drops to 15, two meters higher than it is supposed to.

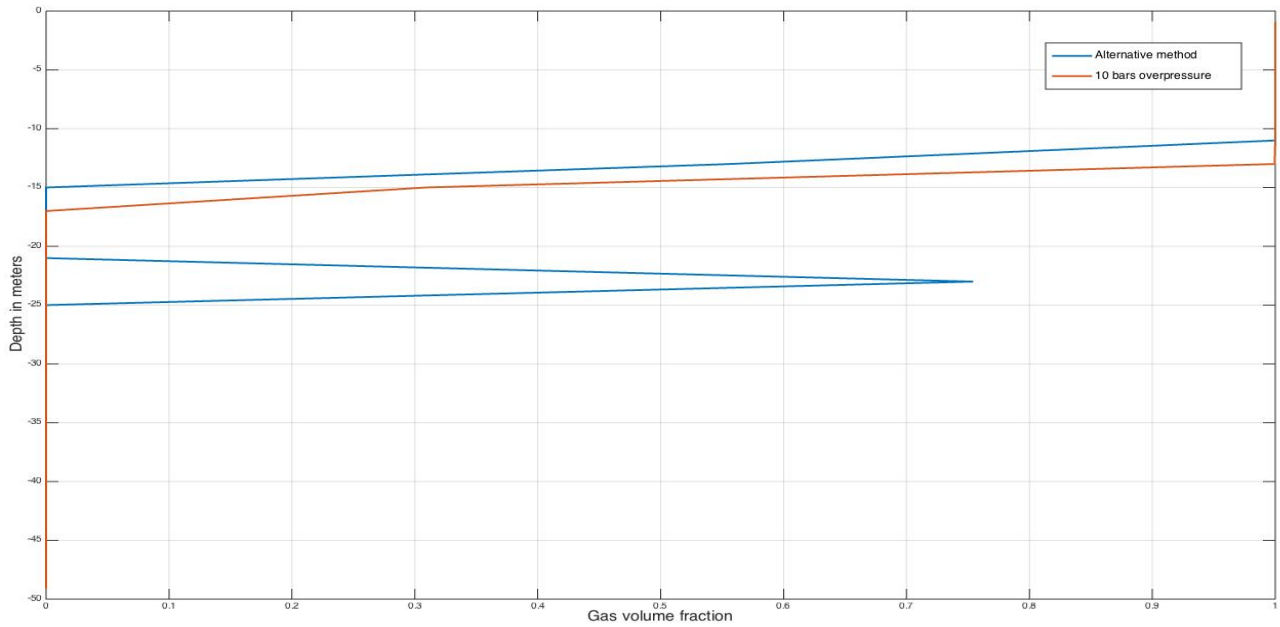

Figure 44: Gas volume fraction vs. depth, alternative method, 50 sec

To check which method gives a more realistic result, hand calculations similar to the ones performed in 5.1.1 were carried out. The total amount of liquid pumped out of the system equals to:

$$Mout = M_{5-10} + M_{10-30} + M_{30-35} = 1.25kg + 20sec * 0.5kg + (5sec * 0.5kg/s - 1.25kg) = 12{,}5kg \quad (28)$$

Corresponding volume is:

$$V = \frac{Mout}{\rho} = \frac{12.5kg}{1000(\frac{kg}{m^3})} = 0.0125m^3 \quad (29)$$

With the overpressure method the midpoint for the drop in mud level is 14.5 meters, which corresponds to $0.0123m^3$. This is quite a good match between the simulation results and the hand calculations. For the alternative method the midpoint is 13.9 meters, which corresponds to $0.0113m^3$. This value is lower by $0.001m^3$, however, if we take into account the volume of the gas bubble and add them together we get better matching results. The gas bubble is located between 21 and 25 meters with maximum concentration of 0.754 at 23 meters. If we assume that half of that distance is represented by gas with the volume fraction of 0.754, the volume of the bubble then becomes:

$$V = A * H = \frac{\pi}{4} * (OD^2) * H * \alpha_g = \frac{\pi}{4} * (0{,}033^2 m) * 2m * 0{,}754 \quad (30)$$

$$= 0.0013m^3$$

The total volume of the liquid sucked from the system according to alternative method is then:

$$V_{tot} = V_{bubble} + V_{top} = 0{,}0013m^3 + 0{,}0113m^3 = 0{,}0126m^3 \quad (31)$$

This proves that both methods deliver realistic results. In general, to use the alternative method for simulation is more preferable, since there is no need for over pressuring the system. The results can then be easily compared to experimental studies conducted with the small-scale loop in the future. The pressure behavior with this method is more realistic and smooth. The only difficulty is the non-physical gas bubble at the suction point, which needs further investigation. This problem can be resolved with increased number of discretization boxes. To test this, simulation with 50 boxes was performed. Time-step dt parameter had to be halved due to lower dx value, which resulted in a longer simulation time. The result is plotted in Figure 45.

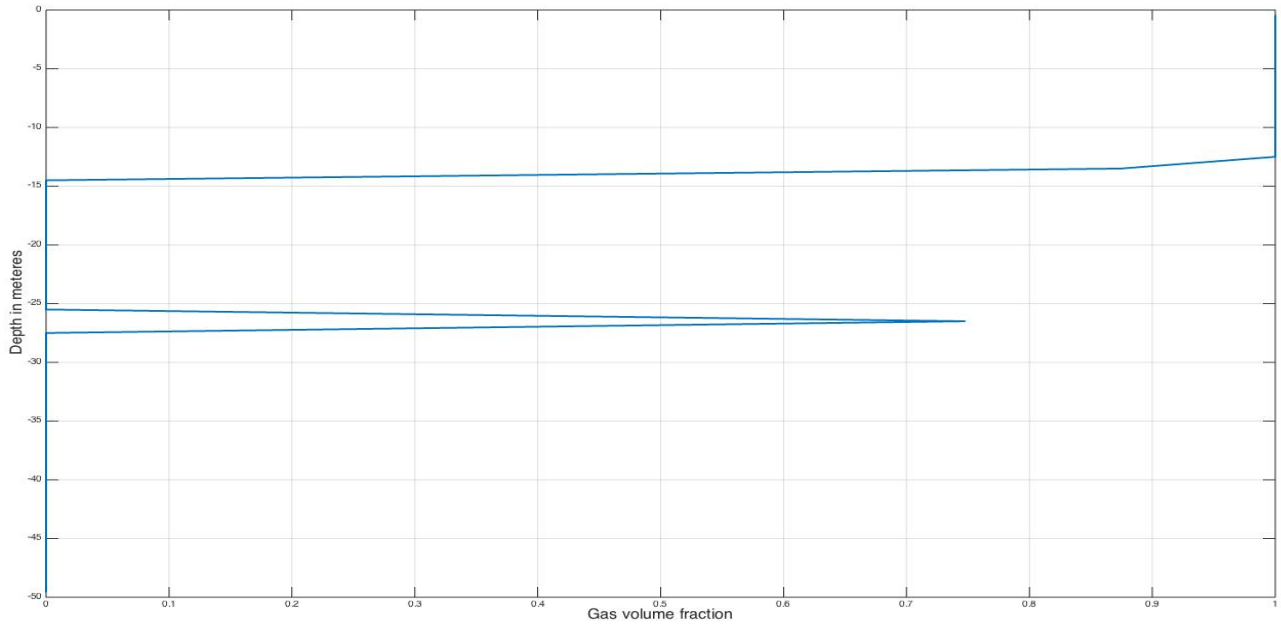

Figure 45: Gas volume fraction vs. depth, alternative method 50 boxes, 50 sec

The distance occupied by gas bubble has halved, now being between 27.5 to 25.5 meters. Hence, the volume effect will be less as well. Increasing the number of boxes

even further would eliminate the problem, if not completely, but quite close to that. However, this will result in a longer computational time, which is an undesired factor.

Motivated by the results in Simulation One, the problem of the 1st order scheme delivering negative velocity fields for static conditions was investigated in Simulation Two as well. Different time situations were taken similarly to Simulation One, and depth plots of liquid and gas velocities were studied. However, none of the observations confirmed the problem related to the 1st order scheme. One may speculate that since the small-scale model differs from the full-scale model with a high inclination angle, this problem might be somehow related to the gravity. The well geometry in Simulation Two is nearly horizontal, which is opposite to Simulation One where the well considered is vertical. Hence, gravity is more pronounced in Simulation One, where well depth reaches 2000 meters.

7 Conclusion

The literature survey on CML involved 17 publications in total. The survey was divided in several parts according to the material in the publications. First, historical development was reviewed. The rest of the survey was divided in non-commercial studies and commercial applications. The part dedicated to non-commercial studies reviewed the really first development of the concept at NTNU. EC-Drill was identified as a leading commercial application of CML technology with 11 publications out of 17. The main conceptual and technical aspects were described. Advantages and disadvantages of this commercially available technology were summarized in a separate sub-chapter. Well control and well control procedures in the end of the survey were broadly described in a separate sub-chapter. The following conclusions have been made:

- The successful applications of EC-Drill in regions like Azerbaijan, GOM, Brazil, The Caribbean and NCS as well as the rising interest and investments from leading oil companies like Statoil proves the importance of this technology for the industry.
- The main advantage of CML is active mud level control in the riser, which results in highly accurate BHP control. Active reduction or increase of hydrostatical pressure component results in several operational advantages like drilling with higher flow rates and hence assuring proper cuttings transport, simpler and time saving procedures for well testing, constant BHP during connections, higher mud density and hence presence of riser margin during any operation.
- One of the main advantages of this technology is early kick detection. Different configurations of the system can provide early kick detection through monitoring parameters like subsea pump speed, pressure inside the riser or power consumption of the subsea pump. Field experience claims that kick detection takes less than one minute.
- The main disadvantage of this technology is u-tube effect when circulation is stopped due to different mud levels in the annulus and the drill pipe. As a solution a DSV can be installed or fingerprinting can be used.

- Well control procedures similar to Driller's method have been developed and tested for this technology. An additional barrier like mud funnel has been installed on top of the riser to avoid gas accumulation.

A hydraulic model for an active mud level control is required. The model used for this thesis is the Drift Flux model, which was solved by the AUSMV numerical scheme. The most recent edition of the AUSMV 2nd order scheme was adopted for CML case scenario and simulations were performed. The main challenge was to specify the outlet pressure flux. Three methods were investigated, setting the flux to the fixed value equal to 1 bar atmospheric pressure and two extrapolation methods. After identifying the best method, the results were compared to the 1st order scheme. Several conclusions can be made on these simulations:

- All three methods for outlet pressure flux worked. The two extrapolation methods worked only after setting the outlet gas fluxes to 0, otherwise they generated an unphysical pressure build-up. Setting the outlet pressure flux equal to 1 atm was the only method that delivered realistic results. The indicator for this was a more adequate drop in friction after the system started to adjust the mud level in the well. Both extrapolation methods delivered unphysical friction pressure drop equal to 8 bars.
- The 2nd order scheme delivered more accurate results compared to the 1st order. The numerical diffusion was reduced with the 2nd order. The simulations confirmed the main problem of the 1st order scheme by delivering negative velocity fields for static conditions. This was evident in the depth plots for liquid velocity in the first simulation scenario where gravity is the dominant factor. The 2nd order scheme showed more adequate results in this case.
- The pressure pulses seen during adjustments of the liquid rates were discussed in relation to friction. During the circulations, when friction is present, the effect of these pressure pulses is less noticeable since friction damps the pulses. If the well is static it can take longer time for pulses to be damped.
- Some of the disturbances seen in the depth plots for velocity of liquid and gas when considering the region around the mud/gas interface can be caused by the numerical boundary treatment. However, they do not seem to affect the correctness of the simulation results.

- The outlet pressure at the start of the simulation showed higher pressure than expected. It was calculated by using the values in the top box. However, this does not seem to affect the pressure in other locations as it was confirmed by hand calculations. The cause for this should be investigated in future research for example by checking if this could be caused by the boundary treatment.

The AUSMV 2nd order scheme was then adapted for the small-scale model at UIS. In the future, comparing the simulation results of a CML case with actual experiments on the small-scale loop will test the reliability of the scheme. Several points can be made:

- The scheme was adapted to the small-scale approximated model with real small-scale geometry data. Numerical problems occurred since the pressures simulated were very close to the atmospheric conditions due to the configuration of the model. In this case pressure pulses or negative friction could lead to a situation where the pressure in boxes becomes lower than 1 atm. Because of this, the pressure condition first implemented for handling the free gas region was unintentionally interfering in other boxes filled with liquid.
- To resolve these problems two methods were introduced. The first method involves pressurizing the system by adding a surface pressure on the top. Then the risk for having pressures below 1 atm is reduced. The second method adjusts the specific pressure condition in the code by separating liquid and gas boxes with the help of volume fraction.
- Since it is not easy to pressurize the experimental set-up, the second method is closer to describing the real experimental case. A small gas bubble emerged in the box containing the subsea pump. This was a side effect of the numerical fix related to the pressure condition. However, this problem can be mitigated by increasing the number of discretization boxes or by additional simple hand calculations for correcting the results.
- The simulation results showed that the model is extremely friction dominated. The effect from the reduction in the hydrostatic pressure component due to the drop in mud level was almost entirely masked by the negative friction effect observed in both simulation cases. When mud continues to drop and more air

is sucked from the top of the well, the overall mixture viscosity is reduced. This lowers the magnitude of the negative friction pressure component. As a result, the BHP increases despite the fact that the mud level continues to drop.

- The problem of the 1st order scheme delivering negative velocity fields in static conditions was investigated in these simulations as well. However, this time it was not observed. This led to the conclusion that this problem might be somehow related to the gravity aspect, since the model in these simulations is almost horizontal.

Studying the CML case with this experimental flow-loop might be difficult in the future since CML technology mostly relies on changes in the hydrostatic pressure component by reducing the mud level. In the simulations conducted in this thesis the suction point was placed always in the middle of the well. As a possible solution to this problem one may move the suction point higher up in the well. This will reduce the height of the fluid column above the suction point, which is the main contributor to the negative friction effect.

8 References

Aadnøy, B.S. 2010. *Modern Well Design, Second edition*. Chapter 2, Rock Mechanics, pp. 9-14. Leiden, The Netherlands: CRC Press/Balkena

Alford, S., Asko, A., Campbell, M. et al. 2005. Silicate-Based Fluid, Mud Recovery System Combine to Stabilize Surface Formations of Azeri Wells Paper SPE 92769-MS presented at the IADC/SPE Drilling Conference, Amsterdam, The Netherlands, 23-25 February. DOI: http://dx.doi.org/10.2118/92769-MS

Breyholtz, Y., Nygaard, G., Nikolaou, M. et al. 2009. Advanced Automatic Pressure Control for Dual-Gradient Drilling Paper SPE 124631-MS presented at the SPE Annual Technical Conference and Exhibition, New Orleans, Louisiana, USA, 4-7 October. DOI: http://dx.doi.org/10.2118/124631-MS

Choe, J., Schubert, J., Juvkam-Wold, H. et al. 2007. Analyses and Procedures for Kick Detection in Subse Mudlift Drilling Paper SPE 87114-PA, *SPE Journal* **22** (4). DOI: http://dx.doi.org/10.2118/87114-PA

Chustz, M., May, J., Wallace, C. et al. 2007. Managed-Pressure Drilling With Dynamic Annular Pressure-control System Proves Successful in Redevelopment Program on Auger TLP in Deepwter Gulf of Mexico Paper SPE 108348-MS presented at the IADC/SPE Managed Pressure Drilling and Underbalanced Operation Conference, Galveston, Texas, USA, 28-29 March. DOI: http://dx.doi.org/10.2118/108348-MS

Cohen, J., Kleppe, J., Grønås, T. et al. 2010. Golf of Mexico's First Application of Riserless Mud Recovery for Top-hole Drilling – A case Study Paper OTC 20939-MS presented at the Offshore Technology Conference, Houston, Texas, USA, 3-6 May. DOI: http://dx.doi.org/10.4043/20939-MS

Cohen, J., Stave, R., Hauge, E. et al. 2015. Field Trial of Well Control Solutions with a Dual Gradient Drilling System Paper SPE 173822-MS presented at the IADC/SPE Managed Pressure Drilling and Underbalanced Operations Conference and Exhibition, Dubai, UAE, 13-14 April. DOI: http://dx.doi.org/10.2118/173822-MS

Dowell, J. 2010. Deploying the World's First Commercial Dual Gradient Drilling System Paper SPE 137319-MS presented at the SPE Deepwater Drilling and Completions Conference, Galveston, Texas, USA, 5-6 October. DOI: http://dx.doi.org/10.2118/137319-MS

Eggemeyer, J., Akins, M., Brainard, R. et al. 2001. Subsea Mudlift Drilling: Design and Implementation of a Dual Gradient Drilling System Paper SPE 71359-MS presented at the SPE Annual Technical Conference and Exhibition, New Orleans, Louisiana, USA, 30 September-3 October. DOI: http://dx.doi.org/10.2118/71359-MS

Erivwo, O. and Adeleye, O. et al. 2012 Narrow Margin Drilling in Deepwater: Solution Concepts Paper SPE 156254 presented at the SPE Deepwater Drilling and Completions Conference, Galveston, Texas, USA, 20-21 June. DOI: http://dx.doi.org/10.2118/156254-MS

Falk, K., Fossli, B., Lagerberg, C. et al. 2011. Well Control When Drilling With a Partly-Evacuated Marine Drilling Riser Paper SPE 143095-MS presented at the IADC/SPE Managed Pressure Drilling and Underbalanced Operations Conference and Exhibition, Denver, Colorado, USA, 5-6 April. DOI: http://dx.doi.org/10.2118/143095-MS

Fjelde, K., Frøyen, J., Ghauri, A. et al. 2016. A Numerical Study of Gas Kick Migration Velocities and Uncertainty Paper SPE 180053-MS presented at the SPE Bergen One Day Seminar, Bergen, Norway, 20 April. DOI: http://dx.doi.org/10.2118/180053-MS

Fossli, B. and Sangesland S. et al. 2004. Controlled Mud-Cap Drilling for Subsea Applications: Well-Control Challenges in Deep Waters Paper SPE 91633-MS presented at the IADC/SPE Underbalanced Technology Conference and Exhibition, Houston, Texas, USA, 11-12 October. DOI: http://dx.doi.org/10.2118/91633-MS

Fossli, B. and Stave R. et al. 2014. Drilling Depleted Reservoirs using Controlled Mud Level Technology in Marine Subsea Fields Paper SPE 169178-MS presented at the SPE Bergen One Day Seminar Bergen, Norway, 2 April. DOI: http://dx.doi.org/10.2118/169178-MS

Godhavn, J., Gaassand, S., Hansen, K. et al. 2015. Development and First Use of Controlled Mud Level System in US Deepwater GoM Paper SPE 173814-MS presented at the IADC/SPE Managed Pressure Drilling and Underbalanced Operations Conference and Exhibition, Dubai, UAE, 13-14 April. DOI: http://dx.doi.org/10.2118/173814-MS

Godhavn, J., Gaassand, S., Hansen, K. et al. 2015. Development and First Use of Controlled Mud Level System in US Deepwater GoM Paper SPE 173814-MS presented at the IADC/SPE Managed Pressure Drilling and Underbalanced Operations Conference and Exhibition, Dubai, UAE, 13-14 April. DOI: http://dx.doi.org/10.2118/173814-MS

Godhavn, J., Hauge, S., Molde, D. et al. 2014. ECD Management Toolbox for Floating Drilling Units Paper OTC 25292-MS presented at the Offshore Technology Conference, Houston, Texas, USA 5-8 May. DOI: http://dx.doi.org/10.4043/25292-MS

Halkyard, J., Anderson, M., Maurer, W. et al. 2014. Hollow Glass Microspheres: An Option for Dual Gradient Drilling and Deep Ocean Mining Lift Paper OTC 25044-MS presented at the Offshore Technology Conference-Asia, Kuala Lumpur, Malaysia, 25-28 March. DOI: http://dx.doi.org/10.4043/25044-MS

Hannegan, D. 2006. Case studies-Offshore Managed Pressure Drilling Paper SPE 101855-MS presented at the SPE Annual Technical Conference and Exhibition, San Antonio, Texas, USA, 24-27 September. DOI: http://dx.doi.org/10.2118/101855-MS

Hauge, E., Godhavn, J., Molde, D. et al. 2015. Analysis of Field Trial Well Control Results with a Dual Gradient Drilling System Paper OTC 26056-MS presented at the Offshore Technology Conference, Houston, Texas, USA, 4-7 May. DOI: http://dx.doi.org/10.4043/26056-MS

Malloy, K., Stone, R., Medley, G. et al. 2009. Managed-Pressure Drilling: What It Is and What It Is Not Paper SPE 122281-MS presented at the IADC/SPE Managed Pressure Drilling and Underbalanced Operations Conference and Exhibition, San Antonio, Texas, USA, 12-13 February. DOI: http://dx.doi.org/10.2118/122281-MS

Malt, J. and Stave, R. et al. 2014. Ed-Drill MPD Dual Gradient Drilling for Challenging Pressure Regimes Paper OTC 25455-MS presented at the Offshore Technology Conference, Kuala Lumpur, Malaysia, 25-28 March. DOI: http://dx.doi.org/10.4043/25455-MS

Mirrajabi, M., Toftevag, K., Stave, R. et al. 2012. First Application of EC-Drill in Ultra Deepwater: Proven Subsea Managed Pressure Drilling Method Paper SPE 151100-MS presented at the SPE Drilling and Completions Conference, Galveston, Texas, USA, 20-21 June. DOI: http://dx.doi.org/10.2118/151100-MS

Rahman, s., Holt, C., Dowell, D. et al. 2015. Successful Testing of Single Gradient Subsea MudLift Drilling Technology in Deep Water Gulf of Mexico Paper SPE 174881-MS presented at the SPE Annual Technical Conference and Exhibition, Houston, Texas, USA, 28-30 September. DOI: http://dx.doi.org/10.2118/174881-MS

Rajabi, M., Rohde, B., Maguire, N. et al. 2012. Successful Implementations of Tophole Managed Pressure Cementing and Managed Pressure Drilling in the Caspian Sea Paper SPE 156889-MS presented at the IADC/SPE Managed Pressure Drilling and Underbalanced Operations Conference and Exhibition, Milan, Italy, 20-21 March. DOI: http://dx.doi.org/10.2118/156889-MS

Rehm, B., Schubert. J, Haghshenas A. et al. 2008. *Managed Pressure Drilling.* Chapter 3, Constant Bottom-Hole Pressure with Pressure as a Primary Control, pp. 81-107, Chapter 4, MPD with Flow Measurements as a Primary Control, pp. 109-126, Chapter 7, Mud Cap Drilling, pp. 155-180 and Chapter 8, Dual Gradient Drilling, pp. 181-226. Houston, Texas, USA: Golf Publishing Company

Rezk, R. 2013. Safe and Clean Marine Drilling with Implementation of "Reserless Mud Recovery Technology-RMR" Paper SPE 166839-MS presented at the SPE Arctic and Extreme Environments Technical Conference and Exhibition, Moscow, Russia, 15-17 October. DOI: http://dx.doi.org/10.2118/166839-MS

Santos, H., Reid, P., Jones, J. et al. 2005. Developing the Micro-Flux Control Method Part 1: System Development, Field Test Preparation and Results Paper SPE 97025-MS presented at the IADC/SPE Middle East Drilling Technology Conference and Exhibition, Dubai, United Arab Emirates, 12-14 September. DOI: http://dx.doi.org/10.2118/97025-MS

Schubert, J., Juvkam-Wold, H., Choe J., et al. 2006. Well Control Procedures for Dual Gradient Drilling as Compared to Conventional Riser Drilling Paper SPE 87114-PA, *SPE Journal* **21** (4). DOI: http://dx.doi.org/10.2118/99029-PA

Schumacher, J., Dowell, J., Ribbeck, L. et al. 2001. Subsea Mudlift Drilling: Planning and Preparation for the First Subsea Field Test of a Full-Scale Dual Gradient

Drilling System at Green Canyon 136, Gulf of Mexico Paper SPE 71358-MS presented at the SPE Annual Technical Conference and Exhibition, New Orleans, Louisiana, USA, 30 September-3 October. DOI: http://dx.doi.org/10.2118/71358-MS

Smith, D., Tarr, B., Winters, W. et al. 2010. Deepwater Riserless Mud Return System for Dual Gradient Tophole Drilling Paper SPE 130308-MS presented at the IADC/SPE Managed Pressure Drilling and Underbalanced Operations Conference and Exhibition, Kuala Lumpur, Malaysia, 24-25 February. DOI: http://dx.doi.org/10.2118/130308-MS

Smith, K., Bhalla, K., Huey, D. et al. 2013. Concept Alternatives and Feasibility Analyses of Dual Gradient Drilling Riser Systems Paper OTC 24081-MS presented at the Offshore Technology Conference, Houston, Texas, USA, 6-9 May. DOI: http://dx.doi.org/10.4043/24081-MS

Smith, K., Gault, A., Witt, D. et al. 2001. SubSea MudLift Drilling Joint Industry Project: Delivering Dual Gradient Drilling Technology to Industry Paper SPE 71357-MS presented at the SPE Annual Technical Conference and Exhibition, New Orleans, Louisiana, USA, 30 September-3 October. DOI: http://dx.doi.org/10.2118/71357-MS

Stave, R. 2015. Implementation of Dual Gradient Drilling Paper OTC 25222-MS presented at the Offshore Technology Conference, Houston, Texas, USA, 5-8 May. DOI: http://dx.doi.org/10.4043/25222-MS

Stave, R., Farestveit, R., Høyland, S. et al. 2005. Demonstration and Qualification Of A Riserless Dual Gradient System Paper SPE 17665-MS presented at the IADC/SPE Offshore Technology Conference, Houston, Texas, USA, 2-5 May. DOI: http://dx.doi.org/10.4043/17665-MS

Stave, R., Fossli, B., Endresen, C. et al. 2014. Exploration Drilling with Riserless Dual Gradient Technology in Arctic Waters Paper OTC 24588-MS presented at the Offshore Technology Conference, Houston, Texas, USA, 10-12 February. DOI: http://dx.doi.org/10.4043/24588-MS

Terwogt, J., Mäkiaho, L., van Beelen, N. et al. 2005. Pressured Mud Cap Drilling from A Semi-Submersible Drilling Rig Paper SPE 92294-MS presented at the IADC/SPE Drilling Conference, Amsterdam, Netherlands, 23-25 February. DOI: http://dx.doi.org/10.2118/92294-MS

Torsdal, A., 2015, Inclusion of temperature in the AUSMV scheme with simulation examples from Underbalanced and Mud Cap Drilling, MSc thesis. University of Stavanger, Norway. DOI: http://hdl.handle.net/11250/301298

Torsvik, M., 2011. Laboratory model of well drilling process. Construction, instrumentation, startup and regulation, MSc thesis. University of Stavanger, Norway. DOI: http://hdl.handle.net/11250/181755

Udegbunam, J., Fjelde, K., Evje, S. et al. 2015. On the Advection-Upstream-Splitting-Method Hybrid Scheme: A simple Transient-Flow Model for Managed-Pressure-Drilling and Underbalanced-Drilling Applications Paper SPE 168960-PA *SPE Journal* **30** (2). DOI: http://dx.doi.org/10.2118/168960-PA

Ziegler, R., Ashley, P., Malt, R. et al. 2013. Successful Application of Deepwater Dual Gradient Drilling Paper SPE 164561-MS presented at the IADC/SPE Managed Pressure Drilling and Underbalanced Operations Conference and Exhibition, San Antonio, Texas, USA, 17-18 April. DOI: http://dx.doi.org/10.2118/164561-MS

Ziegler, R., Sabri, M., Idris, M. et al. 2013. First Successful Commercial Application of Dual Gradient Drilling in Ultra-Deepwater GOM Paper SPE 166272-MS presented at the SPE Annual Technical Conference and Exhibition, New Orleans, Louisiana, USA, 30 September-2 October. DOI: http://dx.doi.org/10.2118/166272-MS

Appendix A, EC-Drill with 2nd order AUSMV scheme, Matlab code

Comments and inactivate variables in the code are separated by "%" symbol and marked in green, the same way it is in Matlab. All the changes made to the original code are marked in red. The pressure condition described in chapter 4 is marked in red as well. Parts related to the 2nd order scheme are marked in light blue and parts related to the 1st order scheme are marked in purple. The functions used in the main code to calculate densities, friction, fluxes etc. are given right after the main code.

```
% Transient two-phase code based on AUSMV scheme: Gas and Water
% The code assumes uniform geometry and the code is partially vectorized.

clear;
t = cputime
tic,

% Geometry data/ Must be specified
welldepth = 2000;
nobox = 25; %Number of boxes in the well
nofluxes = nobox+1;
dx = welldepth/nobox; % Boxlength
%dt = 0.005;

% Welldepth array
x(1)= -1.0*welldepth+0.5*dx;
for i=1:nobox-1
 x(i+1)=x(i)+ dx;
end

dt= 0.01;  % Timestep
dtdx = dt/dx;
time = 0.0;
endtime = 1000; % Rime for end of simulation
nosteps = endtime/dt;  %Number of total timesteps
timebetweensavingtimedata = 5;  % How often in s we save data vs time for
plotting.
nostepsbeforesavingtimedata = timebetweensavingtimedata/dt;

% Slip parameters used in the gas slip relation. vg =Kvmix+S
k = 1.2;
s = 0.5;


% Viscosities (Pa*s)/Used in the frictional pressure loss model.
viscl = 0.001; % Liquid phase
viscg = 0.0000182; % Gas phase

% Density parameters. These parameters are used when finding the
% primitive variables pressure, densities in an analytical manner.
% Changing parameters here, you must also change parameters inside the
% density routines roliq and rogas.

% liquid density at stc and speed of sound in liquid
  dstc = 1000.0;   %Base density of liquid, See also roliq.
  pstc = 100000.0; % Pressure at standard conditions, 100000 Pascal
  al = 1500; % Speed of sound/compressibility of liquid phase.
  t1 = dstc-pstc/(al*al); % Help variable for calculating primitive
```

```
variables from
  % conservative variables
% Ideal gas law constant
  rt = 100000;

% Gravity constant

  g = 9.81; % Gravitational constant

% Well opening. opening = 1, fully open well, opening = 0 (<0.01), the well
% is fully closed. This variable will control what boundary conditions that
% will apply at the outlet (both physical and numerical): We must change
% this further below in the code if we want to change status on this.

  wellopening = 1.0;  % This variable determines if
%the well is closed or not, wellopening = 1.0 -> open. wellopening = 0
%-> Well is closed. This variable affects the boundary treatment.

  bullheading = 0.0; % This variable can be set to 1.0 if we want to
simulate
% a bullheading operation. But the normal is to set this to zero.


% Specify if the primitive variables shall be found either by
% a numerical or analytical approach. If analytical = 1, analytical
% solution is used. If analytical = 0. The numerical approach is used.
% using the itsolver subroutine where the bisection numerical method
% is used.

  analytical = 1;


% Define and initialize flow variables

% Here we specify the outer and inner diameter and the flow area

   for i = 1:nobox
    do(i)=0.2159
    di(i) = 0.127;
    area(i) = 3.14/4*(do(i)*do(i)- di(i)*di(i));
   end


% Initialization of slope limiters.
  for i = 1:nobox
    sl1(i)=0;
    sl2(i)=0;
    sl3(i)=0;
    sl4(i)=0;
    sl5(i)=0;
    sl6(i)=0;
  end


% Now comes the initialization of the physical variables in the well.
% First primitive variables, then the conservative ones.


% Below we initialize pressure and fluid densities. We start from top of
% the well and calculated downwards. The calculation is done twice with
% updated values to get better approximation. Only hydrostatic
% considerations.

p(nobox)= 100000.0+0.5*dx*9.81*dstc;   % Pressure
dl(nobox)=rholiq(p(nobox));  % Liquid density
dg(nobox)=rogas(p(nobox));   % Gas density

for i=nobox-1:-1:1
p(i)=p(i+1)+dx*9.81*dl(i+1);
dl(i)=rholiq(p(i));
```

```
dg(i)=rogas(p(i));
end

for i=nobox-1:-1:1
p(i)=p(i+1)+dx*9.81*(dl(i+1)+dl(i))*0.5;
dl(i)=rholiq(p(i));
dg(i)=rogas(p(i));

end

% Initialize phase velocities, volume fractions, conservative variables
% The basic assumption is static fluid, one phase liquid.

for i = 1:nobox
  vl(i)=0; % Liquid velocity new time level.
  vg(i)=0; % Gas velocity at new time level
  eg(i)=0;  % Gas volume fraction
  ev(i)=1-eg(i); % Liquid volume fraction
  qv(i,1)=dl(i)*ev(i)*area(i);
  qv(i,2)=dg(i)*eg(i)*area(i);
  qv(i,3)=(dl(i)*ev(i)*vl(i)+dg(i)*eg(i)*vg(i))*area(i);
  fricgrad(i)=0;
  hydgrad(i)=g* qv(i,1);
end

source = zeros(nobox,3);


% Section where we also initialize values at old time level


for i=1:nobox
  dlo(i)=dl(i);
  dgo(i)=dg(i);
  po(i)=p(i);
  ego(i)=eg(i);
  evo(i)=ev(i);
  vlo(i)=vl(i);
  vgo(i)=vg(i);
  qvo(i,1)=qv(i,1);
  qvo(i,2)=qv(i,2);
  qvo(i,3)=qv(i,3);
end


% Initialize fluxes between the cells/boxes

for i = 1:nofluxes
  for j =1:3
   flc(i,j)=0.0; % Flux of liquid over box boundary
   fgc(i,j)=0.0; % Flux of gas over box boundary
   fp(i,j)= 0.0; % Pressure flux over box boundary
  end
end


% Main program. Here we will progress in time. First som   initializations
% and definitions to take out results. The for loop below runs until the
% simulation is finished.

countsteps = 0;
counter=0;
printcounter = 1;
pbot(printcounter) = p(1);
pchoke(printcounter)= p(nobox);
liquidmassrateout(printcounter) = 0;
gasmassrateout(printcounter)=0;
timeplot(printcounter)=time;
kickvolume=0;
bullvolume=0;
```

```
for i = 1:nosteps
   countsteps=countsteps+1;
   counter=counter+1;
   time = time+dt;

% Then a section where the boundary conditions are specified.
% Here we specify the inlet rates of the different phases at the
% bottom of the pipe in kg/s. We interpolate to make things smooth.
% It is also possible to change the outlet boundary status of the well
% here. First we specify rates at the bottom and the pressure at the outlet
% in case we have an open well. This is a place where we can change the
% code to control simulations.

XX = 4;
% XX (kg/s) is a variable for introducing a kick in the well.
YY = 15; % Liquid flowrate (kg/s) (1 kg/s = 1 l/s approx)

if (time<150)
  inletligmassrate=0.0;
  inletgasmassrate=0.0;
elseif((time>=150)&(time<160))
  inletligmassrate=22*(time-150)/10;
  inletgasmassrate=0.0;
elseif((time>=160)&(time<300))
  inletligmassrate=22;
  inletgasmassrate=0.0;
elseif((time>=300)&(time<310))
  inletligmassrate=22-22*(time-300)/10;
  inletgasmassrate=0.0;
elseif((time>=310)&(time<800))
  inletligmassrate=0;
  inletgasmassrate=0.0;
elseif((time>=800)&(time<810))
  inletligmassrate=22*(time-800)/10;
  inletgasmassrate=0.0;
elseif(time>810)
  inletligmassrate=22;
  inletgasmassrate=0.0;
end


kickvolume = kickvolume+inletgasmassrate/dgo(1)*dt;


% specify the outlet pressure /Physical. Here we have given the pressure as
% constant. It would be possible to adjust it during openwell conditions
% either by giving the wanted pressure directly (in the command lines
% above) or by finding it indirectly through a chokemodel where the
wellopening
% would be an input parameter. The wellopening variable would equally had
% to be adjusted inside the command line structure given right above.

 pressureoutlet = 100000.0;

% Based on these boundary values combined with use of extrapolations
techniques
% for the remaining unknowns at the boundaries, we will define the mass and
% momentum fluxes at the boundaries (inlet and outlet of pipe).

% inlet/bottom fluxes first.
   if (bullheading<=0)

     flc(1,1)= inletligmassrate/area(1);
     flc(1,2)= 0.0;
     flc(1,3)= flc(1,1)*vlo(1);


     fgc(1,1)= 0.0;
     fgc(1,2)= inletgasmassrate/area(1);
```

```
      fgc(1,3)= fgc(1,2)*vgo(1);

      fp(1,1)= 0.0;
      fp(1,2)= 0.0;

% Old way of treating the boundary
%     fp(1,3)= po(1)+0.5*(po(1)-po(2)); %Interpolation used to find the
% pressure at the inlet/bottom of the well.

% New way of treating the boundary
      fp(1,3)= po(1)...
            +0.5*dx*(dlo(1)*evo(1)+dgo(1)*ego(1))*g...
            +0.5*dx*fricgrad(1);



   else
     flc(1,1)=dlo(1)*evo(1)*vlo(1);
     flc(1,2)=0.0;
     flc(1,3)=flc(1,1)*vlo(1);

     fgc(1,1)=0.0;
     fgc(1,2)=dgo(1)*ego(1)*vgo(1);
     fgc(1,3)=fgc(1,2)*vgo(1);

     fp(1,1)=0.0;
     fp(1,2)=0.0;
     fp(1,3)=20000000; % This was a fixed pressure set at bottom when
bullheading
   end



% Outlet fluxes (open & closed conditions)

    if (wellopening>0.01)

% Here open end condtions are given. We distinguish between bullheading
% & normal circulation.

        if (bullheading<=0)

            flc(nofluxes,1)= dlo(nobox)*evo(nobox)*vlo(nobox);
            flc(nofluxes,2)= 0.0;
            flc(nofluxes,3)= flc(nofluxes,1)*vlo(nobox);


            fgc(nofluxes,1)= 0.0;
            fgc(nofluxes,2)= dgo(nobox)*ego(nobox)*vgo(nobox);
            fgc(nofluxes,3)= fgc(nofluxes,2)*vgo(nobox);

            fp(nofluxes,1)= 0.0;
            fp(nofluxes,2)= 0.0;
            fp(nofluxes,3)= pressureoutlet;
        else
            flc(nofluxes,1)= inletligmassrate/area(nobox);
            flc(nofluxes,2)= 0.0;
            flc(nofluxes,3)= flc(nofluxes,1)*vlo(nobox);

            fgc(nofluxes,1)=0.0;
            fgc(nofluxes,2)=0.0;
            fgc(nofluxes,3)=0.0;

            fp(nofluxes,1)=0.0;
            fp(nofluxes,2)=0.0;
            fp(nofluxes,3)= po(nobox)...
            -0.5*dx*(dlo(nobox)*evo(nobox)+dgo(nobox)*ego(nobox))*g...
            +0.5*dx*fricgrad(nobox);
        end
```

```
    else

% Here closed end conditions are given

          flc(nofluxes,1)= 0.0;
          flc(nofluxes,2)= 0.0;
          flc(nofluxes,3)= 0.0;

          fgc(nofluxes,1)= 0.0;
          fgc(nofluxes,2)= 0.0;
          fgc(nofluxes,3)= 0.0;

          fp(nofluxes,1)=0.0;
          fp(nofluxes,2)=0.0;

     %    Old way of treating the boundary
     %     fp(nofluxes,3)= po(nobox)-0.5*(po(nobox-1)-po(nobox));

     %    New way of treating the boundary
          fp(nofluxes,3)= po(nobox)...
          -0.5*dx*(dlo(nobox)*evo(nobox)+dgo(nobox)*ego(nobox))*g;
     %     -0.5*dx*fricgrad(nobox); % Neglect friction since well is closed.
         end


   % Include Suction Point

   suckrate = 0;

   if ((time>=400)&(time<410))
     suckrate = 22*(time-400)/10;
     flc(nofluxes,1)=0;
     flc(nofluxes,3)=0;

% To make both extrapolation methods work, gas fluxes are set to 0

%      fgc(nofluxes,2)=0;
%      fgc(nofluxes,3)=0;

% New extrapolation method described in SPE 180053:

%      fp(nofluxes,3)= po(nobox)...
%          -0.5*dx*(dlo(nobox)*evo(nobox)+dgo(nobox)*ego(nobox))*g...
%          -0.5*dx*fricgrad(nobox);

% Old extrapolation method described in SPE 168960:

%      fp(nofluxes,3)=po(nobox)-0.5*(po(nobox-1)-po(nobox));

% Fixed pressure equal to 1 atm delivered the most realistic results:

     fp(nofluxes,3)=100000;

   elseif(time>=410)
    suckrate = 22;
    flc(nofluxes,1)=0;
     flc(nofluxes,3)=0;

% To make both extrapolation methods work, gas fluxes are set to 0

%      fgc(nofluxes,2)=0;
%      fgc(nofluxes,3)=0;

% New extrapolation method described in SPE 180053:

%      fp(nofluxes,3)= po(nobox)...
%          -0.5*dx*(dlo(nobox)*evo(nobox)+dgo(nobox)*ego(nobox))*g...
%          -0.5*dx*fricgrad(nobox);

% Old extrapolation method described in SPE 168960:
```

```
%       fp(nofluxes,3)=po(nobox)-0.5*(po(nobox-1)-po(nobox));

% Fixed pressure equal to 1 atm delivered the most realistic results:

      fp(nofluxes,3)=100000;

    end



 % Implementation of slopelimiters. They are applied on the physical
 % variables like phase densities, phase velocities and pressure.

      for i=2:nobox-1
       sl1(i)=minmod(dlo(i-1),dlo(i),dlo(i+1),dx);
       sl2(i)=minmod(po(i-1),po(i),po(i+1),dx);
       sl3(i)=minmod(vlo(i-1),vlo(i),vlo(i+1),dx);
       sl4(i)=minmod(vgo(i-1),vgo(i),vgo(i+1),dx);
       sl5(i)=minmod(ego(i-1),ego(i),ego(i+1),dx);
       sl6(i)=minmod(dgo(i-1),dgo(i),dgo(i+1),dx);
      end

 % Slopelimiters in boundary cells are set to zero!
      sl1(nobox)=0;
      sl2(nobox)=0;
      sl3(nobox)=0;
      sl4(nobox)=0;
      sl5(nobox)=0;
      sl6(nobox)=0;

  % Ny Kode 11/11-15
      sl1(1)=0;
      sl2(1)=0;
      sl3(1)=0;
      sl4(1)=0;
      sl5(1)=0;
      sl6(1)=0;


% Now we will find the fluxes between the different cells.
% NB - IMPORTANE - Note that if we change the compressibilities/sound
velocities of
% the fluids involved, we need to do changes inside the csound function.

      for j = 2:nofluxes-1

 %%%%%%%%%%%%%%%%%%%%%%%%%%%%%%%%%%%%%%%%%%%%%%%%%%%%
 %%%%%%%%%%%%%%%%%%%%%%%%%%%%%%%%%%%%%%%%%%%%%%%%%%%%
 % First order method is from here:
%         cl = csound(ego(j-1),po(j-1),dlo(j-1),k);
%         cr = csound(ego(j),po(j),dlo(j),k);
%         c = max(cl,cr);
%         pll = psip(vlo(j-1),c,evo(j));
%         plr = psim(vlo(j),c,evo(j-1));
%         pgl = psip(vgo(j-1),c,ego(j));
%         pgr = psim(vgo(j),c,ego(j-1));
%         vmixr = vlo(j)*evo(j)+vgo(j)*ego(j);
%         vmixl = vlo(j-1)*evo(j-1)+vgo(j-1)*ego(j-1);
%
%         pl = pp(vmixl,c);
%         pr = pm(vmixr,c);
%         mll= evo(j-1)*dlo(j-1);
%         mlr= evo(j)*dlo(j);
%         mgl= ego(j-1)*dgo(j-1);
%         mgr= ego(j)*dgo(j);
%
%         flc(j,1)= mll*pll+mlr*plr;
%         flc(j,2)= 0.0;
%         flc(j,3)= mll*pll*vlo(j-1)+mlr*plr*vlo(j);
```

```
%
%        fgc(j,1)=0.0;
%        fgc(j,2)= mgl*pgl+mgr*pgr;
%        fgc(j,3)= mgl*pgl*vgo(j-1)+mgr*pgr*vgo(j);
%
%        fp(j,1)= 0.0;
%        fp(j,2)= 0.0;
%        fp(j,3)= pl*po(j-1)+pr*po(j);

 %  First order methods ends here
 %%%%%%%%%%%%%%%%%%%%%%%%%%%%%%%%%%%%%%%%%%%%%%%%%%%%%%%%%%%%
 %%%%%%%%%%%%%%%%%%%%%%%%%%%%%%%%%%%%%%%%%%%%%%%%%%%%%%%%%%%%



%%%%%%%%%%%%%%%%%%%%%%%%%%%%%%%%%%%%%%%%%%%%%%%%%%%%%%%%%%%%%%%
%%%%%%%%%%%%%%%%%%%%%%%%%%%%%%%%%%%%%%%%%%%%%%%%%%%%%%%%%%%%%%%
% Second order method starts here:
% Here slopelimiter is used on all variables except phase velocoties

       psll = po(j-1)+dx/2*sl2(j-1);
       pslr = po(j)-dx/2*sl2(j);
       dsll = dlo(j-1)+dx/2*sl1(j-1);
       dslr = dlo(j)-dx/2*sl1(j);
       dgll = dgo(j-1)+dx/2*sl6(j-1);
       dglr = dgo(j)-dx/2*sl6(j);

       vlv = vlo(j-1)+dx/2*sl3(j-1);
       vlh = vlo(j)-dx/2*sl3(j);
       vgv = vgo(j-1)+dx/2*sl4(j-1);
       vgh = vgo(j)-dx/2*sl4(j);

       gvv = ego(j-1)+dx/2*sl5(j-1);
       gvh = ego(j)-dx/2*sl5(j);
       lvv = 1-gvv;
       lvh = 1-gvh;

       cl = csound(gvv,psll,dsll,k);
       cr = csound(gvh,pslr,dslr,k);
       c = max(cl,cr);

       pll = psip(vlo(j-1),c,lvh);
       plr = psim(vlo(j),c,lvv);
       pgl = psip(vgo(j-1),c,gvh);
       pgr = psim(vgo(j),c,gvv);
       vmixr = vlo(j)*lvh+vgo(j)*gvh;
       vmixl = vlo(j-1)*lvv+vgo(j-1)*gvv;

       pl = pp(vmixl,c);
       pr = pm(vmixr,c);


      mll= lvv*dsll;
      mlr= lvh*dslr;
      mgl= gvv*dgll;
      mgr= gvh*dglr;

      flc(j,1)= mll*pll+mlr*plr;
      flc(j,2)= 0.0;
      flc(j,3)= mll*pll*vlo(j-1)+mlr*plr*vlo(j);


      fgc(j,1)=0.0;
      fgc(j,2)= mgl*pgl+mgr*pgr;
      fgc(j,3)= mgl*pgl*vgo(j-1)+mgr*pgr*vgo(j);

      fp(j,1)= 0.0;
      fp(j,2)= 0.0;
      fp(j,3)= pl*psll+pr*pslr;
```

```
%%% Second order method ends here
%%%%%%%%%%%%%%%%%%%%%%%%%%%%%%%%%%%%%%%%%%%%%%%%%%%%%%%%%%%%%%%%%%%%%%%
%%%%%%%%%%%%%%%%%%%%%%%%%%%%%%%%%%%%%%%%%%%%%%%%%%%%%%%%%%%%%%%%%%%%%%%

% Here sloplimiters is used on all variables. This
% has not worked so well yet.

%       psll = po(j-1)+dx/2*sl2(j-1);
%       pslr = po(j)-dx/2*sl2(j);
%       dsll = dlo(j-1)+dx/2*sl1(j-1);
%       dslr = dlo(j)-dx/2*sl1(j);
%       dgll = dgo(j-1)+dx/2*sl6(j-1);
%       dglr = dgo(j)-dx/2*sl6(j);
%
%       vlv = vlo(j-1)+dx/2*sl3(j-1);
%       vlh = vlo(j)-dx/2*sl3(j);
%       vgv = vgo(j-1)+dx/2*sl4(j-1);
%       vgh = vgo(j)-dx/2*sl4(j);
%
%       gvv = ego(j-1)+dx/2*sl5(j-1);
%       gvh = ego(j)-dx/2*sl5(j);
%       lvv = 1-gvv;
%       lvh = 1-gvh;
%
%       cl = csound(gvv,psll,dsll,k);
%       cr = csound(gvh,pslr,dslr,k);
%       c = max(cl,cr);
%
%       pll = psip(vlv,c,lvh);
%       plr = psim(vlh,c,lvv);
%       pgl = psip(vgv,c,gvh);
%       pgr = psim(vgh,c,gvv);
%       vmixr = vlh*lvh+vgh*gvh;
%       vmixl = vlv*lvv+vgv*gvv;
%
%       pl = pp(vmixl,c);
%       pr = pm(vmixr,c);
%       mll= lvv*dsll;
%       mlr= lvh*dslr;
%       mgl= gvv*dgll;
%       mgr= gvh*dglr;
%
%       flc(j,1)= mll*pll+mlr*plr;
%       flc(j,2)= 0.0;
%       flc(j,3)= mll*pll*vlv+mlr*plr*vlh;
%
%
%       fgc(j,1)=0.0;
%       fgc(j,2)= mgl*pgl+mgr*pgr;
%       fgc(j,3)= mgl*pgl*vgv+mgr*pgr*vgh;
%
%       fp(j,1)= 0.0;
%       fp(j,2)= 0.0;
%       fp(j,3)= pl*psll+pr*pslr;


    end

% Fluxes have now been calculated. We will now update the conservative
% variables in each of the numerical cells.

%     hydgrad = g*(dlo.*evo+dgo.*ego);
%     fricgrad = dpfric1(vlo,vgo,evo,ego,dlo,dgo,po,do,di,viscl,viscg);

% Alternatively the source terms can be calculated by using a
% for loop instead of the vectorized form above.
% Note that the model is sensitive to how we treat the model
% for low Reynolds numbers (possible discontinuity in the model
      for j=1:nobox
```

```
            fricgrad(j)=dpfric(vlo(j),vgo(j),evo(j),ego(j),dlo(j),dgo(j), .
            ..
          po(j),do(j),di(j),viscl,viscg);
        hydgrad(j)=g*(dlo(j)*evo(j)+dgo(j)*ego(j));
       end

      sumfric = 0;
      sumhyd= 0;

      for j=1:nobox
%

%
       ar = area(j);
%



      qv(j,1)=qvo(j,1)-dtdx*((ar*flc(j+1,1)-ar*flc(j,1))...
                            +(ar*fgc(j+1,1)-ar*fgc(j,1))...
                            +(ar*fp(j+1,1)-ar*fp(j,1)));

      qv(j,2)=qvo(j,2)-dtdx*((ar*flc(j+1,2)-ar*flc(j,2))...
                            +(ar*fgc(j+1,2)-ar*fgc(j,2))...
                            +(ar*fp(j+1,2)-ar*fp(j,2)));

      qv(j,3)=qvo(j,3)-dtdx*((ar*flc(j+1,3)-ar*flc(j,3))...
                            +(ar*fgc(j+1,3)-ar*fgc(j,3))...
                            +(ar*fp(j+1,3)-ar*fp(j,3)))...
                   -dt*ar*(fricgrad(j)+hydgrad(j));

%
      sumfric=sumfric+fricgrad(j)*dx;
      sumhyd=sumhyd+hydgrad(j)*dx;


% We define the box number and initiate suction from this box:

      if (j==14)
        qv(14,1)=qv(14,1)-dt*suckrate/dx;
      end

      end


% Section where we find the physical variables (pressures, densities etc)
% from the conservative variables. Some tricks to ensure stability. These
% are induced to avoid negative masses.

%      qv(j,1)= qv(j,1)/area(j);
%      qv(j,2)= qv(j,2)/area(j);

     gasmass=0;
     liqmass=0;

     for j=1:nobox


% Remove the area from the conservative variables to find the
% the primitive variables from the conservative ones.


      qv(:,1)=qv(:,1)./area';
      qv(:,2)=qv(:,2)./area';


      if (qv(j,1)<0.00000001)
        qv(j,1)=0.0000001;
      end
```

```
      if (qv(j,2)< 0.00000001)
        qv(j,2)=0.0000001;
      end


      gasmass = gasmass+qv(j,2)*area(j)*dx;
      liqmass = liqmass+qv(j,1)*area(j)*dx;


% Below, we find the primitive variables pressure and densities based on
% the conservative variables q1,q2. One can choose between getting them by
% analytical or numerical solution approach specified in the beginning of
% the program.

    if (analytical == 1)
      % Coefficients:
      a = 1/(al*al);
      b = t1-qv(j,1)-rt*qv(j,2)/(al*al);
      c = -1.0*t1*rt*qv(j,2);

      % Analytical solution:
       p(j)=(-b+sqrt(b*b-4*a*c))/(2*a);  % Pressure
       dl(j)= dstc + (p(j)-pstc)/(al*al); % Density of liquid
       dl(j)= rholiq(p(j));

       % Density of gas
       dg(j) = p(j)/rt;
       dg(j) = rogas(p(j));
    else
      %Numerical Solution:
      [p(j),error]=itsolver(po(j),qv(j,1),qv(j,2)); % Pressure
      dl(j)=rholiq(p(j)); % Density of liquid
      dg(j)=rogas(p(j)); % Density of gas

      % Incase a numerical solution is not found, the program will write out
"error":
      if error > 0
         error
      end
    end


 % Find the phase volume fractions based on new conservative variables and
 % updated densities.

       eg(j)= qv(j,2)/dg(j);
       ev(j)=1-eg(j);

%        eg=qv(:,2)'./dg;
%        ev=1-eg;



%%%%%% INCLUDE VERY IMPORTANT TEST & CORRECTION ON PRESSURE

      if (p(j)<100000)
         p(j)=100000;
         dg(j)=rogas(p(j));
         dl(j)=rholiq(p(j));
         eg(j)=1-qv(j,1)/dl(j);
         ev(j)=1-eg(j);
         qv(j,1)=dl(j)*ev(j);
         qv(j,2)=dg(j)*eg(j);
      end

% Reset average conservative variables in cells with area changes inside.

       qv(j,1)=qv(j,1)*area(j);
```

```
       qv(j,2)=qv(j,2)*area(j);

%       qv(:,1)=qv(:,1).*area';
%       qv(:,2)=qv(:,2).*area';

%     The section below is used to find the primitive variables vg,vl
%    (phase velocities) based on the updated conservative variable q3 and
%     the slip relation.

     end

% Part where we interpolate in the slip parameters to avoid a
% singularities when approaching one phase gas flow.
% In the transition to one-phase gas flow, we need to
% have a smooth transition to no-slip conditions.

   gasvol=0;

   for j=1:nobox


   % The interpolations introduced below are included
   % to omit a singularity in the slip relation when the gas volume
   % fraction becomes equal to 1/K. In addition, S is interpolated to
   % zero when approaching one phase gas flow. In the transition to
   % one phase gas flow, we have no slip conditions (K=1, S=0)

      ktemp=k;
      stemp=s;

      k0(j) = ktemp;
      s0(j) = stemp;
      if ((eg(j)>=0.7) & (eg(j)<=0.8))
        xint = (eg(j)-0.7)/0.1;
        k0(j) =1.0*xint+k*(1-xint);
      elseif(eg(j)>0.8)
        k0(j)=1.0;
      end

      if ((eg(j)>=0.9) & (eg(j)<=1.0))
        xint = (eg(j)-0.9)/0.1;
        s0(j) = 0.0*xint+s*(1-xint);
      end

      if (eg(j)>=0.999999)
        k1(j) = 1.0;
        s1(j) = 0.0;
      else
        k1(j) = (1-k0(j)*eg(j))/(1-eg(j));
        s1(j) = -1.0*s0(j)*eg(j)/(1-eg(j));
      end


      % Variable for summarizing the gas volume content in the well.
      gasvol=gasvol+eg(j)*area(j)*dx;


   end


 %    Below we find the phase velocities by combining the
 %    conservative variable defined by the mixture momentum equation
 %    with the gas slip relation. The code commented away was before
 %    vectorization.

%       help1 = dl(j)*ev(j)*k1+dg(j)*eg(j)*k0;
%       help2 = dl(j)*ev(j)*s1+dg(j)*eg(j)*s0;
%
%       vmixhelpl = (qv(j,3)/area(j)-help2)/help1;
%       vg(j)=k0*vmixhelpl+s0;
```

```
%       vl(j)=k1*vmixhelpl+s1;

       help1 = dl.*ev.*k1+dg.*eg.*k0;
       help2 = dl.*ev.*s1+dg.*eg.*s0;

       vmixhelpl = (qv(:,3)'./area-help2)./help1;
       vg=k0.*vmixhelpl+s0;
       vl=k1.*vmixhelpl+s1;

% Old values are now set equal to new values in order to prepare
% computation of next time level.

   po=p;
   dlo=dl;
   dgo=dg;
   vlo=vl;
   vgo=vg;
   ego=eg;
   evo=ev;
   qvo=qv;


% Section where we save some time dependent variables in arrays.
% e.g. the bottomhole pressure. They will be saved for certain
% timeintervalls defined in the start of the program in order to ensure
% that the arrays do not get to long!

  if (counter>=nostepsbeforesavingtimedata)
    printcounter=printcounter+1;
    time

    % Outlet massrates vs time
    %liquidmassrateout(printcounter)=dl(nobox)*ev(nobox)*vl(nobox)*area(nobo
x);

liquidmassrateout(printcounter)=flc(nofluxes,1)*area(nobox)+suckrate;
    liquidmassratein(printcounter)=flc(1,1)*area(1);
    %gasmassrateout(printcounter)=dg(nobox)*eg(nobox)*vg(nobox)*area(nobox);
    gasmassrateout(printcounter)=fgc(nofluxes,2)*area(nobox);
    gassmassrateinontop(printcounter)=-    1.0*gasmassrateout(printcounter);

    % Hydrostatic and friction pressure in well vs time
    hyd(printcounter)=sumhyd/100000;
    fric(printcounter)=sumfric/100000;

    % Volume of gas in well vs time

    volgas(printcounter)=gasvol;

    % Total phase masses in the well vs time
    massgas(printcounter)=gasmass;
    massliq(printcounter)=liqmass;
    % pout defines the exact pressure at the outletboundary!
    pout(printcounter)=p(nobox)-0.5*dx*...
    (dlo(nobox)*evo(nobox)+dgo(nobox)*ego(nobox))*g-dx*0.5*fricgrad(nobox);

    % pin defines the exact pressure at the bottom boundary
    %pout(printcounter)=p(nobox)/100000
    pin(printcounter)=
p(1)+0.5*dx*(dlo(1)*evo(1)+dgo(1)*ego(1))*g+0.5*dx*fricgrad(1);
   % pin(printcounter)=hyd(printcounter)+ fric(printcounter);

    % Time variable
    timeplot(printcounter)=time;

    counter = 0;


  end
end
```

```
% end of stepping forward in time.



% Printing of results section


countsteps % Marks number of simulation steps.


% Plot commands for variables vs time. The commands can also
% be copied to command screen where program is run for plotting other
% variables.

toc,
e = cputime-t

% Plot bottomhole pressure
plot(timeplot,pin/100000)

% Show cfl number used.
disp('cfl')
cfl = al*dt/dx


%plot(timeplot,liquidmassrateout)
%plot(timeplot,gasmassrateout)

%Plot commands for variables vs depth/Only the last simulated
%values at endtime is visualised

%plot(vl,x);
%plot(vg,x);
%plot(eg,x);
%plot(p,x);
%plot(dl,x);
%plot(dg,x);
```

Function for finding the sound velocity

```
function mixsoundvelocity = csound(gvo,po,dlo,k)
% Note that at this time k is set to 1.0 (should maybe be
% included below

temp= gvo*dlo*(1.0-gvo);
a=1;
if (temp < 0.01)
  temp = 0.01;
end

cexpr = sqrt(po/temp);

if (gvo <= 0.5)
 mixsoundvelocity = min(cexpr,1500);
else
 mixsoundvelocity = min(cexpr,316);
end
```

Function for the friction model

```
function friclossgrad =
dpfric(vlo,vgo,evo,ego,dlo,dgo,pressure,do,di,viscl,viscg)


% Works for two phase flow. The one phase flow model is used but mixture
% values are introduced.


 vmixfric = vlo*evo+vgo*ego;
 viscmix =  viscl*evo+viscg*ego;
 densmix = dlo*evo+dgo*ego;

 % Calculate mix reynolds number
 Re = ((densmix*abs(vmixfric)*(do-di))/viscmix);

 % Calculate friction factor. For Re > 3000, the flow is turbulent.
 % For Re < 2000, the flow is laminar. Interpolate in between.

 if (Re<0.001)
   f=0.0;
 else
  if (Re >= 3000)
   f = 0.052*Re^(-0.19);
  elseif ( (Re<3000) & (Re > 2000))
   f1 = 24/Re;
   f2 = 0.052*Re^(-0.19);
   xint = (Re-2000)/1000.0;
   f = (1.0-xint)*f1+xint*f2;
  else
   f = 24/Re;
  end
 end

  friclossgrad = ((2*f*densmix*vmixfric*abs(vmixfric))/(do-di));


end
```

Functions for finding the fluxes with AUSMV scheme

Function PM

```
function pmvalue = pm(v,c)


  if (abs(v)<=c)
    pmvalue = -1.0*(v-c)*(v-c)/(4*c)*(-2.0-v/c)/c;
  else
    pmvalue = 0.5*(v-abs(v))/v;
  end
end
```

Function PP

```
function pmvalue = pp(v,c)

  if (abs(v)<=c)
    pmvalue = (v+c)*(v+c)/(4*c)*(2.0-v/c)/c;
  else
    pmvalue = 0.5*(v+abs(v))/v;
  end
end
```

Function PSIM

```
function pmvalue = psim(v,c,alpha)

  if (abs(v)<=c)
    pmvalue = -1.0*alpha*(v-c)*(v-c)/(4*c)+(1-alpha)*(v-abs(v))/2;
  else
    pmvalue = 0.5*(v-abs(v));
  end
end
```

Function PSIP

```
function pmvalue = psip(v,c,alpha)


  if (abs(v)<=c)
    pmvalue = alpha*(v+c)*(v+c)/(4*c)+(1-alpha)*(v+abs(v))/2;
  else
    pmvalue = 0.5*(v+abs(v));
  end
end
```

Appendix B, EC-Drill with 2nd order AUSMV scheme, small-scale flow-loop, Matlab code

Comments and inactivate variables in the code are separated by "%" symbol and marked in green, the same way it is in Matlab. All the changes made to the original code are marked in red. The pressure condition described in chapter 4 is marked in red as well as the modified pressure condition for the alternative method in chapter 6. Parts related to the 2nd order scheme are marked in light blue and parts related to the 1st order scheme are marked in purple. The functions used in the main code to calculate densities, friction, fluxes etc. are given in the end of the Appendix A. The geometry data for the approximated small-scale flow-loop model is taken from chapter 5.

```
% Transient two-phase code based on AUSMV scheme: Gas and Water
% The code assumes uniform geometry and the code is partially vectorized.

clear;
t = cputime
tic,

% Geometry data/ Must be specified
welldepth = 50;
nobox = 25; %Number of boxes in the well
nofluxes = nobox+1;
dx = welldepth/nobox; % Boxlength
%dt = 0.005;

% Welldepth array
x(1)= -1.0*welldepth+0.5*dx;
for i=1:nobox-1
 x(i+1)=x(i)+ dx;
end

dt= 0.00025;  % Timestep
dtdx = dt/dx;
time = 0.0;
endtime = 50; % Rime for end of simulation
nosteps = endtime/dt;  %Number of total timesteps
timebetweensavingtimedata = 0.1;  % How often in s we save data vs time for
plotting.
nostepsbeforesavingtimedata = timebetweensavingtimedata/dt;

% Slip parameters used in the gas slip relation. vg =Kvmix+S
k = 1.0;
s = 0.5;


% Viscosities (Pa*s)/Used in the frictional pressure loss model.
viscl = 0.05; % Liquid phase
viscg = 0.0000182; % Gas phase

% Density parameters. These parameters are used when finding the
% primitive variables pressure, densities in an analytical manner.
% Changing parameters here, you must also change parameters inside the
% density routines roliq and rogas.
```

```
% liquid density at stc and speed of sound in liquid
  dstc = 1000.0;   %Base density of liquid, See also roliq.
  pstc = 100000.0; % Pressure at standard conditions, 100000 Pascal
  al = 1500; % Speed of sound/compressibility of liquid phase.
  t1 = dstc-pstc/(al*al); % Help variable for calculating primitive
variables from
  % conservative variables
% Ideal gas law constant
  rt = 100000;

% Gravity constant

  g = 9.81; % Gravitational constant

% Well opening. opening = 1, fully open well, opening = 0 (<0.01), the well
% is fully closed. This variable will control what boundary conditions that
% will apply at the outlet (both physical and numerical): We must change
% this further below in the code if we want to change status on this.

  wellopening = 1.0;  % This variable determines if
%the well is closed or not, wellopening = 1.0 -> open. wellopening = 0
%-> Well is closed. This variable affects the boundary treatment.

  bullheading = 0.0; % This variable can be set to 1.0 if we want to
simulate
% a bullheading operation. But the normal is to set this to zero.


% Specify if the primitive variables shall be found either by
% a numerical or analytical approach. If analytical = 1, analytical
% solution is used. If analytical = 0. The numerical approach is used.
% using the itsolver subroutine where the bisection numerical method
% is used.

  analytical = 1;


% Define and initialize flow variables

% Here we specify the outer and inner diameter and the flow area

   for i = 1:nobox
    do(i)=0.033;
    di(i) = 0.0;
    area(i) = 3.14/4*(do(i)*do(i)- di(i)*di(i));
   end


% Initialization of slope limiters.
  for i = 1:nobox
    sl1(i)=0;
    sl2(i)=0;
    sl3(i)=0;
    sl4(i)=0;
    sl5(i)=0;
    sl6(i)=0;
  end


% Now comes the initialization of the physical variables in the well.
% First primitive variables, then the conservative ones.


% Below we initialize pressure and fluid densities. We start from top of
% the well and calculated downwards. The calculation is done twice with
% updated values to get better approximation. Only hydrostatic
% considerations.

% Overpressure method with 10 bars
```

```
% p(nobox)= 1000000.0+0.5*dx*9.81*dstc*cosd(84);   % Pressure

% Alternative method
p(nobox)= 100000.0+0.5*dx*9.81*dstc*cosd(84);   % Pressure
dl(nobox)=rholiq(p(nobox));  % Liquid density
dg(nobox)=rogas(p(nobox));   % Gas density

for i=nobox-1:-1:1
p(i)=p(i+1)+dx*9.81*dl(i+1)*cosd(84);
dl(i)=rholiq(p(i));
dg(i)=rogas(p(i));
end

for i=nobox-1:-1:1
p(i)=p(i+1)+dx*9.81*(dl(i+1)+dl(i))*0.5*cosd(84);
dl(i)=rholiq(p(i));
dg(i)=rogas(p(i));

end

% Initialize phase velocities, volume fractions, conservative variables
% The basic assumption is static fluid, one phase liquid.

for i = 1:nobox
  vl(i)=0; % Liquid velocity new time level.
  vg(i)=0; % Gas velocity at new time level
  eg(i)=0;  % Gas volume fraction
  ev(i)=1-eg(i); % Liquid volume fraction
  qv(i,1)=dl(i)*ev(i)*area(i);
  qv(i,2)=dg(i)*eg(i)*area(i);
  qv(i,3)=(dl(i)*ev(i)*vl(i)+dg(i)*eg(i)*vg(i))*area(i);
  fricgrad(i)=0;
  hydgrad(i)=g* qv(i,1)*cosd(84);
end

source = zeros(nobox,3);


% Section where we also initialize values at old time level


for i=1:nobox
  dlo(i)=dl(i);
  dgo(i)=dg(i);
  po(i)=p(i);
  ego(i)=eg(i);
  evo(i)=ev(i);
  vlo(i)=vl(i);
  vgo(i)=vg(i);
  qvo(i,1)=qv(i,1);
  qvo(i,2)=qv(i,2);
  qvo(i,3)=qv(i,3);
end


% Initialize fluxes between the cells/boxes

for i = 1:nofluxes
  for j =1:3
   flc(i,j)=0.0; % Flux of liquid over box boundary
   fgc(i,j)=0.0; % Flux of gas over box boundary
   fp(i,j)= 0.0; % Pressure flux over box boundary
  end
end


% Main program. Here we will progress in time. First som   initializations
% and definitions to take out results. The for loop below runs until the
% simulation is finished.
```

```
countsteps = 0;
counter=0;
printcounter = 1;
pbot(printcounter) = p(1);
pchoke(printcounter)= p(nobox);
liquidmassrateout(printcounter) = 0;
gasmassrateout(printcounter)=0;
timeplot(printcounter)=time;
kickvolume=0;
bullvolume=0;

for i = 1:nosteps
   countsteps=countsteps+1;
   counter=counter+1;
   time = time+dt;

% Then a section where the boundary conditions are specified.
% Here we specify the inlet rates of the different phases at the
% bottom of the pipe in kg/s. We interpolate to make things smooth.
% It is also possible to change the outlet boundary status of the well
% here. First we specify rates at the bottom and the pressure at the outlet
% in case we have an open well. This is a place where we can change the
% code to control simulations.

XX = 4;
% XX (kg/s) is a variable for introducing a kick in the well.
YY = 15; % Liquid flowrate (kg/s) (1 kg/s = 1 l/s approx)

if (time<5)
  inletligmassrate=0.0;
  inletgasmassrate=0.0;
elseif((time>=5)&(time<30))
  inletligmassrate=0.0;
  inletgasmassrate=0.0;
elseif((time>=30)&(time<35))
  inletgasmassrate=0.0;
  inletligmassrate=0.5*(time-30)/5;
elseif(time>=35)
    inletligmassrate=0.5;
    inletgasmassrate=0;
end



kickvolume = kickvolume+inletgasmassrate/dgo(1)*dt;


% specify the outlet pressure /Physical. Here we have given the pressure as
% constant. It would be possible to adjust it during openwell conditions
% either by giving the wanted pressure directly (in the command lines
% above) or by finding it indirectly through a chokemodel where the
wellopening
% would be an input parameter. The wellopening variable would equally had
% to be adjusted inside the command line structure given right above.

 % Overpressure method with 10 bars

%  pressureoutlet = 1000000.0;

%  Alternative method

 pressureoutlet = 100000.0;


% Based on these boundary values combined with use of extrapolations
techniques
% for the remaining unknowns at the boundaries, we will define the mass and
% momentum fluxes at the boundaries (inlet and outlet of pipe).
```

```
% inlet/bottom fluxes first.
   if (bullheading<=0)

     flc(1,1)= inletligmassrate/area(1);
     flc(1,2)= 0.0;
     flc(1,3)= flc(1,1)*vlo(1);


     fgc(1,1)= 0.0;
     fgc(1,2)= inletgasmassrate/area(1);
     fgc(1,3)= fgc(1,2)*vgo(1);

     fp(1,1)= 0.0;
     fp(1,2)= 0.0;

% Old way of treating the boundary
%     fp(1,3)= po(1)+0.5*(po(1)-po(2)); %Interpolation used to find the
% pressure at the inlet/bottom of the well.

% New way of treating the boundary
      fp(1,3)= po(1)...
            +0.5*dx*(dlo(1)*evo(1)+dgo(1)*ego(1))*g*cosd(84)...
            +0.5*dx*fricgrad(1);



   else
     flc(1,1)=dlo(1)*evo(1)*vlo(1);
     flc(1,2)=0.0;
     flc(1,3)=flc(1,1)*vlo(1);

     fgc(1,1)=0.0;
     fgc(1,2)=dgo(1)*ego(1)*vgo(1);
     fgc(1,3)=fgc(1,2)*vgo(1);

     fp(1,1)=0.0;
     fp(1,2)=0.0;
     fp(1,3)=20000000; % This was a fixed pressure set at bottom when
bullheading
   end



% Outlet fluxes (open & closed conditions)

    if (wellopening>0.01)

% Here open end condtions are given. We distinguish between bullheading
% & normal circulation.

        if (bullheading<=0)

            flc(nofluxes,1)= dlo(nobox)*evo(nobox)*vlo(nobox);
            flc(nofluxes,2)= 0.0;
            flc(nofluxes,3)= flc(nofluxes,1)*vlo(nobox);


            fgc(nofluxes,1)= 0.0;
            fgc(nofluxes,2)= dgo(nobox)*ego(nobox)*vgo(nobox);
            fgc(nofluxes,3)= fgc(nofluxes,2)*vgo(nobox);

            fp(nofluxes,1)= 0.0;
            fp(nofluxes,2)= 0.0;
            fp(nofluxes,3)= pressureoutlet;
        else
            flc(nofluxes,1)= inletligmassrate/area(nobox);
            flc(nofluxes,2)= 0.0;
            flc(nofluxes,3)= flc(nofluxes,1)*vlo(nobox);

            fgc(nofluxes,1)=0.0;
```

```
            fgc(nofluxes,2)=0.0;
            fgc(nofluxes,3)=0.0;

            fp(nofluxes,1)=0.0;
            fp(nofluxes,2)=0.0;
            fp(nofluxes,3)= po(nobox)...
            -0.5*dx*(dlo(nobox)*evo(nobox)+dgo(nobox)*ego(nobox))*g...
            *cosd(84)+0.5*dx*fricgrad(nobox);
        end
    else

% Here closed end conditions are given

         flc(nofluxes,1)= 0.0;
         flc(nofluxes,2)= 0.0;
         flc(nofluxes,3)= 0.0;

         fgc(nofluxes,1)= 0.0;
         fgc(nofluxes,2)= 0.0;
         fgc(nofluxes,3)= 0.0;

         fp(nofluxes,1)=0.0;
         fp(nofluxes,2)=0.0;

    %    Old way of treating the boundary
    %     fp(nofluxes,3)= po(nobox)-0.5*(po(nobox-1)-po(nobox));

    %    New way of treating the boundary
         fp(nofluxes,3)= po(nobox)...
         -0.5*dx*(dlo(nobox)*evo(nobox)+dgo(nobox)*ego(nobox))*g*cosd(84);
    %     -0.5*dx*fricgrad(nobox); % Neglect friction since well is closed.
        end


   % Include Suction Point

   suckrate = 0;

   if ((time>=5)&(time<10))
     suckrate = 0.5*(time-5)/5;
     flc(nofluxes,1)=0;
     flc(nofluxes,3)=0;

% To make both extrapolation methods work, gas fluxes are set to 0

%      fgc(nofluxes,2)=0;
%      fgc(nofluxes,3)=0;

% New extrapolation method described in SPE 180053:

%      fp(nofluxes,3)= po(nobox)...
%          -0.5*dx*(dlo(nobox)*evo(nobox)+dgo(nobox)*ego(nobox))*g...
%          *cosd(84)-0.5*dx*fricgrad(nobox);

% Old extrapolation method described in SPE 168960:

%      fp(nofluxes,3)=po(nobox)-0.5*(po(nobox-1)-po(nobox));

% Fixed pressure equal to 1 atm delivered the most realistic results:

% Overpressure method with 10 bars
%     fp(nofluxes,3)=1000000;
% Alternative mthod
     fp(nofluxes,3)=100000;

   elseif(time>=10)
    suckrate = 0.5;
    flc(nofluxes,1)=0;
     flc(nofluxes,3)=0;
```

```
% To make both extrapolation methods work, gas fluxes are set to 0

%       fgc(nofluxes,2)=0;
%       fgc(nofluxes,3)=0;

% New extrapolation method described in SPE 180053:

%       fp(nofluxes,3)= po(nobox)...
%           -0.5*dx*(dlo(nobox)*evo(nobox)+dgo(nobox)*ego(nobox))*g...
%           *cosd(84)-0.5*dx*fricgrad(nobox);

% Old extrapolation method described in SPE 168960:

%       fp(nofluxes,3)=po(nobox)-0.5*(po(nobox-1)-po(nobox));

% Fixed pressure equal to 1 atm delivered the most realistic results:

% Overpressure method with 10 bars
%      fp(nofluxes,3)=1000000;
% Alternative mthod
     fp(nofluxes,3)=100000;


   end


 % Implementation of slopelimiters. They are applied on the physical
 % variables like phase densities, phase velocities and pressure.

     for i=2:nobox-1
      sl1(i)=minmod(dlo(i-1),dlo(i),dlo(i+1),dx);
      sl2(i)=minmod(po(i-1),po(i),po(i+1),dx);
      sl3(i)=minmod(vlo(i-1),vlo(i),vlo(i+1),dx);
      sl4(i)=minmod(vgo(i-1),vgo(i),vgo(i+1),dx);
      sl5(i)=minmod(ego(i-1),ego(i),ego(i+1),dx);
      sl6(i)=minmod(dgo(i-1),dgo(i),dgo(i+1),dx);
     end

 % Slopelimiters in boundary cells are set to zero!
     sl1(nobox)=0;
     sl2(nobox)=0;
     sl3(nobox)=0;
     sl4(nobox)=0;
     sl5(nobox)=0;
     sl6(nobox)=0;

  % Ny Kode 11/11-15
     sl1(1)=0;
     sl2(1)=0;
     sl3(1)=0;
     sl4(1)=0;
     sl5(1)=0;
     sl6(1)=0;


% Now we will find the fluxes between the different cells.
% NB - IMPORTANE - Note that if we change the compressibilities/sound
velocities of
% the fluids involved, we need to do changes inside the csound function.

     for j = 2:nofluxes-1

 %%%%%%%%%%%%%%%%%%%%%%%%%%%%%%%%%%%%%%%%%%%%%%%%%%%%
 %%%%%%%%%%%%%%%%%%%%%%%%%%%%%%%%%%%%%%%%%%%%%%%%%%%%
 % First order method is from here:
%        cl = csound(ego(j-1),po(j-1),dlo(j-1),k);
%        cr = csound(ego(j),po(j),dlo(j),k);
%        c = max(cl,cr);
%        pll = psip(vlo(j-1),c,evo(j));
%        plr = psim(vlo(j),c,evo(j-1));
```

```
%         pgl = psip(vgo(j-1),c,ego(j));
%         pgr = psim(vgo(j),c,ego(j-1));
%         vmixr = vlo(j)*evo(j)+vgo(j)*ego(j);
%         vmixl = vlo(j-1)*evo(j-1)+vgo(j-1)*ego(j-1);
%
%         pl = pp(vmixl,c);
%         pr = pm(vmixr,c);
%         mll= evo(j-1)*dlo(j-1);
%         mlr= evo(j)*dlo(j);
%         mgl= ego(j-1)*dgo(j-1);
%         mgr= ego(j)*dgo(j);
%
%         flc(j,1)= mll*pll+mlr*plr;
%         flc(j,2)= 0.0;
%         flc(j,3)= mll*pll*vlo(j-1)+mlr*plr*vlo(j);
%
%         fgc(j,1)=0.0;
%         fgc(j,2)= mgl*pgl+mgr*pgr;
%         fgc(j,3)= mgl*pgl*vgo(j-1)+mgr*pgr*vgo(j);
%
%         fp(j,1)= 0.0;
%         fp(j,2)= 0.0;
%         fp(j,3)= pl*po(j-1)+pr*po(j);

 %  First order methods ends here
 %%%%%%%%%%%%%%%%%%%%%%%%%%%%%%%%%%%%%%%%%%%%%%%%%%%%%%%%%%%
 %%%%%%%%%%%%%%%%%%%%%%%%%%%%%%%%%%%%%%%%%%%%%%%%%%%%%%%%%%%



%%%%%%%%%%%%%%%%%%%%%%%%%%%%%%%%%%%%%%%%%%%%%%%%%%%%%%%%%%%%%%%%
%%%%%%%%%%%%%%%%%%%%%%%%%%%%%%%%%%%%%%%%%%%%%%%%%%%%%%%%%%%%%%%%
% Second order method starts here:
% Here slopelimiter is used on all variables except phase velocities

        psll = po(j-1)+dx/2*sl2(j-1);
        pslr = po(j)-dx/2*sl2(j);
        dsll = dlo(j-1)+dx/2*sl1(j-1);
        dslr = dlo(j)-dx/2*sl1(j);
        dgll = dgo(j-1)+dx/2*sl6(j-1);
        dglr = dgo(j)-dx/2*sl6(j);

        vlv = vlo(j-1)+dx/2*sl3(j-1);
        vlh = vlo(j)-dx/2*sl3(j);
        vgv = vgo(j-1)+dx/2*sl4(j-1);
        vgh = vgo(j)-dx/2*sl4(j);

        gvv = ego(j-1)+dx/2*sl5(j-1);
        gvh = ego(j)-dx/2*sl5(j);
        lvv = 1-gvv;
        lvh = 1-gvh;

        cl = csound(gvv,psll,dsll,k);
        cr = csound(gvh,pslr,dslr,k);
        c = max(cl,cr);

        pll = psip(vlo(j-1),c,lvh);
        plr = psim(vlo(j),c,lvv);
        pgl = psip(vgo(j-1),c,gvh);
        pgr = psim(vgo(j),c,gvv);
        vmixr = vlo(j)*lvh+vgo(j)*gvh;
        vmixl = vlo(j-1)*lvv+vgo(j-1)*gvv;

        pl = pp(vmixl,c);
        pr = pm(vmixr,c);


       mll= lvv*dsll;
       mlr= lvh*dslr;
       mgl= gvv*dgll;
```

```
      mgr= gvh*dglr;

      flc(j,1)= mll*pll+mlr*plr;
      flc(j,2)= 0.0;
      flc(j,3)= mll*pll*vlo(j-1)+mlr*plr*vlo(j);


      fgc(j,1)=0.0;
      fgc(j,2)= mgl*pgl+mgr*pgr;
      fgc(j,3)= mgl*pgl*vgo(j-1)+mgr*pgr*vgo(j);

      fp(j,1)= 0.0;
      fp(j,2)= 0.0;
      fp(j,3)= pl*psll+pr*pslr;


%%% Second order method ends here
%%%%%%%%%%%%%%%%%%%%%%%%%%%%%%%%%%%%%%%%%%%%%%%%%%%%%%%%%%%%%%%%%%%%%%%
%%%%%%%%%%%%%%%%%%%%%%%%%%%%%%%%%%%%%%%%%%%%%%%%%%%%%%%%%%%%%%%%%%%%%%%

% Here sloplimiters is used on all variables. This
% has not worked so well yet.

%       psll = po(j-1)+dx/2*sl2(j-1);
%       pslr = po(j)-dx/2*sl2(j);
%       dsll = dlo(j-1)+dx/2*sl1(j-1);
%       dslr = dlo(j)-dx/2*sl1(j);
%       dgll = dgo(j-1)+dx/2*sl6(j-1);
%       dglr = dgo(j)-dx/2*sl6(j);
%
%       vlv = vlo(j-1)+dx/2*sl3(j-1);
%       vlh = vlo(j)-dx/2*sl3(j);
%       vgv = vgo(j-1)+dx/2*sl4(j-1);
%       vgh = vgo(j)-dx/2*sl4(j);
%
%       gvv = ego(j-1)+dx/2*sl5(j-1);
%       gvh = ego(j)-dx/2*sl5(j);
%       lvv = 1-gvv;
%       lvh = 1-gvh;
%
%       cl = csound(gvv,psll,dsll,k);
%       cr = csound(gvh,pslr,dslr,k);
%       c = max(cl,cr);
%
%       pll = psip(vlv,c,lvh);
%       plr = psim(vlh,c,lvv);
%       pgl = psip(vgv,c,gvh);
%       pgr = psim(vgh,c,gvv);
%       vmixr = vlh*lvh+vgh*gvh;
%       vmixl = vlv*lvv+vgv*gvv;
%
%       pl = pp(vmixl,c);
%       pr = pm(vmixr,c);
%       mll= lvv*dsll;
%       mlr= lvh*dslr;
%       mgl= gvv*dgll;
%       mgr= gvh*dglr;
%
%       flc(j,1)= mll*pll+mlr*plr;
%       flc(j,2)= 0.0;
%       flc(j,3)= mll*pll*vlv+mlr*plr*vlh;
%
%
%       fgc(j,1)=0.0;
%       fgc(j,2)= mgl*pgl+mgr*pgr;
%       fgc(j,3)= mgl*pgl*vgv+mgr*pgr*vgh;
%
%       fp(j,1)= 0.0;
%       fp(j,2)= 0.0;
%       fp(j,3)= pl*psll+pr*pslr;
```

```
    end

% Fluxes have now been calculated. We will now update the conservative
% variables in each of the numerical cells.

%     hydgrad = g*(dlo.*evo+dgo.*ego);
%     fricgrad = dpfric1(vlo,vgo,evo,ego,dlo,dgo,po,do,di,viscl,viscg);

% Alternatively the source terms can be calculated by using a
% for loop instead of the vectorized form above.
% Note that the model is sensitive to how we treat the model
% for low Reynolds numbers (possible discontinuity in the model
      for j=1:nobox

            fricgrad(j)=dpfric(vlo(j),vgo(j),evo(j),ego(j),dlo(j),dgo(j), ...
          po(j),do(j),di(j),viscl,viscg);
       hydgrad(j)=g*(dlo(j)*evo(j)+dgo(j)*ego(j))*cosd(84);
      end

      sumfric = 0;
      sumhyd= 0;

      for j=1:nobox
%

%
       ar = area(j);
%



      qv(j,1)=qvo(j,1)-dtdx*((ar*flc(j+1,1)-ar*flc(j,1))...
                           +(ar*fgc(j+1,1)-ar*fgc(j,1))...
                           +(ar*fp(j+1,1)-ar*fp(j,1)));

      qv(j,2)=qvo(j,2)-dtdx*((ar*flc(j+1,2)-ar*flc(j,2))...
                           +(ar*fgc(j+1,2)-ar*fgc(j,2))...
                           +(ar*fp(j+1,2)-ar*fp(j,2)));

      qv(j,3)=qvo(j,3)-dtdx*((ar*flc(j+1,3)-ar*flc(j,3))...
                           +(ar*fgc(j+1,3)-ar*fgc(j,3))...
                           +(ar*fp(j+1,3)-ar*fp(j,3)))...
                  -dt*ar*(fricgrad(j)+hydgrad(j));

%
      sumfric=sumfric+fricgrad(j)*dx;
      sumhyd=sumhyd+hydgrad(j)*dx;


% We define the box number and initiate suction from this box:

      if (j==14)
        qv(14,1)=qv(14,1)-dt*suckrate/dx;
      end

      end


% Section where we find the physical variables (pressures, densities etc)
% from the conservative variables. Some tricks to ensure stability. These
% are induced to avoid negative masses.

%      qv(j,1)= qv(j,1)/area(j);
%      qv(j,2)= qv(j,2)/area(j);

     gasmass=0;
     liqmass=0;
```

```
     for j=1:nobox


% Remove the area from the conservative variables to find the
% the primitive variables from the conservative ones.


      qv(:,1)=qv(:,1)./area';
      qv(:,2)=qv(:,2)./area';


      if (qv(j,1)<0.0000001)
        qv(j,1)=0.0000001;
      end

      if (qv(j,2)< 0.0000001)
        qv(j,2)=0.0000001;
      end


      gasmass = gasmass+qv(j,2)*area(j)*dx;
      liqmass = liqmass+qv(j,1)*area(j)*dx;


% Below, we find the primitive variables pressure and densities based on
% the conservative variables q1,q2. One can choose between getting them by
% analytical or numerical solution approach specified in the beginning of
% the program.

    if (analytical == 1)
      % Coefficients:
      a = 1/(al*al);
      b = t1-qv(j,1)-rt*qv(j,2)/(al*al);
      c = -1.0*t1*rt*qv(j,2);

      % Analytical solution:
       p(j)=(-b+sqrt(b*b-4*a*c))/(2*a);  % Pressure
       dl(j)= dstc + (p(j)-pstc)/(al*al); % Density of liquid
       dl(j)= rholiq(p(j));

       % Density of gas
       dg(j) = p(j)/rt;
       dg(j) = rogas(p(j));
    else
      %Numerical Solution:
      [p(j),error]=itsolver(po(j),qv(j,1),qv(j,2)); % Pressure
      dl(j)=rholiq(p(j)); % Density of liquid
      dg(j)=rogas(p(j)); % Density of gas

      % Incase a numerical solution is not found, the program will write out
"error":
      if error > 0
         error
      end
    end


 % Find the phase volume fractions based on new conservative variables and
 % updated densities.

       eg(j)= qv(j,2)/dg(j);
       ev(j)=1-eg(j);

%        eg=qv(:,2)'./dg;
%        ev=1-eg;
```

```
% With Overpressure method the pressure condition remains the same
%%%%%% INCLUDE VERY IMPORTANT TEST & CORRECTION ON PRESSURE

%       if (p(j)<100000)
 %         p(j)=100000;
 %         dg(j)=rogas(p(j));
 %         dl(j)=rholiq(p(j));
 %         eg(j)=1-qv(j,1)/dl(j);
 %         ev(j)=1-eg(j);
 %         qv(j,1)=dl(j)*ev(j);
 %         qv(j,2)=dg(j)*eg(j);
 %      end

% With the alternative method the pressure condition has been modified
% in the following way

          if (j>=14)
              if (p(j)<100000)
                 if (ev(j)<=0.1)
                    p(j)=100000;
                    dg(j)=rogas(p(j));
                    dl(j)=rholiq(p(j));
                    eg(j)=1-qv(j,1)/dl(j);
                    ev(j)=1-eg(j);
                    qv(j,1)=dl(j)*ev(j);
                    qv(j,2)=dg(j)*eg(j);
                 end
              end
           end


% Reset average conservative variables in cells with area changes inside.

        qv(j,1)=qv(j,1)*area(j);
        qv(j,2)=qv(j,2)*area(j);

%        qv(:,1)=qv(:,1).*area';
%        qv(:,2)=qv(:,2).*area';

%      The section below is used to find the primitive variables vg,vl
%     (phase velocities) based on the updated conservative variable q3 and
%      the slip relation.

      end

% Part where we interpolate in the slip parameters to avoid a
% singularities when approaching one phase gas flow.
% In the transition to one-phase gas flow, we need to
% have a smooth transition to no-slip conditions.

    gasvol=0;

    for j=1:nobox


    % The interpolations introduced below are included
    % to omit a singularity in the slip relation when the gas volume
    % fraction becomes equal to 1/K. In addition, S is interpolated to
    % zero when approaching one phase gas flow. In the transition to
    % one phase gas flow, we have no slip conditions (K=1, S=0)

       ktemp=k;
       stemp=s;

       k0(j) = ktemp;
       s0(j) = stemp;
       if ((eg(j)>=0.7) & (eg(j)<=0.8))
         xint = (eg(j)-0.7)/0.1;
         k0(j) =1.0*xint+k*(1-xint);
```

```
      elseif(eg(j)>0.8)
        k0(j)=1.0;
      end

      if ((eg(j)>=0.9) & (eg(j)<=1.0))
        xint = (eg(j)-0.9)/0.1;
        s0(j) = 0.0*xint+s*(1-xint);
      end

      if (eg(j)>=0.999999)
        k1(j) = 1.0;
        s1(j) = 0.0;
      else
        k1(j) = (1-k0(j)*eg(j))/(1-eg(j));
        s1(j) = -1.0*s0(j)*eg(j)/(1-eg(j));
      end


      % Variable for summarizing the gas volume content in the well.
      gasvol=gasvol+eg(j)*area(j)*dx;


   end


 %    Below we find the phase velocities by combining the
 %    conservative variable defined by the mixture momentum equation
 %    with the gas slip relation. The code commented away was before
 %    vectorization.

%       help1 = dl(j)*ev(j)*k1+dg(j)*eg(j)*k0;
%       help2 = dl(j)*ev(j)*s1+dg(j)*eg(j)*s0;
%
%       vmixhelpl = (qv(j,3)/area(j)-help2)/help1;
%       vg(j)=k0*vmixhelpl+s0;
%       vl(j)=k1*vmixhelpl+s1;

      help1 = dl.*ev.*k1+dg.*eg.*k0;
      help2 = dl.*ev.*s1+dg.*eg.*s0;

      vmixhelpl = (qv(:,3)'./area-help2)./help1;
      vg=k0.*vmixhelpl+s0;
      vl=k1.*vmixhelpl+s1;

% Old values are now set equal to new values in order to prepare
% computation of next time level.

   po=p;
   dlo=dl;
   dgo=dg;
   vlo=vl;
   vgo=vg;
   ego=eg;
   evo=ev;
   qvo=qv;


% Section where we save some time dependent variables in arrays.
% e.g. the bottomhole pressure. They will be saved for certain
% timeintervalls defined in the start of the program in order to ensure
% that the arrays do not get to long!

  if (counter>=nostepsbeforesavingtimedata)
    printcounter=printcounter+1;
    time

    % Outlet massrates vs time
    %liquidmassrateout(printcounter)=dl(nobox)*ev(nobox)*vl(nobox)*area(nobo
x);
```

```
liquidmassrateout(printcounter)=flc(nofluxes,1)*area(nobox)+suckrate;
    liquidmassratein(printcounter)=flc(1,1)*area(1);
    %gasmassrateout(printcounter)=dg(nobox)*eg(nobox)*vg(nobox)*area(nobox);
    gasmassrateout(printcounter)=fgc(nofluxes,2)*area(nobox);
    gassmassrateinontop(printcounter)=-1.0*gasmassrateout(printcounter);

    % Hydrostatic and friction pressure in well vs time
    hyd(printcounter)=sumhyd/100000;
    fric(printcounter)=sumfric/100000;

    % Volume of gas in well vs time

    volgas(printcounter)=gasvol;

    % Total phase masses in the well vs time
    massgas(printcounter)=gasmass;
    massliq(printcounter)=liqmass;
    % pout defines the exact pressure at the outletboundary!
    pout(printcounter)=p(nobox)-0.5*dx*...
    (dlo(nobox)*evo(nobox)+dgo(nobox)*ego(nobox))*g*cosd(84)
-dx*0.5*fricgrad(nobox);

    % pin defines the exact pressure at the bottom boundary
    %pout(printcounter)=p(nobox)/100000
    pin(printcounter)=
p(1)+0.5*dx*(dlo(1)*evo(1)+dgo(1)*ego(1))*g*cosd(84)+0.5*dx*fricgrad(1);
   % pin(printcounter)=hyd(printcounter)+ fric(printcounter);

    % Time variable
    timeplot(printcounter)=time;

    counter = 0;


  end
end

% end of stepping forward in time.



% Printing of results section


countsteps % Marks number of simulation steps.


% Plot commands for variables vs time. The commands can also
% be copied to command screen where program is run for plotting other
% variables.

toc,
e = cputime-t

% Plot bottomhole pressure
plot(timeplot,pin/100000)

% Show cfl number used.
disp('cfl')
cfl = al*dt/dx


%plot(timeplot,liquidmassrateout)
%plot(timeplot,gasmassrateout)

%Plot commands for variables vs depth/Only the last simulated
%values at endtime is visualised

%plot(vl,x);
```

```
%plot(vg,x);
%plot(eg,x);
%plot(p,x);
%plot(dl,x);
%plot(dg,x);
```